Dodecylbenzenesulfonic Acid: A Surfactant and Dopant for the Synthesis of Processable Polyaniline and its Copolymers

von der Fakultät für Naturwissenschaften der Technischen Universität Chemnitz genehmigte Dissertation zur Erlangung des akademischen Grades

doctor rerum naturalium

(Dr. rer. nat.)

vorgelegt von

M.Sc. Subrahmanya Shreepathi

geboren am 21.02.1977 in Ananthapur, Indien

eingereicht am 26 Juli 2006

Gutachter: Prof. Dr. Rudlof Holze

Prof. Dr. Werner A. Goedel

PD. Dr. Andreas Bund

Tag der Verteidigung: 07 Dezember 2006

Bibliographische Beschreibung und Referat

Subrahmanya Shreepathi

Dodecylbenzenesulfonic Acid: A Surfactant and Dopant for the Synthesis of Processable Polyaniline and its Copolymers

Das Ziel der vorliegenden Arbeit ist die bessere Verarbeitung von Polyanilin (PANI), da dies bisher ein großer Nachteil unter leitfähigen Polymeren war. Dazu wird ein sperriges Tensid und Dotand, Dodecylbenzensulfonsäure (DBSA) verwendet. Zur Synthese der PANI kommen zwei verschiedene Methoden zur Anwendung, die in dieser Dissertation in zwei Kapiteln beschrieben werden.

Im ersten Teil wurden in einem kleinen Reaktionsvolumen (250 mL) PANI-DBSA-Suspensionen synthetisiert, wobei mit einem binären Gemisch aus 2-Propanol und Wasser als Lösungsmittel gearbeitet wird um die Löslichkeit zu unterstützen. Die micellenunterstützte Synthese produziert grüne Dispersionen, welche nach länger als einem Jahr noch keine sichtbare Ausscheidung zeigen. Eine detaillierte spectroelektrochemische Untersuchung der PANI-DBSA-Nanokolloide wurde durchgeführt und gibt eine bessere Erklärung der Charge-Transfer-Prozesse zwischen PANI-Kolloiden und Elektrodenoberfläche. In einem alkalischen Medium ist das UV-Vis-Spektrum von der Beweglichkeit der Anionen und von einem elektrokinetischen Phänomen abhängig. Um den „metal-to-insulator"-Übergang zwischen PANI-Kolloiden, welcher durch pH-Wert-Änderung des Mediums geschehen kann, zu zeigen, wurden UV-Vis- und pre-resonanz-Raman-Spektroskopie verwendet.

Im zweiten Teil der Dissertation wird zur Polymerisation von Anilin sowie seinen Copolymeren mit *o*-Toluidin eine neue Technik der Polymerisation beschrieben, welche durch inverse Emulsion erfolgt. Diese benutzt Benzoylperoxid, ein ungewöhnlicheres organisches Oxidationsmittel. Die erhaltenen PANI sind in gebräuchlichen organischen Lösungsmitteln, wie in Chloroform, vollständig löslich. Mit einer klar-transparenten, grünen Lösung von PANI können metallische Oberflächen oder Glas leicht tropfenbeschichtet werden. Zyklische Voltammetrie und spektroelektrochemische Verfahren kamen zum Einsatz, um die Elektroaktivität, das UV-Vis-Verhalten und die „metal-to-insulator"-Übergänge der chemisch synthetisierten PANI als Funktion des verwendeten Elektrodenpotentials zu untersuchen. Die elektrische Leitfähigkeit der Materialien ist relativ hoch ($R = 10\ \Omega$). SEM-Untersuchungen zeigen, dass die Menge des zugesetzten DBSA die Morphologie des Polymers stark beeinflusst. Aus *in situ* UV-Vis-spektroskopischen Messungen lässt sich eine gute elektrochromische Reversibilität des Polymers erkennen. DBSA kann Poly(o-toluidin) (POT) effektiv dotieren, auch wenn von der Methylgruppe eine sterische Hinderung ausgeht. Die spektroskopischen Untersuchungen, wie UV-Vis, FT-IR, Raman-Spektroskopie und zyklische Voltammetrie, zeigen deutlich, dass wirkliche Copolymere gebildet werden und die Möglichkeit von Kompositen nicht in Betracht kommt. Das entstandene Poly(anilin-*co*-*o*-toluidin) (PAT) ist in schwach polaren Lösungsmitteln wie Chloroform löslich. Wie erwartet, sind die elektrischen Leitfähigkeiten der Copolymere viel kleiner als die Leitfähigkeit von PANI-DBSA.

Stichworte: Kolloidale Dispersionen, Spektroelektrochemie, Inverse Emulsion, Benzoylperoxid, PANI-DBSA, pre-resonanz Raman-Spektroskopie.

Abstract

Subrahmanya Shreepathi

Dodecylbenzenesulfonic Acid: A Surfactant and Dopant for the Synthesis of Processable Polyaniline and its Copolymers

An attempt has been made to improve the poor processability of polyaniline (PANI), a major drawback in the area of conducting polymers, by using dodecylbenzenesulfonic acid (DBSA), a bulky molecule containing a polar head and a long non-polar chain which functions both as a surfactant and dopant. Two different methods for the synthesis of PANI have been described in this dissertation and are discussed in two parts.

In the first part, chemical synthesis of PANI-DBSA suspensions in smaller reaction volumes (250 mL) has been described using a binary mixture of 2-propanol+water as the solvent to aid the solubility of DBSA. The micelle aided synthesis yields green dispersions which do not undergo macroscopic precipitation for more than a year. Due to excellent electrochromism of PANI, its colloidal dispersions can be directly applied in optoelectronic industry which is an added advantage of synthesizing stable PANI dispersions. Hence, a detailed study on spectroelectrochemistry of PANI-DBSA nanocolloids has been carried out which provides a better understanding of charge transfer processes between PANI colloids and electrode surfaces. UV-Vis and pre-resonance Raman spectroscopies have been used to monitor the metal-to-insulator transition of the PANI colloids induced by pH change of the medium. The shape of the colloidal particles has been investigated using transmission electron microscopy (TEM). The influence of feed ratios of DBSA to aniline on the morphology of PANI colloids has also been discussed.

In the second part of the dissertation, a new inverse emulsion polymerization technique using benzoyl peroxide, a less commonly used organic oxidant, has been described for the polymerization of aniline and its copolymers with *o*-toluidine. DBSA has been selected as dopant because it also functions as surfactant. The new inverse emulsion protocol developed yields PANI which is completely soluble in weakly polar solvents such as chloroform and a 2:1 mixture of toluene+2-propanol. A clear transparent green solution of PANI can be easily drop-, dip- or spun-coated on metallic or glass substrates. Cyclic voltammetry and spectroelectrochemical investigations were carried out to study the electroactivity, UV-Vis response and the metal-to-insulator transition of the chemically synthesized

PANI as a function of applied electrode potential. *In situ* UV-Vis spectroscopy measurements reveal good electrochromic reversibility for the polymer similar to the response of PANI synthesized electrochemically. *In situ* UV-Vis spectroscopy was also used to investigate the ease of permeability of different anions into PANI-DBSA film immersed in aqueous solution containing the anion. *In situ* electrical conductivity measurements, which are mainly employed for electrochemically synthesized polymers, have been used to monitor the change in conductivity of the chemically synthesized PANI. Electrical conductivity of the material is relatively high as the minimum resistance value is nearly 10 Ω. Pre-resonance Raman investigations have been carried out to monitor the metal-to-insulator transition of PANI induced by applied potential changes. Scanning electron microscopy has been used to investigate the influence of the feed concentration of DBSA on the morphology of the polymer. A correlation between bulk morphology and post processed nano-scale morphology has been achieved by transmission electron microscopy.

The same inverse emulsion procedure has been extended for the synthesis of poly(*o*-toluidine) (POT) and poly(aniline-*co*-*o*-toluidine)s (PATs). The efficiency of benzoyl peroxide to polymerize *o*-toluidine in the presence of DBSA has been studied. Electrochemical activity and the structural information of the polymers have been carried out using cyclic voltammetry and spectroscopic methods such as UV-Vis, Raman and FTIR. These techniques are also used to confirm the formation of real copolymers. A comparison between the solubility of PANI and POT shows unusual results where solubility of POT is less than that of PANI. Influence of morphology on physical properties of POT and co-polymers has been investigated. Spectroelectrochemical behaviors of the chemically synthesized copolymers have been studied to understand the structural/conformational differences between the chemically and electrochemically synthesized copolymers. Electrical conductivities of the copolymers, as expected, are much lower than that of PANI-DBSA. *In situ* Raman spectroscopy has been used to monitor the metal-to-insulator transition induced by the change in applied potential. All the above mentioned techniques have been used to correlate the physical properties of the copolymers with PANI and POT.

Keywords: Colloidal dispersions; Spectroelectrochemistry; Inverse emulsion; Benzoyl peroxide; PANI-DBSA; Pre-resonance Raman spectroscopy.

Die vorliegende Arbeit wurde in der Zeit von Januar 2003 bis Januar 2006 unter Leitung von Prof. Dr. Rudolf Holze am Lehrstuhl für Physikalische Chemie/Elektrochemie der Technischen Universität Chemnitz durchgeführt.

Acknowledgements

To express all that I want to say, of people who have made it possible for me to come up to this stage is a rather onerous task which I shall have to try and make the best of. I would first of all like to express my most sincere appreciation and gratitude to my supervisor **Prof. Dr. Rudolf Holze** for his timely support, advices and cooperation. I owe special thanks to Prof. Dr. M. Hietschold, Dr. S. Schulze and Mrs. G. Baumann, Institute of Physics, TU Chemnitz, Germany for their help in recording TEM and SEM images.

I am highly obliged and indebted to Prof. D. N. Sathyanarayana, Indian Institute of Science, Bangalore for introducing me to the field of conducting polymers. I would also like to acknowledge Prof. P. G. Ramappa, Prof. Siddaramaiah and Dr. H.D. Revanasiddappa, University of Mysore, India for their continuous cooperation.

I wish to express my sincere feelings to my lab mates for their help at various stages of my work and for keeping a congenial atmosphere during my stay in the department. I would like to thank Mr. Hung for performing anti-corrosion tests of my polymer samples and for his friendship. Special thanks are due to Mrs. Susanne Vogel, Ms. Susanne Mecklenburg and Ms. Evelyn Richter for the timely support both inside and outside the campus and constant encouragement.

Above all, I wish to acknowledge from the depth of my heart the untiring sacrifices made by my parents to achieve the highest degree in the field of education. I fall short of words in expressing my abounding feelings for my sister, Nagaratna, for her love and affection, understanding and patience. I warmly acknowledge the love and blessings showered by my relatives and friends.

My special thanks go to my wife Sudeshna and children for their love, cooperation, support and encouragement.

It gives me fabulous delectation to convey my thanks to all the members of ACCUMOL. Thanks are also due to Chemnitz Cricket Club (CCC) for weekend entertainments.

Last but not the least, I gratefully acknowledge DFG for research fellowship.

To my beloved parents

Table of Contents

PART I

CHAPTER 1

1   Introduction

List of Abbreviations and Symbols

B	Benzoid
CSA	Camphorsulfonic acid
CV	Cyclic voltammogram
DBSA	Dodecylbenzenesulfonic acid
DMF	Dimethylformamide
DMSO	Dimethylsulfoxide
DNNSA	Dinonylnaphthalenesulfonic acid
EB	Emeraldine base
ED	Electron diffraction
EM	Emeraldine
ES	Emeraldine salt
FTIR	Fourier-transform infrared
GCE	Glassy carbon electrode
IR	Infrared
ITO	Indium doped tin oxide
LE	Leucoemeraldine
NMP	N-Methylpyrrolidone
NP 40	Nonylphenolethoxylate
PANI	Polyaniline
PANI-DBSA	Polyaniline-dodecylbenzenesulfonate
PANI-EB	Polyaniline in emeraldine base form
PANI-ES	Polyaniline in emeraldine salt form
PAT	Poly(aniline-*co*-*o*-toluidine)
PAT-37	PAT with 3:7 molar feed ratio of aniline-to-*o*-toluidine
PAT-55	PAT with equimolar feed ratio of aniline-to-*o*-toluidine
PAT-73	PAT with 7:3 molar feed ratio of aniline-to-*o*-toluidine
PN	Pernigraniline
POT	Poly(*o*-toluidine)
POT-6	POT with DBSA-to-*o*-toluidine feed ratio of 7:1

PTSA	*p*-Toluenesulfonic acid
PVC	Poly(vinyl chloride)
Q	Quinoid
SCE	Saturated calomel electrode
SDS	Sodiumdodecyl sulfate
SEM	Scanning electron microscopy
SQR	Semiquinone radical
TBAP	Tetrabutylammonium persulfate
TEM	Transmission electron microscopy
TIP-5	Soluble PANI-DBSA with DBSA-to-aniline feed ratio of 5:1
TIP-6	Soluble PANI-DBSA with DBSA-to-aniline feed ratio of 7:1
TIP-7	Soluble PANI-DBSA with DBSA-to-aniline feed ratio of 10:1
UV-Vis	Ultraviolet-visible
w	Weak band
A	Absorbance
C_{ani}	Concentration of aniline
C_{total}	Total concentration
$E_{Ag/AgCl}$	Electrode potential (*vs* Ag/AgCl in acetonitrile)
$E_{ox,\,1}$	First oxidation peak potential
$E_{ox,\,2}$	Second oxidation peak potential
E_{SCE}	Electrode potential (*vs* SCE)
I_{pa}	Anodic peak current
I_{pc}	Cathodic peak current
λ	Wavelength
λ_0	Laser excitation wavelength
λ_{max}	Wavelength at band maximum

PART I

Chapter 1

Introduction

The evolution of conducting polymers began in 1975 with the discovery of a linear conjugated organic polymer, polyacetylene, by Shirakawa. However, the material showed metallic properties (improvement in conductivity by 9–13 orders of magnitude) only after its oxidation by iodine, which was reported two years after its discovery [1]. This gave rise to a surge of activity directed towards the exploration, synthesis and characterization of this class of material, also known as 'Synthetic Metals' [2]. These new materials combine typical properties of organic polymers such as low density, environmental stability, resistance to corrosion and low cost of synthesis with the conductivity of metals. The desirable properties of these materials can be achieved among other possibilities through engineering at the molecular level by modifying the parent monomers.

1.1 Conducting Polymers

A conducting polymer is a highly delocalized π-electron system with alternative single and double bonds in the polymer backbone. The π-conjugation of the polymer chain generates high energy occupied and low energy unoccupied molecular orbitals leading to a system that can be readily oxidized or reduced [3]. Their electronic conductivity is called intrinsic as it is caused by the presence of particular molecular structure elements which enable electric charges to move around without any added conducting materials (e.g. metals, graphite). In most of the cases, these polymers are insulators in their neutral state and they become conducting only after introduction of electron acceptors/donors by a process known as 'doping'. One should keep in mind that the term doping used in the field of conducting polymers is somewhat different from the term used in the field of conventional inorganic semiconductors. This discrepancy arises from the amount of dopant which, in some cases, may constitute up to 50 per cent of the final weight of the conducting polymer. Dopants interact with polymers by oxidizing or reducing them and do not participate in the charge transport mechanism directly. An unpaired spin is generated near the valence band or a vacancy in the conduction band is filled when an electron is removed (p-doping) or

added (n-doping) to the polymer. Out of several possible ways of doping a polymer, chemical and electrochemical doping techniques are the most widely used ones [4].

Polyacetylene, the first ever discovered conducting polymer, despite its high conductivity, is environmentally unstable. It has led to the discovery of other conducting polymers such as polypyrrole, polythiophene, polyphenylene, polyphenylenevinylene, polyaniline etc. The electrical behavior of these polymers and their derivatives is similar to that of polyacetylene. Moreover, they show higher stability and better processability [5–7]. Of all these conducting polymers, polyaniline (PANI) is now establishing itself as a novel material due its potential technological applications and low cost of synthesis [8].
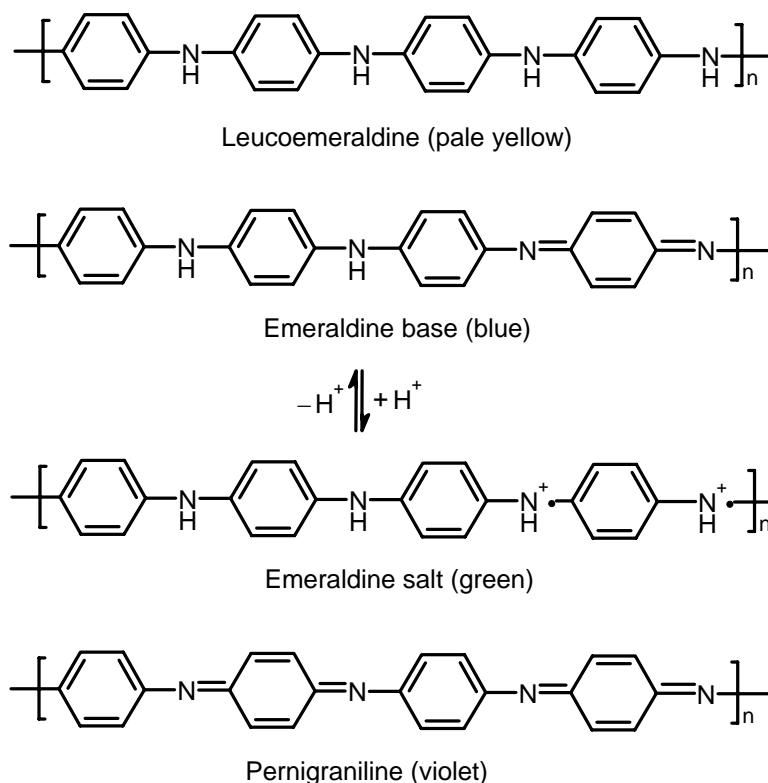
1.2 Polyaniline

PANI has been investigated extensively for over 100 years and has attracted special interest as a conducting material for several important reasons; the monomer is inexpensive, the polymerization reaction is straightforward and proceeds with high yield and PANI has excellent stability [9]. A first fairly detailed description of this product which was earlier known as 'aniline black' was provided by Green and Woodhead [10]. The later discoveries on polyaniline dealt with its electrical conductivity and other properties like electrochemical redox activity, reversible doping/dedoping, electrochromism etc. [11]. Further attention has been focused on PANI due to two prime reasons: (i) It can be synthesized easily both by electrochemical and chemical oxidation processes and (ii) it shows a particular sensitivity to the proton activity of its environment [12].

1.2.1 Structure of Polyaniline

Green and Woodhead [10, 13] were the first to depict PANI as a chain of aniline molecules coupled head-to-tail at the *para* position of the aromatic ring. They have proposed a linear octameric structure for PANI. Polyaniline, a typical phenylene based polymer, has a chemically flexible –NH– group[*] in the polymer chain flanked by phenyl rings on either sides. The diversity in physicochemical properties of PANI is traced to the –NH– group. The difference in the composition of amine and imine segments of PANI generates several oxidation states of this material ranging from completely reduced leucoemeraldine

---

[*] The –NH– group is chemically flexible because it is sensitive to the pH of the medium and the counter ions used in the synthesis. Depending on the nature of the protonating medium, the physicochemical and the electronic properties of the PANI vary.

to completely oxidized pernigraniline states as shown in Scheme 1.1. The different forms of PANI can be readily converted to one another by simple redox methods (Scheme 1.2; Page 17). Out of several possible oxidation states, the 50 % oxidized emeraldine salt state shows electrical conductivity [4].

Leucoemeraldine (pale yellow)

Emeraldine base (blue)

$-H^+ \Updownarrow +H^+$

Emeraldine salt (green)

Pernigraniline (violet)

Scheme 1.1. Various possible oxidation states of polyaniline.

1.2.2 Doping in Polyaniline: Acid Doping

Doping in most of the known conducting polymers is achieved by partial oxidation or partial reduction of the π-system of the polymer which leads to either increase or decrease in the number of electrons associated with it [4]. The uniqueness of PANI arises from the sensitivity of its emeraldine oxidation state (EM) towards the pH which yields emeraldine base (EB) and emeraldine salt (ES) forms of PANI. An interesting feature of PANI arises from the fact that the non-conducting EB form of PANI can be doped to a highly conducting regime (ES) without changing the total number of electrons associated with it [9]. Such a doping is achieved by a simple protonation of the –NH group of EB by mineral or organic protonic acids and is known as 'acid doping' (Scheme 1.2). The acid

doping process increases the conductivity of PANI by more than eight orders of magnitude [14]. Positive charges accumulated on the polymer backbone during protonation of PANI are neutralized by the negatively charged counter ions of the dopant. The protonation is also accompanied by the drastic change in the electronic structure, crystallinity, solubility, etc. [4]. The degree of protonation and the resulting conductivity can be readily controlled by changing the pH of the dopant acid solution. Inorganic mineral acids such as HCl, H_2SO_4, etc. are the most frequently used dopants but the metallic PANI produced, in most of the cases, is completely insoluble. More details about the solubility of PANI are discussed in Section 1.2.7.
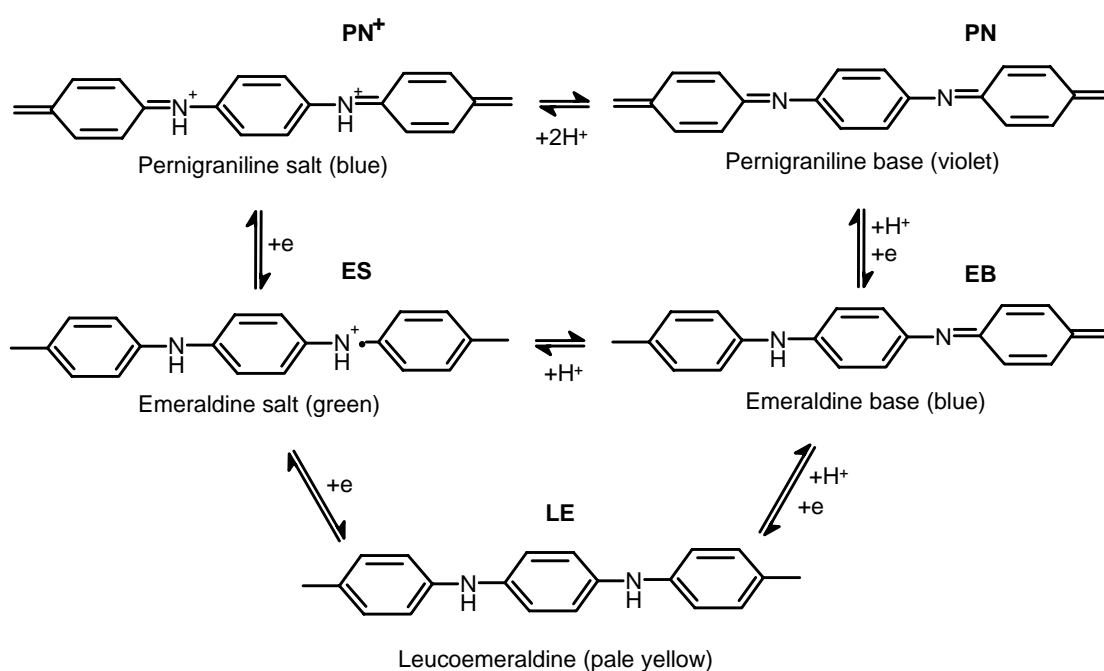
Scheme 1.2. Interconversion of different oxidation states of polyaniline *via* redox procedure.

1.2.3 Synthesis of Polyaniline

There are two principal methods for the synthesis of PANI. The first one is the direct oxidation of aniline by chemical oxidants and the second way is through electrooxidation on an inert electrode.

1.2.3.1 Chemical Synthesis

PANI–ES can be easily obtained as dark green powder by polymerization of aniline in aqueous media using oxidizing agents such as ammonium persulfate, potassium iodate,

hydrogen peroxide, potassium dichromate etc. [15]. The main advantage of chemical synthesis is its ease and capability to produce large volumes of PANI in good yield. The reaction is mainly carried out in acid medium at pH between 0 and 2. The concentration of the monomer employed varies between 0.01 and 1 **M**. Generally, a stoichiometric equivalent of oxidant is used to avoid degradation of the polymer [15]. Oxidative chemical polymerization is generally carried out at low temperatures (–15 to 5 °C) in order to obtain PANI with high molecular weight. One of the disadvantages of this method stems from the experimental observation that an excess of the oxidant and higher ionic strength of the medium leads to materials that are essentially intractable.

In a typical synthesis, aniline (0.1 **M**) is dissolved in 1 **M** solution of protonic acid such as HCl, H_2SO_4, $HClO_4$, etc. and is cooled to 0–5 °C. A precooled solution of the oxidant (0.1 **M**) with or without protonic acid is added drop-wise with continuous stirring for 20–30 minutes. After about 10–15 minutes, the solution gradually develops a green tint. The dark green/blue-green precipitate (ES) formed after 6 h is filtered, washed with excess of dilute acid and then with organic solvents and dried in vacuum for 48 h. Polyemeraldine base (EB) can be obtained by stirring the ES powder in 0.05 **M** solution of NH_4OH for 10–12 h. The dark blue powder of EB is further washed with 0.05 **M** NH_4OH and dried under vacuum.

Several other methods such as emulsion polymerization, dispersion polymerization, interfacial polymerization, and so forth are also available for the polymerization of aniline by chemical means. The possible polymerization routes and availability of list of oxidants have been thoroughly reviewed in the literature [4, 15, 16].

1.2.3.2 Electrochemical Synthesis

The anodic oxidation of aniline is generally carried out on an inert electrode material which is usually platinum. However, other electrode materials such as iron, copper, zinc, lead, etc. have also been used [15]. Polymerization of aniline is carried out in a three electrode single compartment or H–cell containing aqueous acidic solution of aniline. The two mainly employed electrochemical routes are galvanostatic and potentiostatic modes. In the latter case, potential can be fixed (E_{SCE} = 0.7–1.2 V) or cycled (in the range of E_{SCE} = – 0.2 to 0.7–1.2 V). A more homogeneous product is obtained when PANI is synthesized *via* potential cycling [15]. The anodic oxidation is normally carried out in an inert atmosphere at ambient temperature. For many conceivable applications, deposition of the polymer as a

thin film or thick coating is desirable which can be easily achieved using electrochemical polymerization.

1.2.4 Polymerization Mechanisms

The wide variety of methods employed for preparation of PANI leads to products whose nature and properties differ greatly. The mechanism and kinetics of PANI formation has been extensively studied for the identification of the intermediates and the steps involved. This knowledge is essential to correlate the relationships between possible reaction pathways and properties of the polymeric products [12]. Information concerning the mechanism of PANI formation has invariably been gathered with the aid of electrochemical methods. Various polymerization mechanisms and electrochemical aspects of the formation of PANI have been proposed by different authors depending on the protocol used in the synthesis of PANI and have been reviewed in detail [12, 15].

The polymerization reaction is a self-catalyzing reaction and obeys the law: $i/nFA = K_C$, where K_C is the autocatalytic rate constant and has a value of ~0.47 s^{-1} for a 140 nm thick PANI film [17]. The most accepted first step in the reaction mechanism is the formation of a radical cation which is resonance stabilized by several canonical forms and is represented in Scheme 1.3.
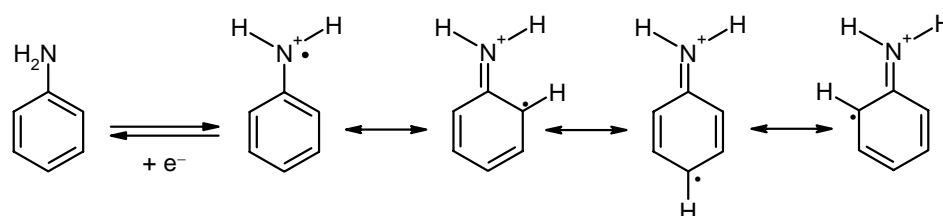
Scheme 1.3. Formation of radical cation and its resonance stabilized canonical forms.

Mohilner and coworkers [18] were the first to predict that in H$_2$SO$_4$ medium (pH 2–5), the oxidation of aniline is an ECE reaction, i.e., a succession of rapid electrochemical-chemical-electrochemical reactions, mainly resulting in *para*-coupled chains. However, *para*-coupling is not exclusive; radical coupling at the *ortho* position may lead to low yields of other products [15]. The first reaction intermediate can undergo further oxidation or it can react with a free monomer. Based on fast scan cyclic voltammetry results, Yang

and Bard [19] deduced a dimer (*p*-aminodiphenylamine) as a first intermediate product (Scheme 1.4).
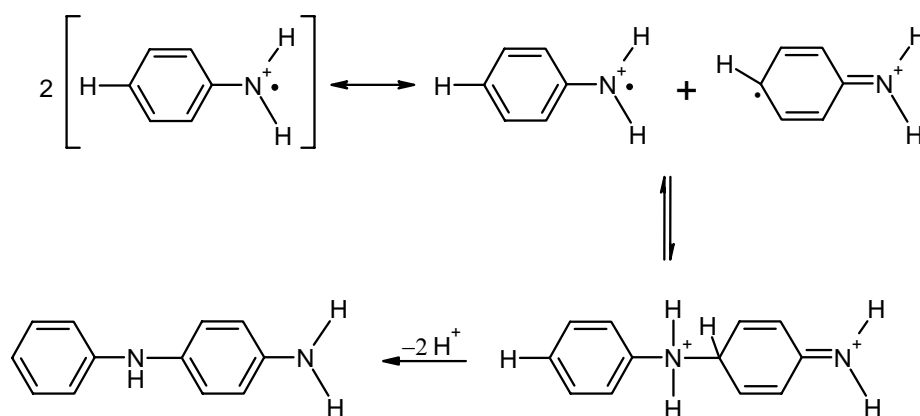
Scheme 1.4. Formation of *p*-aminodiphenylamine from the monomeric radical cation.

The next steps in the polymerization of *p*-aminodiphenylamine are rapid and Mohilner *et al.* [18] proposed that the process occurs by formation of a tetramer, and then octamer, which polymerizes even further resulting in a polymer whose structure is that of emeraldine. The polymerization mechanism is characterized as 'autocatalytic' because electrooxidation of the oligomers occurs at less positive potentials than that of aniline monomer. Such an autocatalytic effect is observed only in aqueous solutions of considerable acidity [12].

1.2.5 Mechanism of Conductivity

The electrical conductivity of doped conducting polymers can be varied up to metallic state in the range of more than ten orders of magnitude. Charge transport in these polymers has been extensively investigated but still remains poorly understood [4]. The conjugation arising from chemical unsaturation of the carbon atom in conducting polymers is the main cause for charge transport. The presence of localized electronic states of energies less than the band gap arising due to the changes in the local bond order have lead to the possibility of new types of charge conduction phenomenon in these conjugated polymers [4]. All conducting polymers have intrinsic topological defects which are introduced during polymerization and their ground states are non-degenerate. Removal of a charge from the valance band generates a radical cation whose energy lies in the band gap. In solid

state physics, such a radical cation which is partially delocalized over some polymer segments is called a 'small polaron'. It stabilizes itself by polarizing the medium around it and hence its name. Formation of polaron is associated with the distortion of lattice and the presence of two localized electronic states in the gap. According to the model proposed by Brazovski-Kirova [20], formation of a polaron leads to the possibility of three new optical transitions (Figure 1.1).

VB = valence band; CB = conduction band
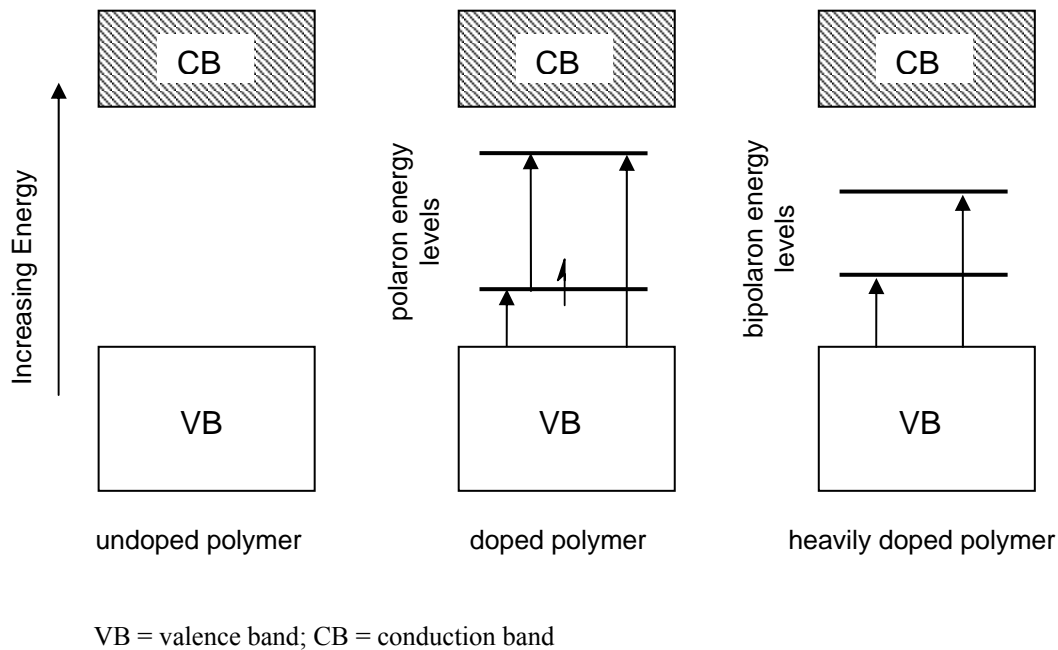
Figure 1.1. Illustration of energy levels and allowed transitions of polarons and bipolarons.

When a second electron is removed from the system, it may come from either a different segment of the polymer chain creating another polaron, or from the first polaron to generate a dication which, in solid state physics, is referred to as a bipolaron (Figure 1.1). A bipolaron is also associated with structural deformation and the two charges are not independent but act as a pair. Application of an external electric field makes both polaron and bipolaron mobile *via* the rearrangement of conjugation.

In the case of PANI, the charged species are formed during protonation of the polymer, which are subsequently responsible for the increase in conductivity [21]. Several other mechanisms are also proposed for the conductivity of PANI. Salaneck and coworkers [22, 23], based on temperature dependent conductivity studies, have proposed a one-dimensional variable range hopping or three-dimensional fluctuation-induced tunneling models.

1.2.6 Characterization of Polyaniline

Polyaniline synthesized either chemically or electrochemically is characterized by several physicochemical techniques as discussed below.

1.2.6.1 Elemental Analysis

The basic characterization tool used in synthetic chemistry is elemental analysis which gives elemental composition of the sample material. Generally, elemental analysis gives percentage weight (wt %) of carbon, hydrogen, nitrogen and sulfur present in the sample which can be used to calculate the stoichiometry of the sample. When sulfuric acid or organic sulfonic acids are used as dopants, elemental analysis can be used to estimate the extent of doping in the PANI chain.

1.2.6.2 UV-Visible Spectroscopy

As mentioned in the previous sections, different oxidation states of PANI have different color which makes UV-Vis spectroscopy a useful technique for characterization of PANI. The sensitivity of PANI to pH of a medium is also reflected by the color change and can be easily traced using this spectroscopy. Electronic absorption spectra of electrochemically deposited film of PANI or PANI dissolved in a suitable solvent gives qualitative information about the level of doping, extent of conjugation and the presence of radical cations in the polymer. The conductor-to-insulator transition arising from the change in pH of the medium can be clearly monitored. Further, *in situ* UV-Vis spectroscopy as a function of applied potential helps to understand the interconversion of different oxidation states of PANI and allows correlating the electrical conductivity with the observed change in the absorbance values. In some cases, electronic absorption spectroscopy can also be used to trace the kinetics of aniline polymerization [12]. Interaction of the solvent with PANI in which it is dissolved can also be studied by this method.

1.2.6.3 Fourier Transform Infrared (FTIR) Spectroscopy

Structure of PANI has been elucidated using this vibrational spectroscopic tool [15]. Formation of the intermediate product of polymerization has also been characterized using this technique. FTIR spectroscopy of PANI reveals that PANI is formed by 1,4-

coupling of aniline monomers and eliminates the possibility of formation of *ortho* coupled product to a considerable extent [15]. One can gain information about the presence of the bands corresponding to both imine and amine type of rings in emeraldine state of PANI. Formation of copolymers, presence of a functional group on the polymer backbone or change in the protonation-deprotonation equilibrium of emeraldine can be deduced from the presence of corresponding bands in the FTIR spectrum.

1.2.6.4 Raman Spectroscopy

Raman spectroscopy is used as a complementary technique to infrared spectroscopy. It provides definite structural characterization of PANI because of the characteristic dependence of the Raman spectral pattern on the disposition of the ring constituents of aromatic compounds. The advantage of Raman spectroscopy arises from the resonance enhancement of the Raman signals. Presence of several optical transitions in the UV-Vis spectrum of PANI leads to the use of different laser excitation wavelengths to enhance the intensity of the scattered signals. When the laser excitation wavelength matches with one of the band maxima in the UV-Vis spectra, the intensity of the scattered light is strongly increased. This is called 'resonance enhancement' [24]. The enhancement of the intensity of Raman signals is also possible when the laser excitation wavelength lies in the longer or shorter wavelength wing of an electronic absorption band and is called as 'pre-resonance enhancement' [25, 26]. Raman spectroscopy when coupled to electrochemistry (Raman spectra as a function of applied potential) allows monitoring of the metal-to-insulator transition arising due the change in the oxidation state of PANI. Thus, an *in situ* coupling is useful in the structural study of complex multichromophore materials like PANI. Information on each chromophore can be obtained separately by proper choice of exciting wavelength.

1.2.6.5 Cyclic Voltammetry

Cyclic voltammetry is a powerful electrochemical tool to gain information about the electrochemical behaviors and interconversion of oxidation states of PANI. It has not only been used to characterize PANI but also to synthesize PANI. Kinetics of aniline polymerization can be deduced with this technique. The peaks in the cyclic voltammogram (CV), which are ascribed to the electrochemical responses of PANI, give clear knowledge

of the charge injected during interconversion of any two oxidation states of PANI. Effect of different anions in the supporting electrolyte or polymerization medium on the conductivity or morphology of PANI can also be studied using cyclic voltammetry.

1.2.6.6 In Situ Conductivity Measurements

Most conductivity measurements reported in the literature were made *ex situ* with samples prepared and doped chemically [4]. Usually, the conductivity measurements of PANI are performed on pressed pellets using constant currents applied to the samples; the measured voltage drop across the sample in a two- or four-probe arrangement corresponds to resistance of the sample. A new, much easier to handle, *in situ* electrochemical conductivity technique using a two-band electrode has been developed in our laboratory [27]. This technique has been frequently used for electrochemically synthesized conducting polymers. The advantage of this *in situ* measurement is that the change in resistance values on changing the oxidation state of PANI can easily be monitored. In this dissertation, *in situ* measurements are performed on chemically synthesized PANI to monitor the change in resistance upon electrochemical doping.

1.2.6.7 Scanning Electron Microscopy

It is well established that morphology of the polyaniline film synthesized electrochemically or bulk PANI powder synthesized chemically strongly influences the properties of PANI [15]. In most cases, morphology of PANI has been investigated using SEM. The wide range of magnification makes it suitable for investigation of microstructures and sometimes nanostructures of PANI. With the help of SEM images, one can correlate the electrical conductivity, crystallinity, mechanical properties, etc. of PANI with its surface morphology.

1.2.6.8 Transmission Electron Microscopy

The high resolution of the transmission electron microscope makes it a useful characterization technique for determination of nanostructures of PANI. Conducting polymers have significant contribution in the area of nanotechnology as active components of nanoscale molecular electronic devices. Hence, investigation of nanostructures of PANI is essential and can be done with transmission electron microscopy. The additional information

gained from this technique is the crystal structure of PANI deduced from electron diffraction pattern of nanoparticles.

1.2.7 Solubility of Polyaniline

Solubility of PANI has gained special importance, both scientifically and commercially. Scientifically, it provides a medium more conducive to the production of well reproducible analytical data, especially in the determination of molecular weight which helps in elucidating molecular configuration and structure in the conducting and insulator states. In commercial applications, solutions of PANI enhance its applicability in manufacturing technological devices [2]. Most electrically conducting polymers are insoluble in their doped, conducting state [28]. The chemically synthesized green-black ES form of PANI is also insoluble in common organic solvents thereby exhibiting poor processability [29]. Heeger [9], in his Nobel review article, reported that discovery of PANI was a breakthrough in overcoming the processability problems of conducting polymers. However, he quoted that high molecular weight PANI could not be processed into useful objects and devices. PANI cannot be melt processed like conventional thermoplastic polymers because it is unstable at melt process temperatures [30].

In 1999, Wessling [31] showed that solubility of PANI is governed by its basic thermodynamic properties like unmoldability, unfavorable entropy of dissolution and the extremely high lattice energy (ca. 1,100 KJ mol^{-1}). In another work, the poor solubility of PANI as reported by Gregory [32], is due to non-availability of suitable solvents which can simultaneously dissolve both the hydrophilic dopant part and the hydrophobic organic part of the polymer. However, the non-metallic EB form of PANI exhibits partial solubility in N-methyl-2-pyrrolidone (NMP) [33], dimethylsulfoxide (DMSO) [34–36] and dimethylformamide (DMF) [18]. In the last two decades, much attention has been paid to improve the solubility of PANI and thereby its processability. Several methodologies have been developed to improve the processability of PANI. These include the use of substituted anilines as monomers, use of suitable anionic dopants which favor dissolution, synthesis of blends and composites of PANI with conventional thermoplastics, copolymers of aniline with its derivatives, dispersions of PANI and so forth which are briefly discussed below.

1.2.8 Poly(Substituted Anilines)

Solubility of PANI can be improved by polymerizing a derivative of aniline, particularly by choosing the substituent which has solubilizing effect. The substituents used to modify the solubility of polyaniline range from alkyl [37], alkoxy [38] groups to phosphonic [39] and sulfonic acid [40] groups. These substituted polyanilines, especially those with acid substituent groups were found to be more soluble, some of them being water soluble and also showing higher thermal stability. Polymerization of substituted anilines, like their parent monomer, can also be carried out either chemically [41] or electrochemically [42]. The major drawback of these ring substituted PANIs is the fact that solubility is achieved at the cost of conductivity [43].

1.2.9 Functionalized Protonic Acid as Dopant

Cao, Smith, and Heeger [44] in 1992 used functionalized protonic acids to convert PANI into the metallic form and, simultaneously, render the resulting PANI complex soluble in common organic solvents. The functionalized counter ion acts like a 'surfactant' in that the charged head group is ionically bound to the oppositely charged protonated PANI chain, and the 'tail' is chosen to be compatible with nonpolar or weakly polar organic liquids [9]. This approach is also known as 'counter-ion-induced processability'. More details regarding this approach will be provided in the second part of the dissertation.

1.2.10 Blends of Polyaniline

A physical mixture of two or more polymers with different chemical compositions is known as 'blend'. Progress in the processability of PANI resulted in the fabrication of several types of conductive blends of PANI [45, 46]. The main idea behind the synthesis of blends is to introduce flexibility and toughness to PANI thereby making it melt processable. A phase separation between the two components of the blends leads to drastic loss in the mechanical strength of the material [47]. However, by keeping the PANI composition (wt %) less than 16 %, materials with good flexibility can be obtained [46]. Several conductive blends of PANI salt with thermoplastic polymers such as polystyrene [48], poly(vinyl chloride) [49], polyamides [50], poly(vinyl alcohol) [51], and so forth have been extensively studied.

1.2.11 Copolymers

Copolymerization is generally carried out to combine the diverse physicochemical properties of different polymers to a single polymeric system. As described in the preceding sections, mere homopolymerization of substituted anilines drastically reduces the conductivity of the polymer. Copolymerization of aniline with ring or N-substituted anilines leads to polymers which have conductivity like PANI and solubility of substituted anilines [52–54]. More details about copolymers will be described in the second part of the dissertation.

1.2.12 Polyaniline Dispersions

Dispersion polymerization is a well known technique in conventional polymer synthesis for the preparation of polymer particles in both aqueous and non-aqueous media [55, 56]. The benefits of dispersion polymerization (also known as suspension polymerization) over bulk polymerization include ease of temperature (and hence, reaction) control and the formation of a directly usable product. One of the widely used and technologically important ways of tackling the problem of poor solubility of PANI is synthesis of its colloidal dispersions [57]. Dispersions of PANI, which can be applied in place of true solutions, are also used in the synthesis of blends of PANI with commodity polymers [58]. Dispersions of PANI have been studied extensively during the past decade because they can be used directly in commercial applications such as electromagnetic shielding materials, sensors, electrooptics, and light-emitting diodes [59].

1.2.12.1 Polymer Stabilized Polyaniline Dispersions

Generally, PANI in colloidal form or as suspension is synthesized by chemical polymerization of aniline in the presence of various polymeric steric stabilizers such as methyl cellulose [60], carboxymethyl cellulose [57], poly(vinyl alcohol) [61], poly(vinyl methyl ether) [62], poly(ethylene oxide) [63], poly(N-vinylpyrrolidone) [61], etc. Armes and coworkers [64] have synthesized colloidal PANI by chemical grafting of PANI onto several tailor made copolymer surfactants. In such polymer-stabilized PANI dispersions, the monomer (aniline) is soluble in the reaction medium whereas the resulting polymer (PANI) is insoluble and its macroscopic coagulation is prevented by steric stabilizers [65]. The possible synthetic routes and the properties of PANI colloids have recently been re-

viewed by Stejskal [66]. The size and morphology of the colloidal particles strongly depend on the steric stabilizer, oxidizing agent and reaction conditions [67]. However, the use of polymeric stabilizers drastically lowers the electrical conductivity of PANI.

1.2.12.2 Role of Surfactants

The chemical polymerization of aniline in well-organized systems such as micelles not only accelerates polymerization but also yields PANI with relatively high molecular weight [68]. Such acceleration was also observed during the electropolymerization of aniline in the presence of sodiumdodecyl sulfate (SDS) because of a higher local concentration of aniline in the reaction medium [69]. Surfactants like SDS were also used in the synthesis of colloidal PANI dispersions [68, 70, 71]. Kuramoto *et al.* [68] have synthesized HCl doped PANI dispersions in SDS micelle medium and the conducting polyemeraldine in the dispersions was stable up to pH = 8. Recently, Hassan *et al.* [67] reported that both micelle size and monomer concentration influence the size of the polymer particles when polymerization is carried out using SDS as a surfactant. In a micelle-aided polymer synthesis, the reaction takes place mainly at the micelle-water interface and the micelles are in dynamic equilibrium with surfactant monomers in the solution. The intermediate products of polymerization have increased hydrophobicity due to poor solubility in water; therefore, they are readily incorporated into micelles. In the end, polymer particles are stabilized by adsorbed and incorporated SDS molecules through electrostatic repulsive interactions [71].

1.2.12.3 Role of Bulky Organic Acids

Cao *et al.* [44] reported for the first time that functional protonic acids such as camphorsulfonic acid (CSA) and dodecylbenzenesulfonic acid (DBSA) increase the solubility of PANI in common organic solvents. Thereafter, the synthesis of PANI using organic acids as dopants has gained special attention [72, 73]. DBSA, being a bulky molecule, can act both as a surfactant and dopant; therefore, several researchers have attempted the synthesis of PANI-DBSA suspensions in the last few years [69, 74–76]. CSA was also used in the electrochemical synthesis of PANI colloids by pumping the electrolyte solution into an anodic chamber which was separated from cathodic chamber by an ion-exchange membrane [77]. Kuramoto and Tomita [69] have synthesized stable PANI-DBSA suspensions in water using ammonium persulfate as oxidant but the exact reaction volumes are not defined.

Haba *et al.* [75] have observed that in the initial stages of polymerization of aniline-DBSA complex, agglomerates containing spherical PANI particles are formed whereas in the later stages the voids between these particles are filled, forming a smooth surface of PANI ag-glomerates. Non-aqueous microgel-coated PANI-DBSA colloids show core-shell mor-phology composed of a cross-linked acrylic core and PANI-DBSA shell [76]. The effects of aniline-to-oxidant mole ratio, DBSA concentration, temperature, period of polymeriza-tion on the kinetics, yield and conductivity of the PANI-DBSA colloids have been exten-sively investigated [74, 75].

1.3 Aim and Scope of the Work

As mentioned in the preceding sections, doping of PANI with DBSA not only im-proves the solubility but also yields PANI with high conductivity and good yield. The main advantage of using DBSA in the synthesis of colloidal PANI is that it does not require any additional surfactant or steric stabilizer. Generally, PANI-DBSA suspensions are obtained by polymerization of aqueous dispersion of anilinium-DBSA complex. Solid DBSA has very low solubility in water and, therefore, the white turbid dispersion of anilinium-DBSA complex is prepared by mixing aniline and DBSA in large volume of water (~1 *l*) for more than 3 hours [75]. Hence, additional attention is necessary to prevent air oxidation of ani-line during such a long period of mixing. Small scale synthesis of dispersions of PANI-DBSA is hindered by larger reaction volumes associated with the formation of anilinium-DBSA complex. Recently, Han *et al.* [72] have shown that formation of turbidity can be avoided using a mixture of 2,2,4-trimethylpentane, isooctane and water. Hence, use of a secondary solvent, which has lower dielectric constant than water as well as high miscibil-ity in water will open a new way towards the small scale synthesis of DBSA doped colloi-dal PANI.

The basic aim of this work is to develop a new small scale synthetic route for the polymerization of aniline in presence of DBSA which yields a highly stable colloidal PANI dispersion. A significant decrease in the reaction volumes of formation of complex has been achieved by using a binary mixture of 2-propanol+water. It is also interesting to study the influence of feed ratios of DBSA to aniline on the morphology, particularly the shape and size of PANI particles, of the dispersions. The shape of the colloidal particles was studied with TEM. PANI is well known for its electrochromism as evidenced by plenty of reports on electrochromic behaviors of electrochemically synthesized or post-processed

PANI films [78, 79]. However, voltammetric responses of PANI colloids have not been reported. In this dissertation, a detailed study of spectroelectrochemistry of PANI-DBSA nanocolloids has been carried out which provides a better understanding of charge transfer processes between PANI and electrode surfaces. UV-Vis and pre-resonance Raman spectroscopies are used to monitor the metal-to-insulator transition of the PANI colloids

Chapter 2

Experimental

2.1 Chemicals

Aniline (VEB Laborchemie Apolda, analytical grade) was distilled under reduced pressure and stored under nitrogen. DBSA (70 wt % in 2-propanol, 70% solution, Aldrich) and ammonium persulfate (Aldrich) were used as received. Deionized water (Seralpur pro 90 C) was used in the synthesis and for all other purposes. All other chemicals were analytical grade and were used as received. Indium doped tin oxide (ITO)-coated glass sheets ($R = 20$ Ω cm^{-2}) used in spectroelectrochemical studies were supplied by Merck.

2.2 Synthesis of PANI-DBSA Colloidal Dispersions

The reaction sequence involved in the formation of anilinium-DBSA complex and its polymerization is described in Scheme 2.1 (see next page). In a typical experiment, 11.7 mL of DBSA (70 wt % in 2-propanol) (0.1 **M**) and 13.3 mL of 2-propanol were added to 200 mL of deionized water taken in a 500 mL conical flask. 0.23 mL of aniline (0.01 **M**) was added to the above mixture followed by 25 mL of 0.01 **M** ammonium persulfate. The reaction mixture was kept under mechanical stirring for 24 h. Nearly 45–50 minutes after the addition of the oxidant, the colorless homogeneous solution slowly turns to blue and then to dark green. In the end PANI-DBSA suspensions were obtained as a stable dark green solution and a part of the dispersion was stored without further purification for investigations. The above suspension (170 mL) was poured into a 500 mL beaker containing 250 mL of methanol and the mixture was kept undisturbed for 10 h. The precipitated polyaniline was filtered, washed several times with water and dried in an oven at 45 °C for 24 hours.

Polyaniline-DBSA dispersions with different mole ratios of DBSA to aniline (2:1, 3.3:1, 5:1, 10:1 and 20:1) in the feed were synthesized in a similar fashion. Codes assigned to the different dispersions are given in Table 2.1.
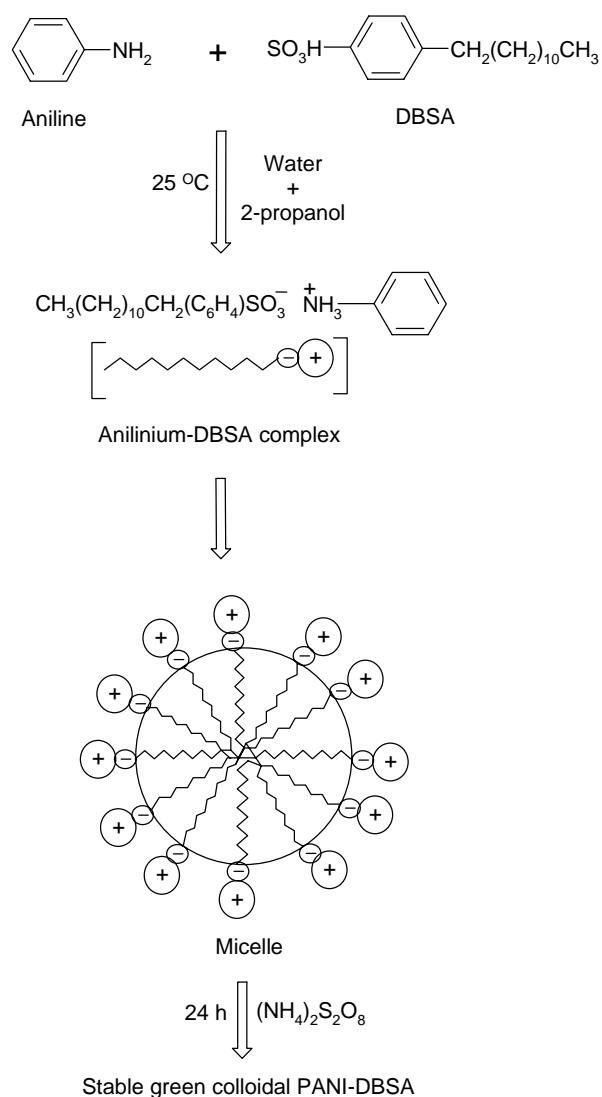
Scheme 2.1. Reaction scheme for the polymerization of aniline by formation of micelles.

Table 2.1. Feed concentrations of the reactants, DBSA-to-aniline feed ratios and codes assigned to different PANI-DBSA dispersions.

Sl No.	Aniline (**M**)	DBSA (**M**)	$(NH_4)_2S_2O_8$ (**M**)	[DBSA]/[Aniline]	Sample code
1	0.05	0.1	0.05	2	PANI–1
2	0.03	0.1	0.03	3.3	PANI–2
3	0.02	0.1	0.02	5	PANI–3
4	0.01	0.1	0.01	10	PANI–4
5	0.005	0.1	0.005	20	PANI–5a
6	0.005	0.05	0.005	10	PANI–5d
7	0.005	0.025	0.005	5	PANI–5e

2.3 Characterization

UV-Vis spectra were recorded on a Shimadzu UV-2101PC spectrophotometer. Quartz cuvettes with a 1 cm path length were used to record the spectra of the dispersions. *In situ* UV-Vis spectra of thin layers of dispersions at different applied potentials were recorded using a special home built set up (Figure 2.1) [80, 81]. A thin layer of the PANI dispersion is formed when a sheet of ITO-coated glass and a glass sheet separated by Teflon tape were dipped into a pool of dispersion fitted with a platinum wire as a counter electrode and a salt bridge connected to a saturated calomel (SCE) reference electrode. Sheets of ITO-coated glass and glass dipped into deionized water were used in the reference compartment. The radiation beam passes through the active layer of the dispersion formed between the ITO glass and glass sheet only. *In situ* measurements were carried out under ambient conditions without any additional electrolyte and the potential was increased in steps of 100 mV starting from $E_{SCE} = -0.4$ to 1.4 V. UV-Vis spectra were recorded five minutes after applying each potential.
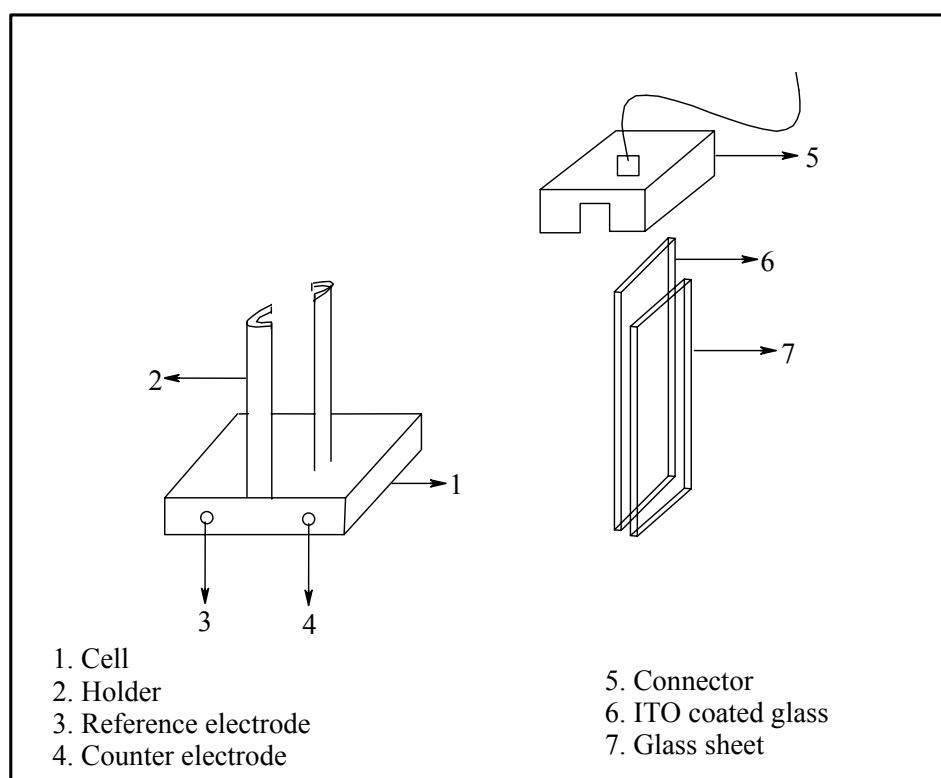

1. Cell
2. Holder
3. Reference electrode
4. Counter electrode

5. Connector
6. ITO coated glass
7. Glass sheet

Figure 2.1. Home built set-up for *in situ* UV-Vis spectroelectrochemical measurements of thin layers of PANI-DBSA dispersions.

Raman spectra of the liquid samples were measured on an ISA 64000 spectrometer equipped with a liquid-nitrogen-cooled CCD camera detector at a resolution of 2 cm^{-1}. Samples of different pH values, taken in a glass capillary, were illuminated with 476.5 nm laser light from a Coherent Innova 70 argon ion laser.

TEM images were recorded on a Philips CM 20 FEG transmission electron microscope. The samples were prepared by depositing a drop of well-diluted PANI suspension onto a carbon (1 0 0)-coated copper grid and dried in an oven at 55 °C for two hours. Elemental analysis was performed using an elemental analyzer (Vario EL; Elementar Analysen Systeme GmbH, Hanau). PANI-DBSA powders obtained by precipitating PANI dispersions were used in elemental analysis.

Chapter 3
Results and Discussion

A mixture of 2-propanol+water and DBSA dissolved in 2-propanol has been used for the synthesis of PANI-DBSA colloidal dispersions to minimize the period of mixing of DBSA with aniline and the total reaction volume. Generally, alcohols are better media for PANI dispersions because they facilitate the adsorption of PANI particles on the steric stabilizer [82]. The synthesis of PANI-DBSA colloids was carried out at different feed ratios of DBSA/aniline; however, stable dispersions (stable for more than a year) were formed only when the mole ratio is greater than 3.33. Below this mole ratio, reaction mixtures became a thick paste that nevertheless can be diluted to form a stable dispersion. All dispersions were synthesized above the critical micelle concentration for DBSA, which in water is $\sim 8.4 \times 10^{-3}$ **M** [83]. The dispersions were characterized by different techniques without purification in order to study the behavior of PANI particles in the presence of ionic byproducts. PANI-DBSA particles in the above synthesized dispersions do not sediment even after centrifugation at 15 000 rpm for 1 h.

3.1. Polymerization Process

Electronic absorption spectroscopy was used to observe the changes during polymerization of aniline. UV-Vis spectra of the reaction mixture were recorded soon after the addition of the oxidant up to 5 h of polymerization. The later stage of polymerization was also traced by UV-Vis spectroscopy but the spectra are recorded at larger time intervals (100 min). There was no color change in the reaction mixture during the initial few minutes (induction period) as confirmed by the absence of any band in the UV-Vis spectra. Polymerization of aniline progresses very quickly after the induction period and the clear transparent reaction mixture turns blue and finally dark green [68]. The induction period duration depends on the concentration of aniline in the feed; it is shorter at higher feed concentrations of aniline. For example, when the concentration of aniline in the feed is 0.03 **M**, the reaction is initiated after 25 min, whereas, an induction period of 60 min is observed at a concentration of 0.005 **M** aniline.

The UV-Vis spectrum of chemically synthesized PANI-salt dissolved in solvents such as DMSO generally exhibits three bands at 730–800 nm, 430 nm (both originating from polaron transitions) and 350 nm ($\pi^* \leftarrow \pi$ transition) [84]. These three transitions are also present in PANI dispersions, however, their positions are shifted depending upon the synthetic route, dopants and solvents employed. Figure 3.1 shows the growth of the band at 670–750 nm of PANI–5a during polymerization. After the induction period, a band at 680–690 nm appears before the bands at 350 and 430 nm and its position is blue shifted by 10–15 nm for the first few minutes indicating generation of PANI in completely oxidized per-nigraniline state that later on is transformed into the emeraldine state [75]. The absorbance value at the band maximum of the band at 670–750 nm increases by 2–3 orders of magnitude, reaching a constant value in just 2 to 3 minutes after the induction period [85] (Figure 3.1).
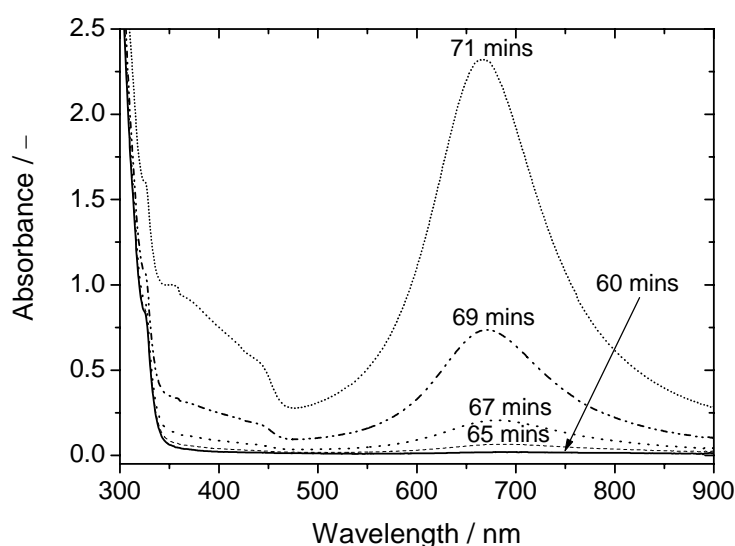

Figure 3.1. UV-Vis spectra of reaction mixture recorded during polymerization of anilinium-DBSA complex (PANI–5a).

A few minutes after the induction period (7–12 min), with increase in the polymerization time, the band at 700 nm shifts into the red indicating an increase in conjugation length of the polymer backbone (Figure 3.2). The area of all of the bands increases during the polymerization. The band in the region of 670–700 nm attains a constant position (750–770 nm) approximately 3 h after the addition of ammonium persulfate irrespective of the concentration of aniline in the feed (Figure 3.2). This indicates that the polymerization reaction is completed 3 h after the addition of oxidant. Similar results were observed by

Svelko *et al.* [83] during the polymerization of aniline in the presence of various surfactants.
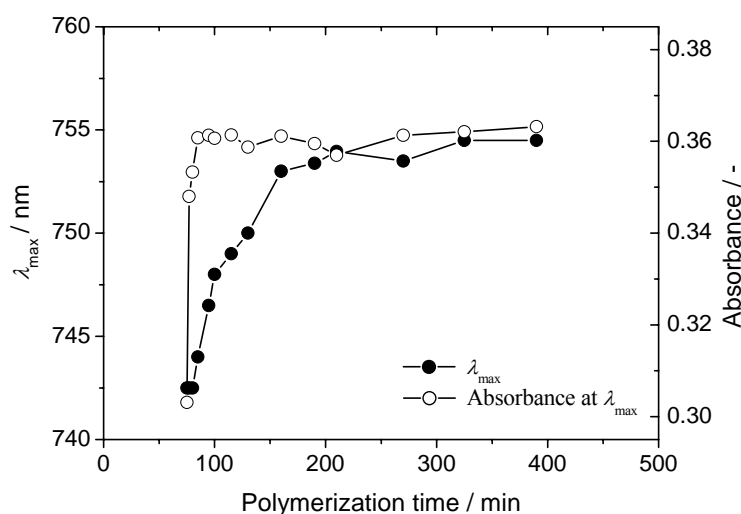

Figure 3.2. Changes in the position and absorbance of the band at 670–770 nm with respect to polymerization time.

3.2 Elemental Analysis

Elemental analysis was carried out for PANI-DBSA powder obtained after precipitation and washing of the dispersion. N/S ratios obtained from elemental analysis were used to calculate the extent of doping (%) of the polymer. Elemental composition and doping percentage for all solid PANI-DBSA samples are given in Table 3.1 (Page 38). It is clear from the table that doping of the polymer backbone increases with increasing feed ratios of DBSA/aniline. Higher doping at higher DBSA/aniline mole ratio is due to the strong complexation of DBSA with the PANI backbone in the presence of excess counter ions in the micelles. Previous results show 40–50 % doping for PANI-DBSA salt [73, 83].

3.3 Polymerization Yield

Part of the PANI-DBSA dispersions which were precipitated and washed to get PANI powder were weighed and used to estimate the polymerization yield. Assuming 100 % doping of the nitrogen atoms in the polymer backbone (1:1, **M/M** of aniline and DBSA), the percentage yield was calculated using the equation:

$$\text{Percentage yield} = \frac{\text{Weight of PANI-DBSA}}{\text{Weight of } x\,\mathbf{M} \text{ aniline} + \text{Weight of } x\,\mathbf{M} \text{ DBSA}} \times 100$$

Using the present method, PANI-DBSA salts can be synthesized in good yield (up to 92 %) which strongly depends on the mole ratio of DBSA/aniline in the feed (Table 3.1). Polymerization yield increases when the mole ratio of DBSA/aniline in the feed is increased. Higher yields at higher concentration of DBSA are due to a decrease in the pH of the reaction medium.

Table 3.1. Elemental composition (mol %), percentage doping values and percentage yields of PANI-DBSA dispersions synthesized at various concentration of aniline and DBSA.

Sample code	C (%)	N (%)	S (%)	Percentage doping	Yield (%)
PANI–1	5.675	0.329	0.195	66.7	38.0
PANI–2	5.702	0.336	0.196	58.5	43.1
PANI–3	5.812	0.301	0.181	59.9	56.7
PANI–4	5.971	0.25	0.163	65.5	68.6
PANI–5a	6.152	0.171	0.163	95.3	92.3
PANI–5d	5.962	0.271	0.168	62.1	56.5
PANI–5e	5.732	0.346	0.188	54.3	33.6

3.4 UV-Vis Spectroscopy

Electronic absorption spectra of all the dispersions show three bands in the region of 760–800 nm, 410–430 nm and 350–355 nm indicating that the polymer is in its emeraldine salt form [67]. Of these three bands, the band at 760–800 nm is sensitive to changes in the environment such as pH, feed concentration of the monomer/dopant, etc. [76]. Figure 3.3 (Page 39) shows the plot of the absorbance of the band at 760–800 nm *vs* the feed concentration of aniline (C_{ani}). It is evident from the figure that the absorbance exhibits linear dependency when $C_{ani} \leq 0.02$ **M**. Thus, below this concentration PANI-DBSA dispersions obey the Beer-Lambert law. This indicates that in the Beer-Lambert concentration limit the real polymerization yield of the dispersions (the fraction of monomer transformed into polymer) is constant. Hence, in this concentration range UV-Vis spectroscopy can be used as an analytical tool to detect the concentration of aniline used in the synthesis of the dispersion. At fixed aniline concentration, the ratio of absorbance of the low energy band

to the high energy band (A_{770}/A_{350}) is almost the same (1.7–1.9) irrespective of the amount of DBSA in the feed indicating almost the same level of protonation. The higher A_{770}/A_{350} ratios indicate better protonation of the polymer backbone in these suspensions. Elemental analysis of precipitated pure PANI-DBSA revealed that extent of doping is increased with increasing amounts of DBSA in the feed (Table 3.1, see previous page). The rather unusual behavior observed for the dispersions may be due to the interference of the ionic byproducts of the oxidant, presence of free acid and dilution. The band at 770 nm shows a hypsochromic shift when the concentration of DBSA in the feed is increased from 0.025 (λ_{max} = 786 nm) to 0.1 **M** (λ_{max} = 766 nm). This is rather unexpected because an increase in the concentration of DBSA decreases the pH of the medium thereby decreasing the band gap due to higher protonation. Such a blue shift was also observed by Yin and Ruckenstein [86] for PANIs codoped with HCl and DBSA. They suggested that an increase in the amount of HCl in the polymer increases the compact coil conformation of the polymer, leading to a hypsochromic shift. Such a trend was also observed for PANI-DBSA dissolved in chloroform where scanning electron microscopy images clearly show the change in conformation with increasing concentration of DBSA in the feed as discussed in the second part of the dissertation.
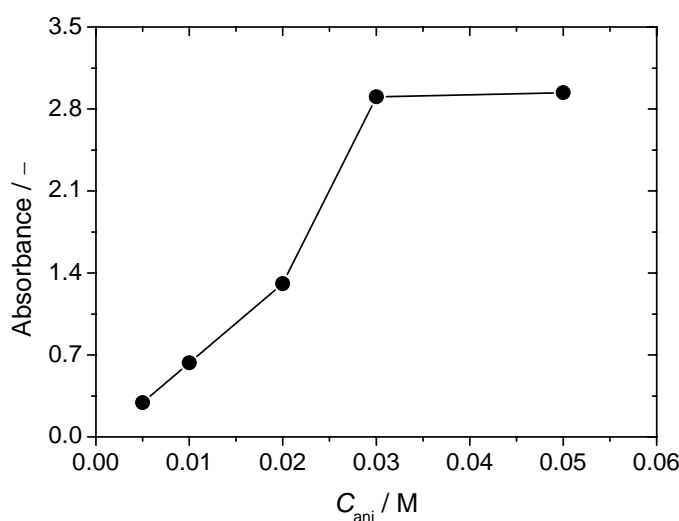

Figure 3.3. Plot of the absorbance of the band at 760–800 nm *vs* the concentration of aniline in the feed.

3.4.1 Effect of pH on UV-Vis Spectra

The pH of the dispersion has a pronounced effect on the protonation-deprotonation equilibrium of conducting ES and non-conducting EB forms of polyaniline. The pH of the

PANI-DBSA dispersion is controlled either by the addition of 0.1 **M** HCl or 0.01 **M** NaOH, keeping the total volume of the sample constant. Polyemeraldine base exhibits only two bands at 550–600 and 315–330 nm corresponding to $\pi* \leftarrow$ n and $\pi * \leftarrow \pi$ transitions, respectively [83]. Figure 3.4 shows UV-Vis absorption spectra of PANI–5a recorded at progressively increasing pH. The absorbance at 770 nm linearly decreases when the pH of the dispersion is increased from 1 to 8 and above this pH, a new band that is characteristic of the EB form of PANI in the region of 570–600 nm is observed. The decrease in absorbance is attributed to the decrease in protonation of the polymer backbone which in turn decreases the number of polarons. The position of this band shows a red shift when pH of the dispersion is increased from 1 to 8. It is assumed that the addition of NaOH to the PANI suspension leads to the aggregation of colloidal particles thereby increasing the conjugation length and decreasing the band gap. The above assumption is confirmed by the gradual macroscopic precipitation of PANI colloids under strongly basic conditions (pH > 10). Kuramoto and Genies [68] have observed a similar trend for PANI–HCl colloids synthesized in SDS aided micelle system but no explanation has been given for the observed changes. Interestingly, Svelko *et al.* [83] observed blue shift in the position of the band at 770 nm with increasing pH of PANI colloids synthesized in the presence of nonylphenolethoxylate (NP 40). Again, there is no explanation for the observed shifts.
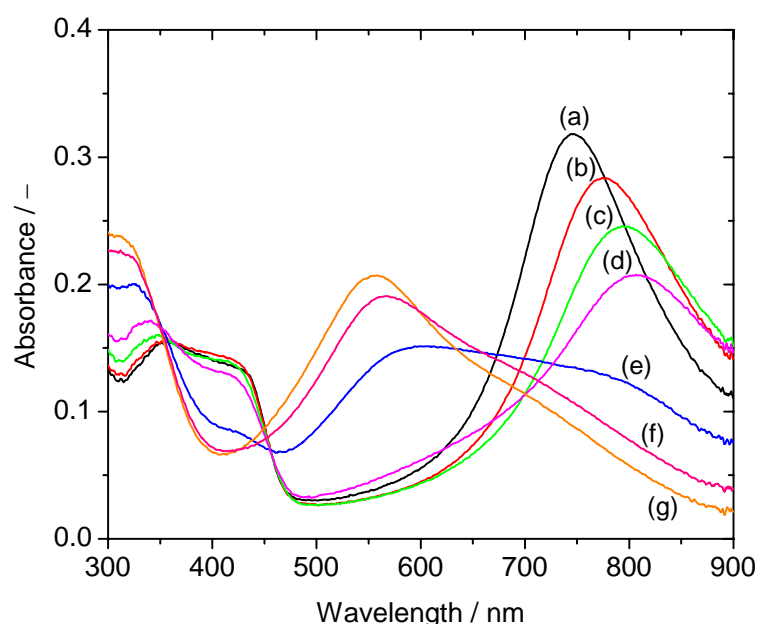

Figure 3.4. Electronic absorption spectra of PANI–5a recorded at progressively increasing pH values of (a) 1.8, (b) 3.5, (c) 5.6, (d) 8.0, (e) 9.2, (f) 10.0 and (g) 10.6.

When the pH of the suspension is greater than 8, the band at 770 nm shows a blue shift and there is a sharp increase in the absorbance of the new band at 560–600 nm. This reveals that in this pH range, the benzoid segments formed by protonation are gradually transformed into quinoid segments [83]. At pH > 10, UV-Vis spectra characteristic of EB have been observed. Both polaron bands (770 and 420 nm) exist up to pH = 9–10 which reveals that conductivity of the PANI particles is not completely lost even at pH 10. Figure 3.5 shows the absorbance change of the PANI–5d dispersion at 770 and 570 nm at various pH values. The observed spectral changes illustrated in two plots are attributed to the transformation of protonated benzoid structures to unprotonated quinoid structures. The two plots intersect at pH ~10 which confirms the presence of the ES state of PANI. The ES-to-EB transition is observed in the range of pH = 9–10 for all of the PANI dispersions irrespective of the mole ratio of DBSA/aniline in the feed. Previous results have shown stability of the ES state of PANI up to pH = 4 for conventional HCl doped PANI and pH = 7–8 for PANI-DBSA suspensions as well as for PANI particles synthesized in the presence of NP 40 [68, 69, 83]. The higher stability of the ES state of PANI particles observed in the present study may be due to the strong complexation of DBSA with the polymer backbone in the 2-propanol+water mixture.
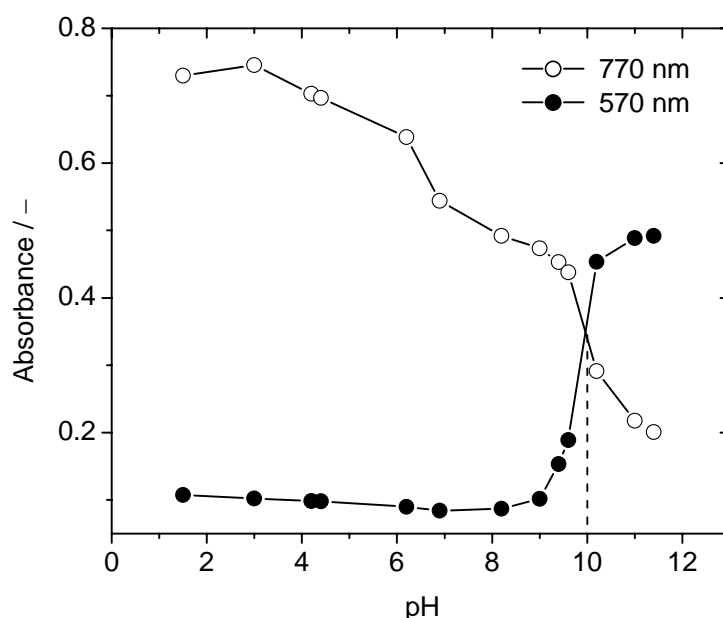

Figure 3.5. Changes in the absorbance of the bands at 770 and 570 nm as a function of pH for PANI–5d.

The position and the absorbance of the band at 350 nm are unaffected when the pH < 8. Further increases in the pH increase the absorbance of this band exhibiting a blue shift because of the ES-to-EB transformation in this pH range. The band at 420 nm, assigned to the polaron transition, disappears for pH > 9. The existence of the low energy polaron band (770 nm) at pH > 9 depends on the mole ratio of DBSA/aniline in the feed. This band disappears at pH = 9.5 when the mole ratio of DBSA/aniline is 3.33 whereas it persists as a hump even at pH = 11 when the mole ratio is increased to 20.

3.4.2 Spectroelectrochemical Studies at Acidic pH

The electrochromic properties and electrochemical stability of both chemically and electrochemically synthesized PANI have been extensively studied using *in situ* UV-Vis spectroscopy [73, 87]. In the present work, this idea has been extended to a thin layer of the PANI-DBSA dispersion as mentioned in Chapter 2 (Section 2.3). The aim is to understand how the colloidal particles of PANI respond to a change in the applied potential. Thin layers of PANI-DBSA dispersions show changes in the band positions and the absorbance when the applied potential is gradually increased in steps from $E_{SCE} = -0.4$ V to $E_{SCE} = 1.4$ V.

Figure 3.6 (Page 43) shows *in situ* UV-Vis spectra of PANI–5e at different potentials successively shifting into the anodic direction. Again, the band that is most sensitive to the change in the applied potential is the low energy polaron band (770 nm). The position of this band shows a small bathochromic shift and its absorbance decreases when the applied potential is increased from $E_{SCE} = -0.4$ to 0.2 V. In this potential range PANI exists in the leucoemeraldine state and the increase in the absorbance observed at $E_{SCE} = 0.2$ V can be attributed to the transformation from the leucoemeraldine to the emeraldine salt state of PANI. Further increase in the applied potential shifts this band toward lower wavelengths with progressive increases in the absorbance. These results are similar to those observed for soluble PANI-DBSA salts which are discussed in the second part of the dissertation [73]. Irrespective of the concentration of aniline or DBSA in the feed, the band at 770 nm is shifted to 680 nm when the applied potential $E_{SCE} > 1.1$ V. Generally, such a steep blue shift is attributed to an emeraldine-to-pernigraniline transformation in the PANI backbone [88]. However, this transformation cannot be confirmed in the present study because the other polaron band at 420 nm is present at all applied potentials. The absorbance at 680

nm decreases when the applied potential is further increased to E_{SCE} = 1.4 V which may be due to irreversible degradation of the polymer.
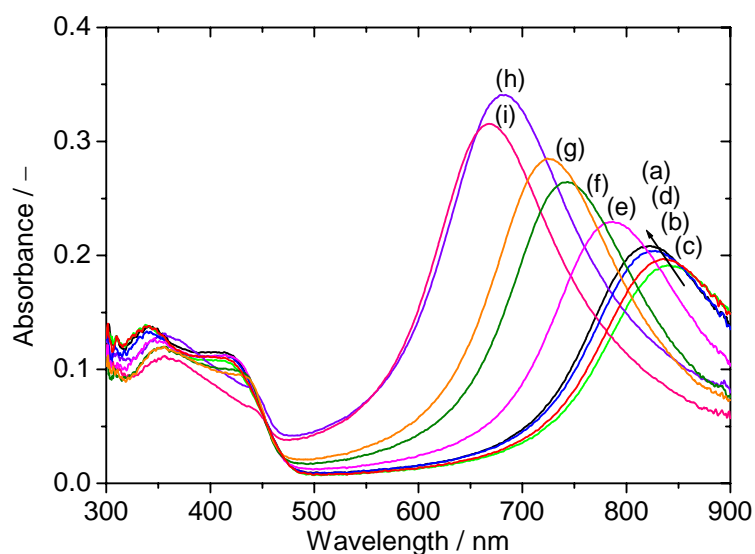

Figure 3.6. *In situ* electronic absorption spectra of PANI–5e recorded in ongoing anodic potential direction of a potential cycle; E_{SCE} (V) = (a) −0.4, (b) −0.2, (c) 0, (d) 0.2, (e) 0.4, (f) 0.6, (g) 0.8, (h) 1.1 and (i) 1.4.

In situ electronic absorption spectra were also recorded in cathodic direction to check the electrochromic reversibility of a thin layer of the dispersion (Figure 3.7; Page 44). Position of the low energy polaron band (770 nm) exhibits a red shift when potential is progressively shifted in cathodic direction from E_{SCE} = 1.4 to 0 V. Its absorbance increases, passes through a maximum at $E_{SCE} \sim$ 0.6 V and then decreases. The overall trend of this band, both in terms of position and absorbance, is similar to the one observed during anodic sweep. Significant differences in the UV-Vis response are observed when $E_{SCE} <$ −0.2 V due to emeraldine-to-leucoemeraldine transformation.

The changes in the position and the absorbance of the band at 770 nm of PANI–5a during a potential cycle (anodic sweep followed by cathodic sweep) are shown in Figure 3.8 (Page 44). It is clear from the figure that both the wavelength and the absorbance show hysteresis during the potential cycle, indicating poor electrochemical and electrochromic reversibility of the PANI-DBSA particles. This may be caused by the poor charge transfer between the thin layer of the dispersion and the surface of the electrode. The system in this case is further complicated by the possible exchange of particles between the active layer and the pool of suspension from which the thin layer is generated.
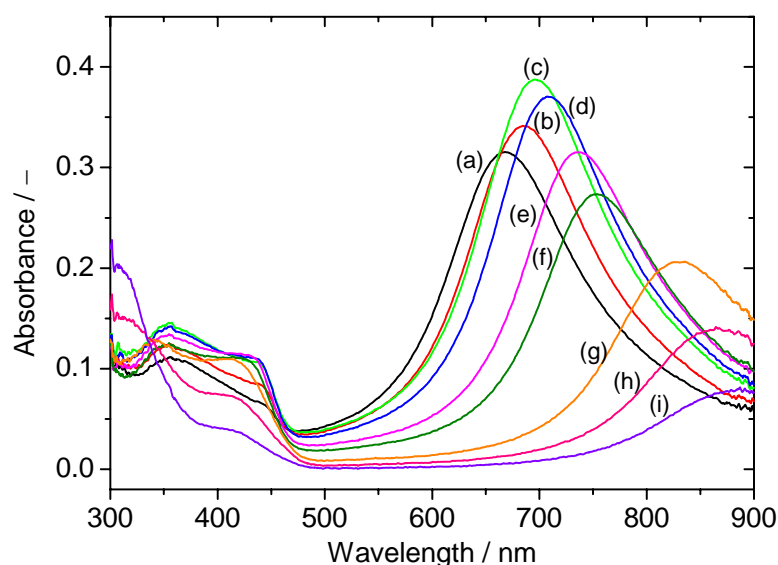
Figure 3.7. *In situ* electronic absorption spectra of PANI–5e recorded in ongoing cathodic potential direction of a potential cycle; E_{SCE} (V) = (a) 1.4, (b) 0.8, (c) 0.6, (d) 0.4, (e) 0.2, (f) 0, (g) −0.2, (h) −0.4 and (i) −0.7.
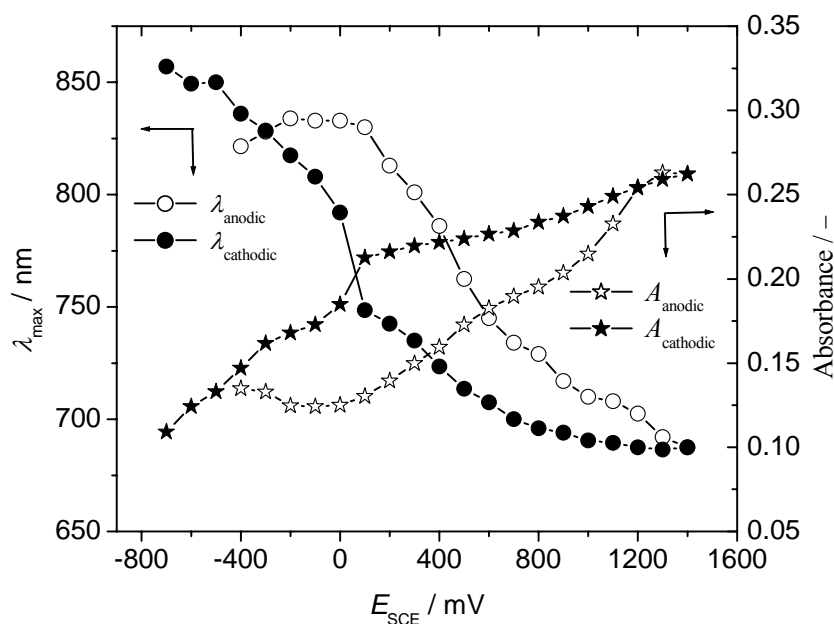
Figure 3.8. Change in the position and the absorbance of the band at 770 nm of PANI–5a in an applied potential cycle (positive and then negative ongoing direction).

The spectroelectrochemical response of PANI particles depends on the total ionic concentration (C_{total}) of the suspension. The UV-Vis spectral response of PANI suspension having lower C_{total} is similar to the chemically synthesized PANI films [73]. For example, a

44

visible transformation from emeraldine to leucoemeraldine was observed in the UV-Vis spectra of PANI–5e (C_{total} = 0.11 **M**) recorded at different applied potentials successively shifting in the negative direction (Figure 3.7; Page 44).

Another polaron band at 400–420 nm progressively shifts to higher wavelength and its absorbance gradually decreases when the applied potential is increased from E_{SCE} = −0.4 V to E_{SCE} = 1.4 V. In the cathodic sweep, the absorbance of this band increases, passes through a maximum at E_{SCE} = 0 to −0.2 V and then decreases. This observation suggests that maximum concentration of radical cations is present in the potential range of E_{SCE} = 0 to −0.2 V [73]. The position of the band at 350 nm shifts to 315 nm and its absorbance increases when E_{SCE} < −0.3 V, where PANI is in the leucoemeraldine state. However, neither its position nor absorbance is greatly affected above this potential.

3.4.3 Spectroelectrochemical Studies at Basic pH

The UV-Vis spectral response of PANI-DBSA dispersions to applied potential at basic pH shows interesting features. As mentioned earlier, UV-Vis spectra of PANI in basic medium exhibit two bands at 550–600 and 315–330 nm. The completely oxidized pernigraniline state also has bands in this region [73]. During an anodic potential sweep from E_{SCE} = −0.4 to 1.4 V, only these two bands are observed. The band at 580 nm shows a red shift when the applied potential is increased from E_{SCE} = −0.4 to 0 V. Further increases in the potential shift this band gradually and then steeply to lower wavelength which is attributed to the conversion of EB to PN. The absorbance of this band slightly decreases with an increase in the applied potential, passes through a minimum at around E_{SCE} = 0.8 to 0.9 V and then slightly increases. PANI is in its conducting emeraldine form in the potential range of E_{SCE} = 0 to 0.8 V. The conducting property of the PANI is related to the absorbance changes in the UV-Vis spectra. The decrease in the absorbance reflects the decreases in the conductivity of the PANI.

New bands in the region of 400–430 nm and 770–860 nm (polaron bands) appear and their absorbance increases during the reverse cathodic sweep. Figure 3.9 (Page 46) shows *in situ* UV-Vis spectra of PANI–5d at pH = 11 recorded at different potentials successively shifted in the cathodic direction. The appearance and the position of the band at 770 nm depend on the amount of DBSA in the feed. The band at 520 nm characteristic of pernigraniline is progressively shifted to 770 nm when the concentration of DBSA in the feed is 0.1 **M** while two distinct bands corresponding to EB and ES states of PANI are ob-

served when the concentration of DBSA is reduced to ≤0.05 **M** (Figure 3.9). The complexation between DBSA and PANI is stronger at higher concentrations of DBSA; therefore, the band at 520 nm (PN) is shifted to 770 nm (ES). At lower concentrations of DBSA, the reduction of pernigraniline to emeraldine yields PANI in both the EB and ES states. The spectral changes are similar to those observed when changing the pH value of the medium. In the latter case, extent of protonation in the emeraldine state is varied, whereas in the former case, the transformation is from pernigraniline to the emeraldine salt.
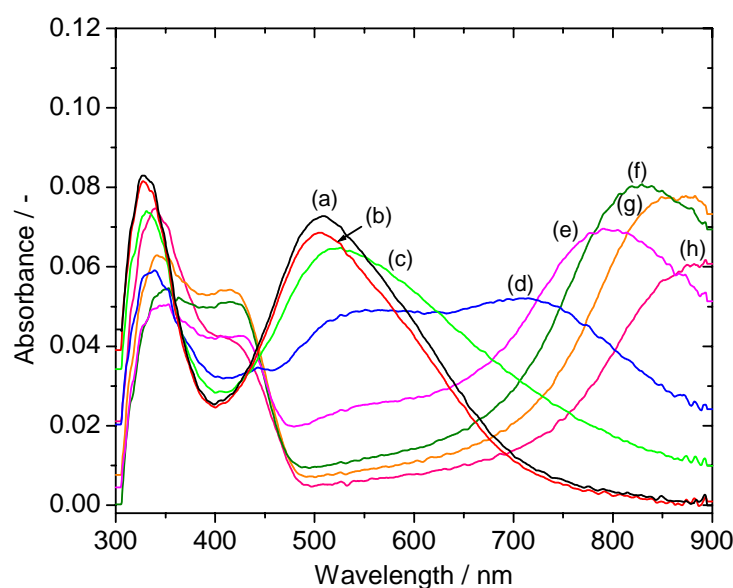
Figure 3.9. *In situ* electronic absorption spectra of PANI–5d at pH 11 recorded by progressively shifting the applied potential in the negative direction of a potential cycle; E_{SCE} (V) = (a) 1.4, (b) 1.0, (c) 0.6, (d) 0.4, (e) 0.2, (f) 0, (g) −0.2 and (h) −0.6.

Generally, a PANI film (chemically or electrochemically synthesized) is electrochemically inactive in neutral/basic solutions; therefore, the polaron bands in the UV-Vis spectra are absent. The presence of polarons in the present study may be attributed to protonation in the presence of bulky counter ions in the medium. The protonation of PANI is not a simple process of inserting and expelling protons. Such changes were not observed for thicker layers of dispersions. When the thin layer of PANI-DBSA colloids was kept at a constant applied potential of E_{SCE} = 1 V for 30–40 minutes, similar transformations were observed during an ongoing anodic scan. Hence, it is assumed that the spectral changes are controlled by the mobility of anions and an electrokinetic effect. Positively charged PANI particles are repelled from the electrode in an anodic potential sweep (electrophoretic phe-

nomenon) and can be easily exchanged from the pool of dispersion. During the following cathodic potential sweep, particles have a tendency to stay near the surface of the electrode and the exchange of particles between the thin layer and the pool of dispersion is minimized. The mobility of the anions (basic pH) is lower than that of the protons (acidic pH). As a result, PANI particles near the electrode surface experience different chemical environment leading to the formation of polarons. The above assumption is supported by the behavior of the absorbance at 420 nm in an acidic solution of PANI colloids which is similar to that of a chemically or electrochemically synthesized PANI film only during a cathodic sweep.

The new bands show up at E_{SCE} = 0.6, 0.4 and 0 V when the mole ratio of DBSA/aniline is 20, 10 and 3.33, respectively. This suggests that the counter ions have a pronounced effect on doping of the PANI backbone. Figure 3.10 (see next page) shows changes in the absorbance at 770 and 570 nm for PANI–5d at different applied potentials that are progressively shifted in the cathodic direction from E_{SCE} = 1.4 to –0.4 V. The two plots intersect at around E_{SCE} = 0.4 V indicating that below this potential, ES state of PANI predominates. The absorbance of the polaron band at 770 nm increases when the applied potential is decreased from E_{SCE} = 0.8 V to E_{SCE} = 0.1 V and then decreases with further decreases in the applied potential. Thus, PANI colloids exist in the emeraldine state in the potential range of E_{SCE} = 0.1 to 0.8 V which is similar to that of electrochemically synthesized PANI [89]. Pernigraniline-to-emeraldine and emeraldine-to-leucoemeraldine transformations are observed at E_{SCE} = 0.9–0.8 and 0.1 V, respectively.

As mentioned above, charge transfer between PANI colloids in a thin layer of suspension and the electrode surface is relatively slow. This effect has been verified by observing the position and absorbance of all the three bands at a fixed applied potential as a function of time. Figure 3.11 (Page 48) shows changes in position of the band at 770 nm as a function of time at four different applied potentials for PANI–5a. In the range of E_{SCE} = 0.4–0.8 V, the position of the band at 770 nm does not depend on time, indicating that PANI dispersions synthesized by the present method do not respond to the applied potential. The position of this band shows red or blue shift as a function of time when the applied potential is E_{SCE} = –0.4 or E_{SCE} = 1.2 V, respectively, indicating irreversible changes in the polymer structure. The position and absorbance of both bands at 350 nm and 420 nm are also independent of time of application of the potential in the potential range of E_{SCE} = 0.4–0.8 V.
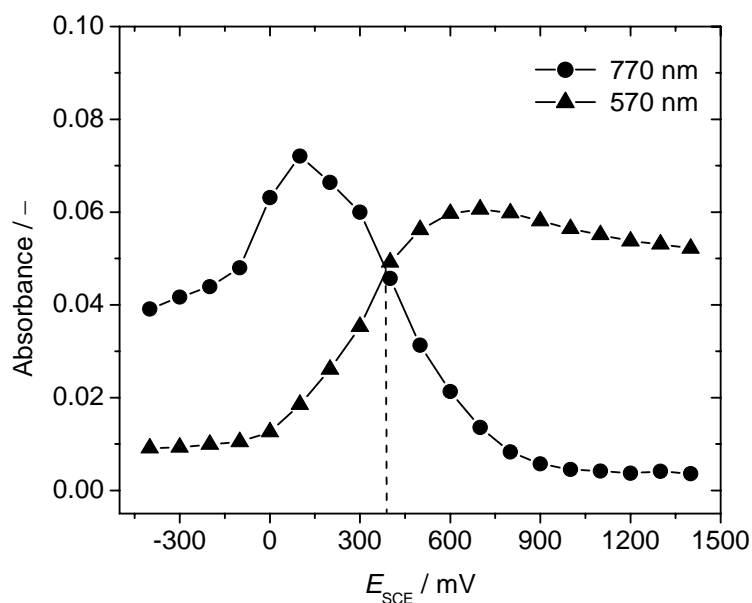
Figure 3.10. Changes in the absorbance of the bands at 770 and 570 nm as a function of applied potential progressively shifted in the negative direction for PANI–5d.
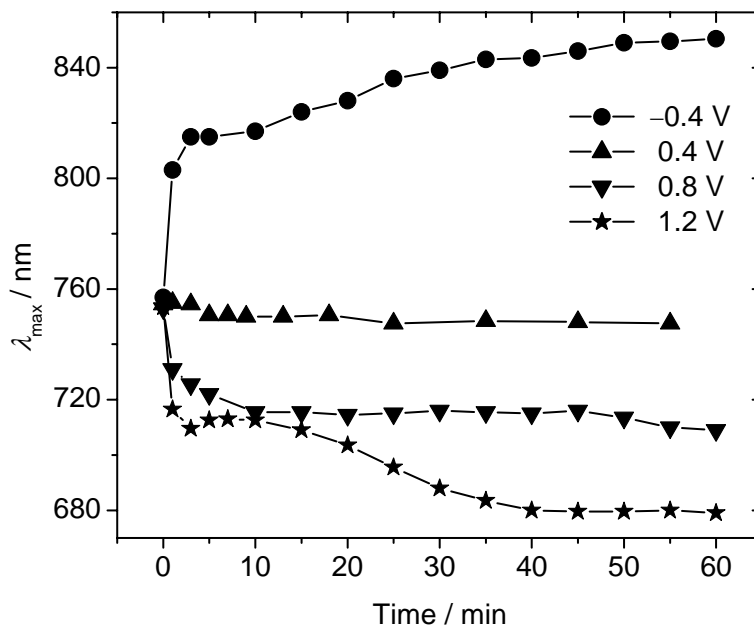

Figure 3.11. Change in position of the band at 770 nm as a function of time at four different applied potentials for PANI–5a.

3.5 Pre-resonance Raman Spectroscopy

Pre-resonance enhancement for the PANI films was observed because the laser excitation wavelength used (λ_0 = 476.5 nm) matches the longer wavelength wing of the absorption band of PANI centered at 420–430 nm [25, 26]. However, pre-resonance enhancement is not effective in the alkaline pH region because of the absence of the band at 420 nm in this pH region. The frequencies of the major Raman bands and their assignments are summarized in Table 3.2. *In situ* UV-Vis spectra at different pH values reveal that during a progressive stepwise increase in the pH of the medium the absorbance of the band at 420 nm shows a small increase, passes through a maximum and then decreases as shown in the Figure 3.12 (Page 50).

Table 3.2. Major Raman bands and their assignments for PANI-DBSA dispersions, λ_0 = 476.5 nm.

Frequency (cm^{-1})	State*	Assignment [90, 91]
1627–1637	B	C–C ring stretching
1590–1597	Q	C–C ring stretching
1540–1546	Q	C–C ring stretching
1506–1516	Q	C=N stretching
1490–1496	Q	C=N stretching
1230–1235	Q	In-plane ring deformation
1200–1205	B	C–H in-plane bending
1171–1177	Q	C–H in-plane bending
890–895	B	In-plane ring deformation
845–855	B	Amine ring deformation
825–830	Q	In-plane ring deformation
800–815	Q	C–H out-of-plane bending
712–724	B	Out-of-plane ring deformation
685–698	Q	Out-of-plane ring deformation
640–645	B	In-plane ring deformation
511–526		Out-of-plane C–N–C torsion
412–420	Q	Out-of-plane C–H wag

*: B = benzoid ring and Q = quinoid ring

At pH = 1, the Raman spectrum shows two strong peaks at 1635 and 1202 cm^{-1} assigned to benzoid rings (Table 3.2). Intensity of almost all the peaks increases when pH is raised to 8 but beyond this value, scattered light intensity decreases. This trend of pH de-

pendent pre-resonance enhancement is very similar to the plot of absorbance at 430 nm (radical cations) *vs* pH (Figure 3.12). This implies that the resonance enhancement depends on the concentration of radical cations in the dispersion. Bartonek *et al.* [92] have observed that strong bands that are mainly due to benzoid segments are present at lower pH, thus we have concluded that the radical cations involved are polarons and not bipolarons. An explanation for the change in intensity of the Raman bands at higher pH (> 8) is complicated because in this pH range Raman band intensity is controlled by three main factors: coagulation of PANI particles, concentration of quinoid segments and pre-resonance enhancement.
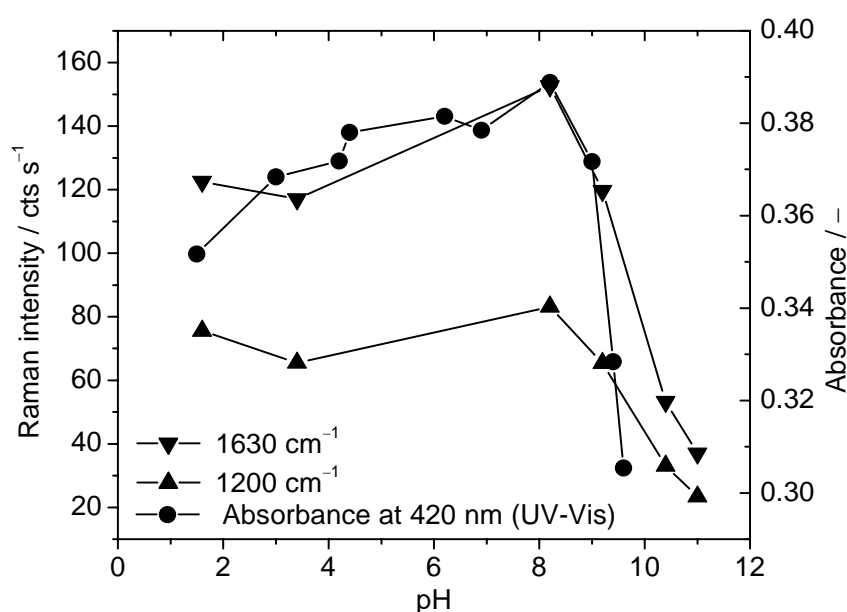
Figure 3.12. Plot of the absorbance at 420 nm and the intensity of Raman bands at 1630 and 1200 cm^{-1} as a function of pH for PANI–5d.

An increase in the pH from 8 to 10 causes a steep decrease in the intensity of bands at 1635 and 1202 cm^{-1} and new bands in the region of 1400–1600 cm^{-1} corresponding to quinoid vibrations appear. Hugot-LeGoff and Bernard [91] stated that there should be three C–C ring stretching modes (1550, 1575 and 1585 cm^{-1}) and two C=N stretching modes (1485 and 1500–1515 cm^{-1}) for quinoid rings. They have also observed that C–C ring stretching modes are sensitive to the applied potential and pH of the medium whereas the multiplicity in C=N stretching arises from the difference in protonation and charge localization on the imine sites. Two C–H bending vibrations at 1200 cm^{-1} and 1175 cm^{-1} corresponding to benzoid and quinoid rings, respectively, are present in this pH range. Quillard

et al. [93] have attributed two such C–H bending vibrations to a radical species having two types of benzene rings. Bands mainly due to quinoid vibrations are present when the pH is increased further (pH > 10) and their intensities are almost independent of the pH of the medium which is consistent with previous results (Figure 3.13) [92]. The C–C ring stretching vibration shows a red shift from 1637 cm^{-1} to 1630 cm^{-1} with an increase in the pH of the medium from 1 to 11. The intensity of the quinoid C=N stretching vibration at 1460 cm^{-1} increases at pH > 9, where the conducting ES is transformed into the non-conducting EB. The band due to amine deformation at 840 cm^{-1} is absent above this pH which confirms the metal-to-insulator transition of PANI.
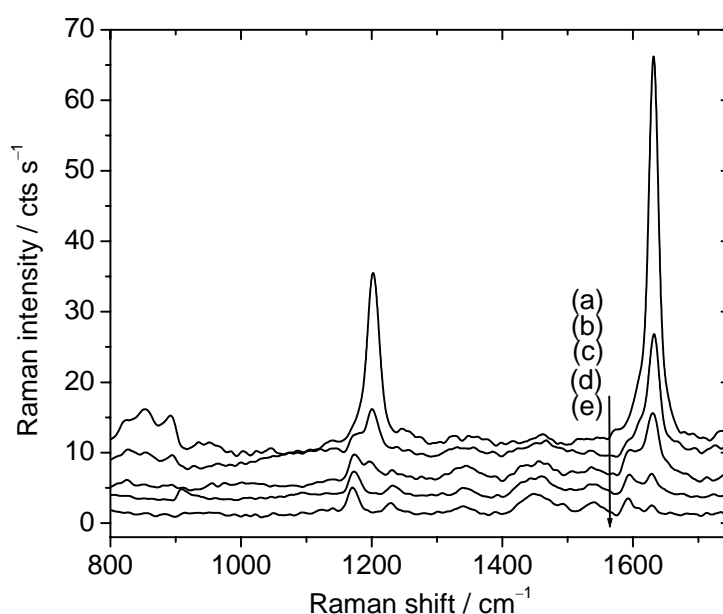
Figure 3.13. Pre-resonance Raman spectra of PANI–5d (stacked for better visibility) at pH (a) 8.2, (b) 9.2, (c) 9.7, (d) 10.4 and (e) 11.

The generation of new bands (1170 cm^{-1} and 1590 cm^{-1}) corresponding to the quinoid ring in the region of pH 9–10 can be clearly seen in Figure 3.13; the intensity of these bands increases at the cost of the bands due to benzoid rings (1635 cm^{-1} and 1200 cm^{-1}). As mentioned earlier, this observation is attributed to the metal-to-insulator transition. Such a transition observed with Raman spectroscopy was also found in UV-Vis spectra of PANI-DBSA particles synthesized by the present method at much higher pH values (~10) compared to the reported ones (pH 4–6) [83, 92]. A benzoid-to-quinoid transformation is also observed in the region 900–800 cm^{-1}. The intensity of the benzoid in-plane bending

vibration observed at 895 cm^{-1} decreases whereas that assigned to the quinoid ring observed at 825–830 cm^{-1} increases when the pH is increased from 8 to 11. The intensity of the out-of-plane C–H wagging mode at 800–815 cm^{-1}, which is present as a broad band near neutral pH, increases and appears as a sharp band when the pH is increased to 11. A band in the range of 1040–1057 cm^{-1} and a band at 1140 cm^{-1} are caused by the dopant, DBSA and are assigned to C–S stretching and S=O out-of-plane bending modes, respectively [94].

3.6 Transmission Electron Microscopy

PANI particles reported so far showed rice grain, needle or spherical morphology depending on the choice of oxidant, steric stabilizers and reaction conditions [71]. Figure 3.14 shows TEM images of PANI-DBSA dispersions at different molar ratios of DBSA/aniline in the feed. Obviously, PANI particles are irregularly shaped. The particles are actually spherically shaped but their high tendency to aggregate hinders the recording of a TEM image with perfectly spherical particles. Such aggregation takes place during sample preparation for TEM where dispersions are evaporated on a carbon-coated copper grid. The size of particles strongly depends on the dilution of the PANI-DBSA dispersion which supports the argument of aggregation. Vincent and Waterson [95] believe that such aggregation during sample preparation is due to inefficient steric stabilization. However, steric stabilization in an aqueous medium of PANI-DBSA particles is very good because they are stable for more than a year and centrifugation does not yield a solid residue. Irregularly shaped particles are observed for PANI dispersions at all DBSA/aniline mole ratios, indicating the absence of any control over the shape of the particles.
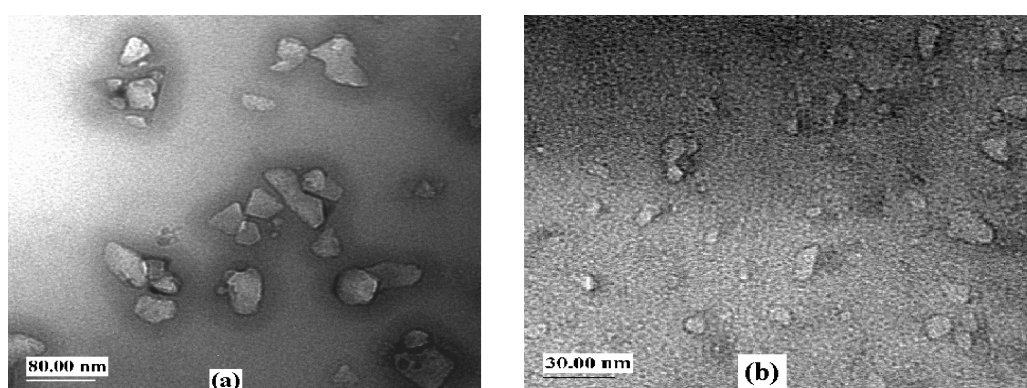

Figure 3.14. TEM images of PANI-DBSA dispersions with DBSA/aniline feed ratios of (a) 3.3 and (b) 5.

Stejskal *et al.* [96] have reported core-shell model for PANI particles where the particles consist of a PANI core and a shell of water soluble polymer. Recently, Han and co-workers [72] have observed needle like particles with an average diameter of 10 nm and lengths of 20–30 nm for PANI-DBSA synthesized *via* reverse micelle polymerization in 2,2,4-trimethylpentane+isooctane+water. PANI-DBSA particles synthesized by the present method do not exhibit such core-shell or needle like pattern.

Electron diffraction (ED) patterns have been recorded for selected regions of cluster of aggregated particles and are shown in Figure 3.15. Electron diffraction pattern exhibit both bright spots or arcs characteristic of the crystalline part and amorphous halos (Figure 3.15a) indicating that bulk PANI is semicrystalline. Crystallinity of PANI-DBSA particles is improved when the concentration of DBSA in the feed is increased (Figure 3.15b). Organically soluble PANI-DBSA, discussed in the second part of the dissertation, exhibit diffraction pattern corresponding to orthorhombic crystal structure, however, in the present case, such a well defined diffraction pattern has not been observed.
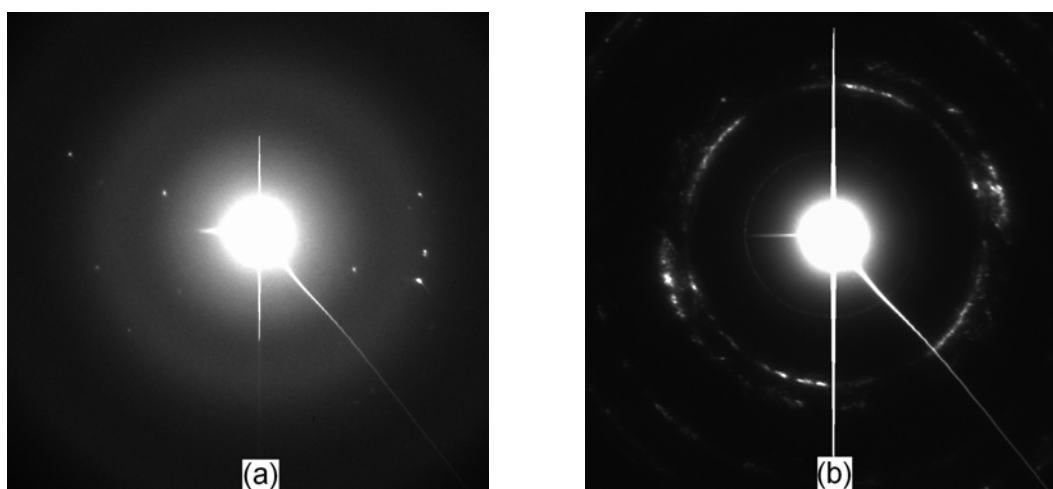

Figure 3.15. ED patterns of PANI-DBSA dispersions with DBSA/aniline feed ratios of (a) 3.33 and (b) 5.

Chapter 4

Conclusions and Remarks

4.1 Conclusions

Stable suspensions of PANI-DBSA have been synthesized *via* micelle aided polymerization using 2-propanol+water as a solvent. DBSA dissolved in 2-propanol (70 % solution) has been used both as surfactant and dopant. The binary mixture of solvent facilitates dissolution of DBSA, thus the polymerization reaction has been successfully carried out in small reaction volumes. The green PANI-DBSA dispersions obtained does not undergo macroscopic precipitation for more than a year even in the presence of ionic byproducts of the oxidant.

Visible color changes during polymerization have been observed only after the induction period whose duration depends on the feed concentration of aniline. Higher concentration of aniline in the feed leads to shorter induction period. UV-Vis studies reveal that polymerization is completed in three hours irrespective of the feed ratio of DBSA/aniline in the feed. Polymerization yield depends on the amount of DBSA in the feed where increased feed concentration of DBSA increases the polymerization yield.

Valuable information on the charge transfer behavior of the PANI-DBSA colloids has been obtained from the pilot attempt made on the UV-Vis spectroscopy of thin layers of dispersions as a function of applied potential. Spectroelectrochemical behavior of a thin layer of dispersion depends on the pH value of the medium. In the acidic pH region, leucoemeraldine-to-emeraldine transformation has been observed, whereas, the second transformation corresponding to emeraldine to pernigraniline could not be assigned due to the presence of polaron band (~420 nm) at all applied potential. The hysteresis formed in the plot of position and absorbance of band at 770 nm as a function of applied potential indicates poor electrochromic and electrochemical stability of these dispersions arising from slower charge transfer processes. Polymer particles in the form of a thin liquid layer are stable in the applied potential region of $E_{SCE} = 0.4$ to 0.8 V.

Interesting changes in the UV-Vis responses have been observed in the basic pH region when the applied potential was swept in positive and then negative direction. In a positive going sweep, bands only due to EB form of PANI have been observed whereas bands corresponding to both ES and EB were observed during cathodic potential sweep.

Different UV-Vis spectral characteristics at basic pH observed during anodic and cathodic sweep indicates that mobility of anions and an electrokinetic effect play dominant role at higher pH.

Both electronic absorption spectroscopy and pre-resonance Raman spectroscopy have been used to monitor the metal-to-insulator transition of the PANI particles taking place by increasing the pH from acidic to basic pH values. The ES (metal)-to-EB (insulator) transition of the PANI-DBSA dispersions synthesized by the present method occurs in the range of pH = 9–10 which is much higher than previously reported ones.

PANI-DBSA particles in presence of ionic byproducts behave similar to pure PANI stabilized by various polymeric stabilizers. TEM investigation reveals that it is practically difficult to achieve control over the shape of the particles. High tendency of aggregation of PANI particles during sample preparation yields irregularly shaped particles. Aggregated clusters of PANI-DBSA particles are semicrystalline in nature and the crystallinity increases with increasing feed concentrations of DBSA.

4.2. Remarks

As mentioned in the preceding paragraphs, highly stable PANI-DBSA colloids have been synthesized in lower reaction volumes and their spectroelectrochemical investigations have been successfully carried out which really gives a broad insight towards the nature of the charge transport in PANI colloids. However, these suspensions suffer from chemical impurity because of the presence of byproducts of oxidant and excess of dopant. The poor electrochromic reversibility and electrochemical stability of the dispersions severely hinders their use in commercial applications. These drawbacks motivated us to work on the synthesis of DBSA doped PANI which is soluble in common organic solvents. The next part of this dissertation deals with the synthesis and characterization of soluble DBSA doped PANI and its copolymers.

PART II

Chapter 5

Introduction

As mentioned in chapter 1, polyaniline, a unique member of the family of conducting polymers, has been studied extensively in recent years due to its interesting acid-base chemistry, high environmental stability and low cost of synthesis. However, the wide variety of technological applications of PANI is limited by its poor solubility which has already been briefed in section 1.2.7. In this chapter more attention is paid to different protocols and oxidizing agents employed by various authors for chemical synthesis of PANI. The role of organic functional acids in tackling the problem of poor processability of PANI, different synthetic protocols for polymerization of aniline and various oxidants employed are discussed below under separate subtitles. A general overview on copolymers of aniline and, in particular, copolymers of aniline and *o*-toluidine is also provided.

5.1 Functionalized Protonic Acid: Counter Ion-induced Processability

As mentioned in section 1.2.9, Cao and coworkers [44] were the first to notice a large improvement in the solubility of metallic PANI when PANI-EB was doped with functionalized protonic acid. They have designated the functionalized protonic acid as $H^+(M^- - R)$ where anionic species $(M^- - R)$ containing R group is compatible with weakly polar or non-polar organic solvents. They have used DBSA, CSA, dinonylnaphthalenesulfonic acid (DNNSA), etc. and have found that PANI-DBSA complex is soluble in xylene, chloroform, toluene, etc. The process of protonating PANI in this way is also called 'counter ion-induced processability' as the solubility of the final PANI complex originates from the counter anionic species used. Such a post-processing method involves two steps: (1) neutralization of PANI-ES to form PANI-EB and (2) re-protonating PANI-EB with a functionalized protonic acid.

Several investigations have been carried out after this report of Cao and coworkers [44]. Tzou and Gregory [97] used this approach and reported that PANI-ES containing carboxyl and amino substituents were soluble in NMP and DMSO. A similar approach was also used by Rannou and coworkers [98] to prepare PANI-ES doped with sulfonic acid and phosphoric acid diesters. *m*-Cresol which is used as a solvent, acts like a secondary dopant

leading to high conductivity of PANI over a wide temperature range. In most of the cases, such post processed PANI-DBSA complex has been used in the synthesis of its blends with insulating polymers such as polyamide, epoxy resin, etc. [99, 100]. Recently, Krzysztof and Nan-Loh [101] have used phosphoric acid diesters as dopants and the resulting PANI was employed in the synthesis of blends of poly(vinyl chloride) (PVC) with PANI. Dufour *et al.* [102] have protonated PANI-EB dissolved in 2,2'-dichloroacetic acid with several sulfosuccinic acid diesters to prepare free-standing films of PANI. The resulting PANI-sulfosuccinates exhibited metallic-type conductivity and improved mechanical properties. Shacklette *et al.* [103] have developed a surface-core doping process in which PANI was doped with one acid at the core of a particle (e.g., *p*-toluenesulfonic acid, PTSA) and a second dopant predominantly at the surface (e.g., DBSA). The surface dopant was chosen to achieve increased compatibility between the PANI particles and a polymer matrix. Angelopoulos *et al.* [104] reported the synthesis of water soluble electrically conducting PANI doped with polystyrenesulfonic acid. The polymeric acid dopants used as template for oxidative polymerization of aniline results in a water soluble PANI.

Despite their improved solubility, counter-ion processed PANI-DBSA has maximum solubility of 0.5 % (wt/wt) in xylene [105]. As mentioned above, the post processing approach is carried out in two steps and the resulting material could not be obtained in its pristine state due to the presence of free and excess protonic acid. In some other cases, PANI-EB to functionalized protonic acid ratio of 0.5 was used which led to less efficient doping of PANI backbone [102]. As a result, several researchers have attempted to develop new synthetic protocols, which in some cases, have shown improved solubility of the produced PANI and are discussed below.

5.2 Various Synthetic Routes

The most widely employed chemical oxidation of aniline in aqueous acidic media using ammonium persulfate oxidant has already been described in section 1.2.3.1. Several other methods of polymerization of aniline have come to forefront because of the sensitivity of PANI to pH and availability of a wide variety of oxidants and dopants. In addition, the growing interest in the field of nanotechnology has also motivated several research groups to develop new polymerization routes to produce PANI nanostructures. Some of the recent synthetic approaches are described below.

Madathil *et al.* [106] developed a new route in which polymerization of aniline was carried out at 23 °C by addition of ammonium persulfate in aqueous medium containing aniline, sodium salt of dodecylbenzenesulfonate and HCl. The reaction mixture turns to a highly viscous gel and a solid gel was obtained at the end of the reaction which was easily cast into thin films. However, the byproducts of the oxidant and excess dopant are always associated with the final PANI-DBSA salt. Li and Zhang [107] have also employed a gelation technique which produces dendritic PANI nanofibers. Formation of the gel containing surfactant, monomer, dopant and oxidant was achieved by mixing all the components in acetic acid+water and quickly cooling to −7 °C.

The environmental concerns and the importance of biocompatibility resulted in a number of reports on a natural way of synthesis of PANI. Horse-radish peroxidase enzyme has been used for the oxidative coupling of aniline/substituted anilines in aqueous or non-aqueous medium containing buffers [108, 109]. Recently, Ma and coworkers [110] have extended this enzymatic approach to synthesize PANI nano-wires on Si surfaces fabricated with DNA.

Kan and coworkers [111] have prepared PANI nano-threads using a simple protocol. They employed a binary mixture of water and ethanol instead of an aqueous acidic media, and the polymerization of aniline was carried out at −20 °C. A much different procedure has been adapted by Wang *et al.* [112] for the synthesis of PANI hollow microspheres. They carried out the polymerization of aniline in an aqueous alkaline medium (NaOH, pH > 12) by dispersing the aniline monomer in NaOH. Ammonium persulfate was used as oxidant and the reaction was carried out at −5 °C.

Dispersion polymerization is another important non-conventional pathway for the synthesis of PANI which is discussed in the first part of the dissertation. Recently, Lee and coworkers [65] have reported a new self-stabilized dispersion polymerization of aniline. A mixture of water and chloroform was used as solvent and self-stabilization was achieved by the oligomers formed during polymerization.

In recent years emulsion, miniemulsion, microemulsion and inverse emulsion polymerization of aniline have come to the forefront and are detailed in the following section.

5.3 Emulsion Polymerization

Emulsion polymerization is a compartmentalized polymerization reaction taking place in a large number of loci dispersed in a continuous external phase. Emulsion polym-

erization methods have several distinct advantages over the conventional *in situ* polymerization. The physical state of the emulsion system makes it easier to control the process. Thermal and viscosity problems are much less significant than in the bulk polymerization. The product of emulsion polymerization can, in many instances, be used directly without further separations. High molecular weight and high reaction rates can be attained simultaneously by these methods. Several authors have reported this process for the synthesis of PANI [113−116]. In these disclosures, aniline, a protonic acid, a surfactant and an oxidant are combined with a mixture of water and a non-polar or a weakly polar liquid, for example, xylene, chloroform or toluene, all of which are sparingly soluble or insoluble in water. Aqueous solution of ammonium persulfate is added to the above emulsion system to initiate the polymerization. In most of the cases, the product was isolated by breaking the emulsion (adding acetone, for example) and collecting the precipitated PANI salt by filtering and washing. In some cases, emulsion flocculates during the course of reaction to form a two-phase system and the PANI remains in organic phase which can be easily separated. The emulsion polymerization described above, sometimes, is also known as 'conventional emulsion polymerization' or 'macroemulsion polymerization'. Several other types of emulsion polymerization have also been reported and are briefed below.

5.3.1. Miniemulsion Polymerization

Miniemulsions contain both droplets of dispersed phase and micelles formed by surfactant and the droplet size is lower than that of macroemulsions. However, the micelle size in both macro- and miniemulsions is the same [117].

Marie *et al.* [29] have synthesized PANI latex particles using a direct miniemulsion polymerization technique. The particles are preformed as droplets (size of 50–500 nm) by applying high shear or stress to a system containing the phase to be dispersed, the continuous phase, a surfactant and osmotic agent (essentially a hydrophobe in this case). The surfactant stabilizes the droplets against collisions and the mass exchange between the droplets is suppressed by the osmotic agent.

5.3.2 Microemulsion Polymerization

Microemulsion is completely devoid of droplets and only micelles are present. It is obtained using larger amounts of surfactant and continuous phase compared to the conventional emulsion. As in miniemulsion, size of micelle is the same in macro- and microemul-

sions [117]. A microemulsion is an organized microheterogeneous system which provides a large interfacial area and is generally less viscous.

Gan and coworkers [118] have employed this technique for the synthesis of PANI-HCl. A solution of aniline in 3 **M** HCl was dispersed in petroleum ether to form a microemulsion and a second microemulsion with an aqueous ammonium persulfate solution was added to initiate the polymerization.

5.3.3. Inverse Emulsion Polymerization

Inverse emulsion (also known as reverse emulsion), is a water-in-oil type of emulsion which consists of an aqueous dispersed phase and organic non-polar or weakly polar continuous phase. Inverse emulsion polymerization consists of an aqueous solution of the monomer which is emulsified in a non-polar organic solvent and the polymerization is initiated with an oil soluble initiator [117]. However, the term inverse emulsion polymerization was used even though a water soluble initiator, ammonium persulfate, was employed as reported by Ruckenstein and Sun [119] for the synthesis of blends of PANI. The reaction carried out in heterogeneous inverted emulsion has several distinct advantages as in the emulsion polymerization. Only a few attempts of inverse emulsion polymerization of aniline were made.

Marie *et al.* [29] reported the synthesis of PANI latex particles using an inverse miniemulsion polymerization technique. In this process, anilinium chloride was dispersed in ISOPAR† or cyclohexane using block copolymer poly[(butylene-*co*-ethylene)-*b*-(ethylene oxide)] as stabilizer and a solution of potassium persulfate in H_2O_2 as oxidizing agent. Recently, Han *et al.* [72] have also used the reverse emulsion method to synthesize PANI-DBSA nano-particles. In this case, ammonium persulfate dissolved in water constitutes dispersed phase whereas DBSA and aniline dissolved in isooctane constitute the continuous phase. This part of the dissertation also employs an inverse emulsion polymerization procedure for the synthesis of PANI and its copolymers with *o*-toluidine and is detailed in the next chapters.

As mentioned in section 5.2, the facile chemistry of PANI allows its synthesis using various oxidizing agents. The different oxidizing agents reported in the literature are mentioned below.

---

† ISOPAR is the brand name for eight grades of high-purity isoparaffinic solvents with narrow boiling ranges.

5.4. Oxidants Employed in the Polymerization of Aniline

Potassium dichromate, ammonium persulfate, potassium bromate, hydrogen peroxide, ceric nitrate, ceric sulfate and chromyl chloride are some of the commonly used oxidants [15]. Rao *et al.* [4], in their review article, have tabulated various oxidants used in the synthesis of PANI. Tetrabutylammonium persulfate (TBAP) [120] and hydrogen peroxide [121, 122] have also been utilized for the polymerization of aniline. Pron *et al.* [123] have compared four different oxidants $(NH_4)_2S_2O_8$, $K_2Cr_2O_7$, H_2O_2 and KIO_3 in the polymerization of aniline and concluded that KIO_3 was the most efficient oxidant, in the sense, that it produced good quality product over a wide range of reaction conditions, whereas, H_2O_2 was not a good oxidizing agent for the synthesis of PANI. Among various oxidizing agents, the most widely used oxidant is ammonium persulfate. However, it being a strong oxidizing agent and aniline polymerization being exothermic, controlling the reaction temperature is rather difficult and consequently polymers with a wide distribution of molecular weights result. The removal of inorganic byproducts (ammonium sulfate) from the polymer formed is also difficult [124]. Rao and coworkers [124, 125], for the first time have employed a novel organic oxidant, benzoyl peroxide, to overcome the above mentioned drawbacks.

5.4.1 Benzoyl Peroxide

Besides being used as an initiator in many polymerization reactions, benzoyl peroxide is also an efficient oxidant for polymerization of aniline. The main advantages of this oxidant are (a) solubility in most of the organic solvents which furnishes selection of a wide range of solvent systems, (b) the organic peroxide (compared to the conventional ammonium persulfate) reduces the possibility of overoxidation of PANI during exothermic reaction of aniline polymerization and (c) byproducts of the oxidant can easily be removed using solvents such as acetone or methanol which is normally used to break the emulsion. Recently, Ram and Palaniappan [125] have synthesized PANI salts doped with several mineral acids using benzoyl peroxide as an oxidant *via* an inverse emulsion polymerization method. Benzoyl peroxide has also been employed as an oxidant in the present dissertation.

5.5 Copolymers of Aniline

A brief introduction to copolymers has already been given in Section 1.2.11. In this section, the advantages of carrying out copolymerization and some of the recent examples

of copolymers of aniline are discussed. More emphasis is given to the copolymers of aniline with toluidines as this dissertation describes synthesis and electrochemical investigations of poly(aniline-*co-o*-toluidine).

Copolymerization involves polymerizing a mixture of two monomers. The product, referred to as copolymer, contains both monomers in the polymer chain in the alternating, statistical, block or graft arrangement depending on the detailed chemistry of the specific monomers and reaction conditions [117]. This technique helps in varying the chemical structure of a polymer to obtain a product with a particular combination of desirable properties. In polymer chemistry, this technique has widely been used to alter the polymer properties such as crystallinity, flexibility, etc. In the field of conducting polymers, copolymerization emerged as an efficient technique to combine the high metallic conductivity of PANI (poor solubility) and solubility of substituted anilines (very low conductivity) to obtain a processable conducting polymer. Further, copolymerization leads to an increase in the number of conducting polymers from the same set of monomers. The above mentioned advantages of copolymerization technique lead to an upsurge in the synthesis and characterization of various copolymers of aniline. A pioneering work on copolymers of aniline has been reported as early as 1990 [126]. Some of the recent contributions to aniline copolymers are reported below.

Rao and Sathyanarayana [127] have employed an inverse emulsion polymerization route to synthesize copolymers of aniline with *o*- and *m*- aminobenzoic acid with relatively better electrical conductivity and improved solubility. They have also employed the same approach for the synthesis of poly(aniline-*co-m*-aminobenzenesulfonic acid) exhibiting higher crystallinity and improved solubility in DMSO and DMF [128]. An inverse emulsion was formed by adding an aqueous solution of surfactant and dopant (HCl in these cases) to chloroform containing oxidant (benzoyl peroxide). Copolymers of aniline and 2,5-dimethoxyaniline which exhibit remarkably improved solubility in solvents such as chloroform, dichloromethane, etc. were also reported [129]. Chemical oxidative copolymerization of aniline and halogen substituted anilines yields copolymers with improved solubility but with very low electrical conductivity [130, 131]. Recently, synthesis of poly(aniline-*co*-aminoacetophenone) possessing enhanced solubility and good electrical conductivity have been reported using both emulsion and inverse emulsion polymerization pathways [54].

Like polyaniline (described in section 1.2.3), its copolymers can also be synthesized either chemically or electrochemically. All of the above mentioned copolymers have been

synthesized through chemical oxidation of their respective monomers. Electrochemical co-polymerization has gained increasing attention in last two decades due to the following reasons: (a) precise tuning of oxidation potential (fixed potential or by cycling in a potential limit) can be easily achieved and (b) wide variety of monomers can be copolymerized, for example, copolymerization of aniline and thiophene [132]. A considerable work has been reported from our laboratory on the electrochemical copolymerization of aniline/alkyl anilines with *o*-aminophenol/phenylenediamines [133−135].

5.5.1 Copolymers of Aniline with Toluidine

Synthesis of poly(aniline-*co*-toluidine) was initiated in 1990 by Wei and coworkers [126]. The main aim was to combine the conductivity of PANI and solubility of poly(*o/m*-toluidines). They have employed both chemical and electrochemical approaches to synthesize copolymers whose conductivity can be controlled in a broad range (0.1-10 S cm^{-1}). Following the pioneering work of Wei and coworkers, several reports have been published on the synthesis of poly(aniline-*co*-toluidine) using different synthetic routes[42, 136−139]. Su *et al.* [140] have reported a chemical oxidative copolymerization of aniline and *o*-toluidine with CSA as a chiral inductor in organic media. A helix inversion of co-polymer backbone in contrast to PANI has been induced by the incorporation of *o*-toluidine units. Recently, copolymer microtubes composed of aniline and *o*-toluidine have been prepared through a template (microporous anodic aluminum oxide) guided polymerization. The copolymer microtubes show improved solubility (up to 3.83 g/L) in DMF and very high conductivity (~17.4 S cm^{-1}) [141]. All these reports have shown a wide range of control over the conductivity of copolymers but failed to achieve the desired solubility in non-polar or weakly polar organic solvents.

Most of the above works have employed aqueous mineral acids as dopants and po-lymerization was carried out chemically using ammonium persulfate or electrochemically. All of them described solubility of the products with respect to EB form of the polymer backbone. The idea of retaining the conductivity of PANI by synthesizing the copolymers of aniline and toluidines has been successfully achieved in all these work. However, in most of the cases, the copolymers are partly soluble in DMSO, DMF, NMP, etc. and spar-ingly soluble in weakly polar solvents such as chloroform.

5.6 Solubility of Parent Polyaniline

Considerable progress has been made in the last few years in the processability of PANI by enhancing its solubility. Several research groups reported enhanced solubility of the parent PANI emeraldine salt when they use bulky acidic groups as dopant or when they apply a different synthetic route [86, 115, 142–146]. Laska and Widlarz [144] have reported synthesis of water-soluble polyaniline with various phosphonic and sulfonic acids as dopants. PANIs in this case are directly produced as dispersions in water and they are stable only for few days. Kinlen *et al.* [115] have reported a synthetic protocol for PANI doped with DNNSA. An emulsion polymerization pathway is employed to prepare PANI-DNNSA in the organic phase, which can be purified and extracted as a suspension in organic solvent. However, authors report that reprecipitated PANI has very low solubility. Ito and Murata [142] have prepared sulfonated polyaniline that can be dissolved up to 88 g/L in water. They adapted a difficult procedure to sulfonate the emeraldine base and solubility of the resulting material depends on the S/N ratio. However, the conductivity of PANI is low in the range of 0.02 to 1×10^{-5} S cm^{-1}. Recently, Athawale and coworkers [146] have synthesized polyaniline co-doped with acrylic acid but PANI synthesized is soluble only in NMP and *m*-cresol. Six years ago, Ruckenstein and coworkers [86] reported synthesis of PANI co-doped with HCl and DBSA and the resulting material was soluble in chloroform. Conductivity of PANI prepared is as high as 7.9 S cm^{-1} but the solubility is not clearly defined. Sathyanarayana and coworkers [84, 124] have used benzoyl peroxide as oxidizing agent for polymerization of aniline with many organic and mineral acids as dopants in good yield and conductivity. The weakly polar organic solvent used by them was either chloroform or a mixture of toluene and isooctane. However, the resulting polymers have low solubility and the authors have not studied PANI doped with DBSA.

5.7 Aim and Scope of the Work

The main goal of the work presented in this dissertation is to synthesize a completely soluble polyaniline. The aim has been achieved by employing a new inverse emulsion polymerization pathway for the synthesis of PANI doped with DBSA using benzoyl peroxide as oxidizing agent. Benzoyl peroxide has been used because of its superiority over the conventional ammonium persulfate (discussed in Section 5.4.1). DBSA has been selected as dopant because of its recognition in improving the solubility of PANI and also its use as a surfactant. An organic component, mixture of toluene+2-propanol, constitutes

the continuous phase of the inverse emulsion. The resulting polymer is completely soluble in chloroform and in 2:1 mixture (vol/vol) of toluene+2-propanol. Spectroelectrochemical investigations of chemically synthesized PANI have successfully been carried out which give a better comparisons with their electrochemically synthesized counterparts.

DBSA, which has been extensively used to dope PANI in order to improve the solubility of PANI-ES has so far, not been used to dope polytoluidines. One of the possible reasons would be the steric factor arising from the methyl substituent of the polymer backbone. In this dissertation, the above described inverse emulsion polymerization technique is also employed to synthesize copolymers of aniline and *o*-toluidine. DBSA has been retained as dopant and surfactant in order to evaluate its efficiency to dope polymer backbone where methyl group exerts steric hindrance to the bulky dopant. The resulting poly(aniline-*co-o*-toluidine) (PAT) is soluble in weakly polar solvents such as chloroform. Spectroelectrochemical behavior of the chemically synthesized copolymers has been studied which is very much essential to understand the structural/conformational differences between the chemically and electrochemically synthesized copolymers.

Chapter 6

Experimental

6.1 Chemicals

The details of aniline, DBSA, deionized water and ITO-coated glass sheets have already been given in Section 2.1 (Part I, Chapter 2). *o*-Toluidine (Merck) was distilled under reduced pressure and stored under nitrogen. Tetrabutylammoniumtetrafluoroborate (Bu$_4$NBF$_4$, Aldrich) and fluoroboric acid (as diethylether complex, Fluka) were used as received. All other chemicals were of analytical grade and used as procured.

6.2 Synthesis

6.2.1 Synthesis of PANI-DBSA

The reaction sequence involved in the formation of a reverse micelle and polymerization of aniline is described in Scheme 6.1 (Page 68). In a typical experiment, 0.303 g of benzoyl peroxide (0.025 **M**) was added to a 100 mL round-bottomed flask containing 35 mL of toluene. The mixture was kept under mechanical stirring. 10 mL of 2-propanol, 1.165 mL of DBSA (0.05 **M**) and 0.05 mL of aniline (0.01 **M**) were added to the above mixture. 5 mL of water were added to this clear solution to form an inverted emulsion. Here aniline-DBSA salt and 2-propanol in water form the dispersed phase whereas benzoyl peroxide and 2-propanol in toluene form the continuous phase. The reaction mixture gradually turns green in 2.5 hours and the stirring was continued for 28 hours at room temperature. At the end of the reaction, organic phase containing the polymer was separated and 50 mL of acetone were added to it. PANI phase, which is relatively denser, was then separated from the acetone phase. The separation process was repeated four times and the solvent associated with PANI was evaporated at room temperature for 24 hours in a petridish. A small amount of acetone was added to a thick coherent film of PANI which then breaks into flakes. The larger flakes were separated by hand picking whereas the smaller particles were separated by filtration and dried in an oven at 50 °C for 4 hours.

Polyanilines with different mole ratios of DBSA to aniline have been prepared in the same way by keeping constant the oxidant-to-monomer ratio and by varying the con-

centration of DBSA. Concentrations of aniline, DBSA and benzoyl peroxide in the feed and the codes assigned to different PANI-DBSA salts are given in Table 6.1.
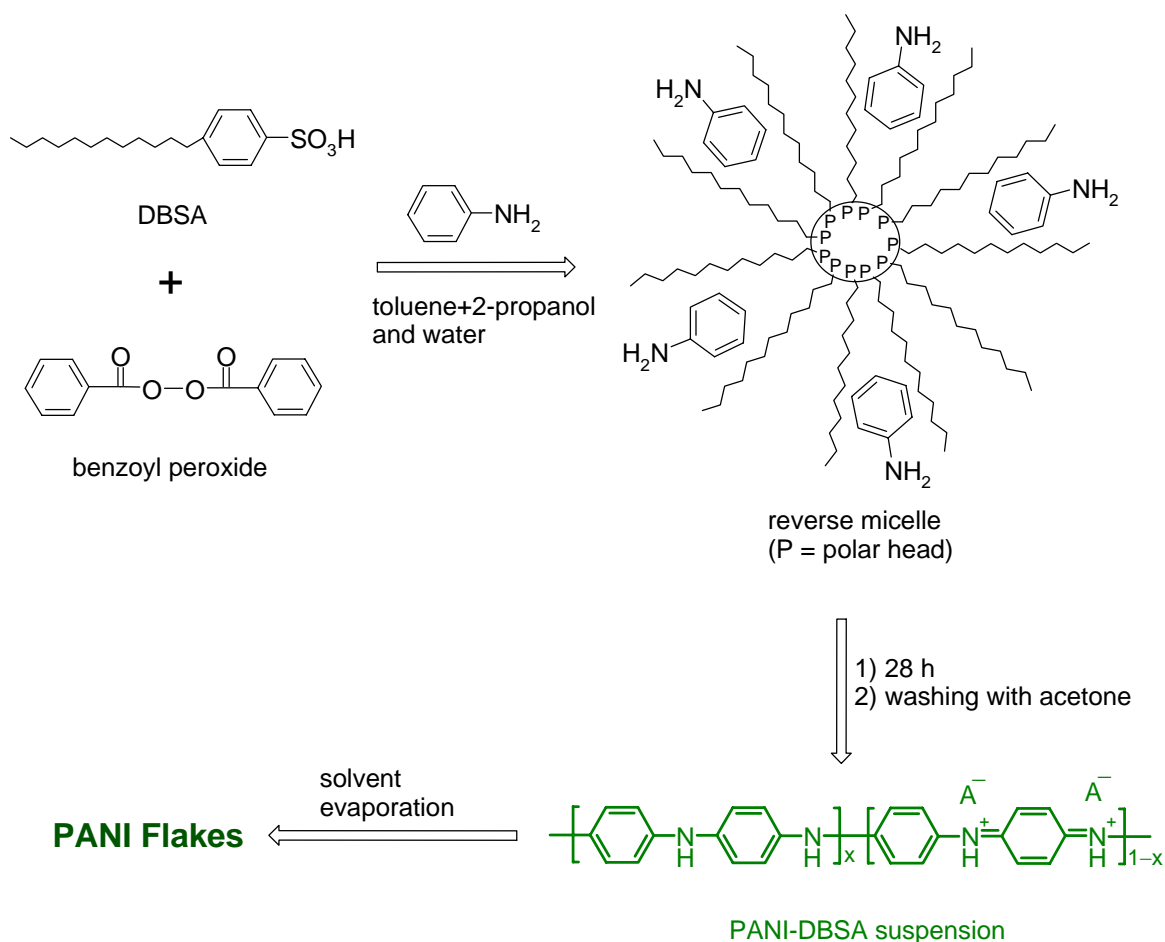
Scheme 6.1. Reaction scheme for the formation of reverse micelle and polymerization of aniline.

Table 6.1. Feed concentrations of the reactants, feed ratio of DBSA to aniline and the codes assigned to different PANI-DBSA salts.

Sl No.	Aniline (M)	DBSA (M)	$(C_6H_5CO)_2O$ (M)	[DBSA]/[Aniline]	Sample code
1	0.01	0.05	0.025	5	TIP-5
2	0.01	0.07	0.025	7	TIP-6
3	0.01	0.10	0.025	10	TIP-7

6.2.2 Synthesis of Poly(aniline-*co-o*-toluidine) (PAT)

Copolymers of different compositions were synthesized using the above mentioned procedure, by varying the molar ratios of monomers in the feed and keeping constant the

total concentration of the monomer (Table 6.2). Molar feed ratio of the dopant to monomer is also fixed to 7. As a representative of the system, synthesis of a copolymer of 1:1 molar ratio of aniline to *o*-toluidine is described below.

Benzoyl peroxide (0.605 g; 0.025 **M**) was added to a 250 mL round-bottomed flask containing 70 mL of toluene and kept under mechanical stirring. 2-propanol (20 mL) and DBSA (3.26 mL; 0.07 **M**) were added to the above mixture followed by the addition of aniline (0.046 mL; 0.005 **M**) and *o*-toluidine (0.054 mL; 0.005 **M**). 10 mL of water were added to this clear solution to form an inverted emulsion. The reaction mixture gradually turns green in ~2 hours and stirring was continued for 28 hours at room temperature. In the end, the organic phase containing the copolymer was separated, washed, solvent evaporated as mentioned in section 6.2.1. The resulting copolymer was dried in an oven at 50 °C for 4 hours.

Homopolymers of aniline and *o*-toluidine were synthesized in a similar fashion maintaining a constant concentration (0.01 **M**) of the monomer. Name of the hom- and copolymers have been abbreviated and tabulated in Table 6.2.

Table 6.2. Molar concentration of the monomers in the feed and the codes assigned to the homo and copolymers.

Sl No.	Aniline (**M**)	*o*-Toluidine (**M**)	Sample code
1	0.01	0	TIP-6
2	0.07	0.03	PAT-73
3	0.05	0.05	PAT-55
4	0.03	0.07	PAT-37
5	0	0.01	POT-6

6.3 Characterization

Elemental analysis was performed using an elemental analyzer (Vario EL; Elementar Analysen Systeme GmbH, Hanau).

UV-Vis spectra were recorded using a Shimadzu 2100 PC spectrophotometer. A quartz cell of 1 cm path length and polymer/copolymer dissolved in different solvents were used. For the *in situ* UV-Vis measurements, PANI/copolymer/POT dissolved in $CHCl_3$ were drop-coated on clean ITO-coated glass sheets that were subsequently used as working electrodes. A quartz cell of 1 cm path length fitted with a platinum wire as counter elec-

trode and saturated calomel electrode (SCE) connected *via* salt bridge as reference electrode served as a three-electrode cell. *In situ* measurements were carried out under ambient conditions.

Cyclic voltammograms were recorded under nitrogen atmosphere in a three-electrode H-cell using a custom built potentiostat connected to a computer with an AD/DA converter. CVs were recorded in three different 1 **N** aqueous acids (sulfuric, perchloric and hydrochloric acids) and in a non-aqueous electrolyte solution. For aqueous systems, polymer/copolymer dissolved in chloroform and drop-coated onto a glassy carbon electrode (GCE) was used as working electrode. A Pt sheet and a saturated calomel electrode were used as counter and reference electrodes, respectively. For non-aqueous systems, polymer/copolymer dissolved in $CHCl_3$ and drop-coated onto a Pt sheet was used as working electrode. Pt sheet electrode and Ag/AgCl in acetonitrile were used as counter and reference electrodes, respectively. CVs were recorded in acetonitrile containing 0.1 **M** Bu_4NBF_4 and 0.075 **M** HBF_4 as supporting electrolyte.

For *in situ* conductivity measurements, a two-band gold electrode [27, 147], a gold sheet electrode and Ag/AgCl in acetonitrile were used as working, counter and reference electrodes, respectively. Polymer/copolymer dissolved in chloroform was drop-coated on gold two-band electrode and dried at room temperature for 30 minutes prior to the measurements. A d.c. voltage of 10 mV was applied to the two-band electrode (Gap between the two strips is ~0.05 mm). The current flowing across the band was measured using an I/V converter with an amplification factor *(Fac)* ranging from 10^2 to 10^6. The film resistance R_x (ohm) is related to the measured voltage U_x and amplification factor *Fac* according to the equation:

$$R_x = (0.01 \times Fac)/U_x$$

Electrode potential was increased stepwise by 100 mV and after approximately 5 min the electrochemical cell was cut off the potentiostat. Conductivity measurements were carried out in acetonitrile containing 0.1 **M** Bu_4NBF_4 and 0.075 **M** HBF_4 as supporting electrolyte.

Fourier transform infrared (FTIR) spectra were recorded with a Perkin-Elmer FTIR 1000 spectrometer using standard KBr pressed pellet technique. The spectra obtained were baseline corrected for better visibility.

In situ Raman spectra were measured on an ISA 64000 spectrometer equipped with a liquid nitrogen cooled CCD camera detector at a resolution of 2 cm^{-1}. Samples were illuminated with 476.5 nm (in the case of PANI) and 514.5 nm (in the case of PAT) laser light from an Argon ion laser Coherent Innova 70. A special three compartment cell containing 1 **N** H_2SO_4 was used in the measurements. Polymer/copolymer dissolved in $CHCl_3$ was drop-coated on a platinum disc electrode polished with γ-Al_2O_3 (0.3 μm) subsequently used as working electrode. A platinum sheet electrode and a saturated calomel electrode were used as counter and reference electrodes, respectively. The electrochemical cell was purged with nitrogen for 6 minutes prior to the measurements. The Raman spectra thus obtained were smoothed and baseline corrected for better visibility.

Scanning electron microscope (SEM) pictures of the solid polymer flakes were recorded using a Philips SEM 515 electron microscope. No gold or platinum coating was applied prior to recording the images. Transmission electron microscope (TEM) images were recorded on a Philips CM 20 FEG transmission electron microscope. The samples were prepared by depositing a drop of well diluted PANI in chloroform on a carbon (1 0 0) coated copper grid (3 mm diameter and 10 μm thick; Plano GmbH, Germany) and dried in an oven at 50 °C for two hours.

Chapter 7
Results and Discussion

7.1. Solubility

All the PANI-DBSAs and poly(aniline-*co-o*-toluidine)s synthesized in the present way are of high purity since excess of benzoyl peroxide, DBSA, oligomers and byproducts of oxidation were readily removed by acetone, which was used to wash the organic phase.

(a) Solubility of PANI-DBSA

Solubility of conducting polymers is always a matter of discussion and many reports have been published in the literature discussing the solubility of PANI [86, 142, 144, 146]. Normally, when a pinch of PANI doped with mineral or organic acid is added to highly polar solvents such as dimethyl sulfoxide (DMSO) or N-methylpyrrolidone (NMP), part of the polymer material (presumably oligomeric or of low molecular weight) is dissolved but a residual mass is always present in the mixture. Such a mixture is filtered and the solubility of PANI (g/L) is calculated by weighing the residual mass. In this article when we quote 'completely soluble' we mean, that the PANI is dissolved in the solvent without leaving any solid residue. PANI-DBSA produced in the present way is completely soluble in chloroform and a 2:1 mixture of toluene+2-propanol. In both the solvents, it gives a clear green solution (Figure 7.1a; Page 73), which can be spin- or drop-coated on metallic and glass substrates. Such films show strong adherence to the substrate. Figure 7.1b shows a photograph of a dip-coated PANI film on a glass substrate. The transparency of the material is confirmed by the clear visibility of the text (PANI-DBSA), which is nearly eight to ten centimeters behind the film. Slight solubility is also observed for PANI-DBSA in NMP and in dichloromethane.

(b) Solubility of Poly(aniline-co-o-toluidine)

It is well known that copolymerization of aniline and toluidine improves the solubility of PANI, especially PANI-EB form, in solvents such as NMP, DMSO and THF [126, 136]. A partial solubility of PATs in their ES form in DMSO, DMF, NMP, THF, CHCl$_3$

etc. has also been reported [139, 148]. In most cases, the partial solubility of ES form of the copolymer arises from the undoped segments of the polymer backbone and can be easily confirmed from the UV-Vis spectra where strong band characteristic of EB form is observed [139].
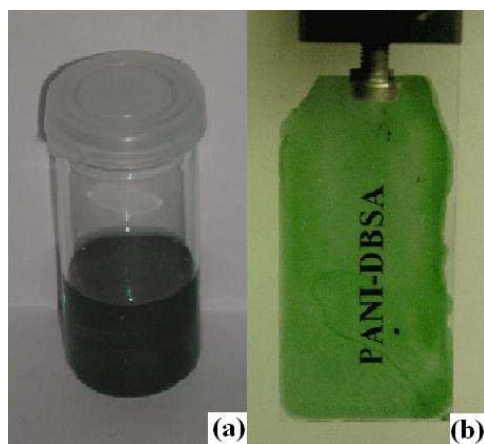

Figure 7.1. (a) Solution of PANI in a 2:1 mixture of toluene+2-propanol and (b) its dip-coated film on glass substrate.

Poly(aniline-*co-o*-toluidine)s, synthesized using the present protocol, are soluble in weakly polar solvents such as chloroform and a 2:1 mixture of toluene+2-propanol. They also show partial solubility in NMP and dichloromethane. Strong green coloration of the solution indicates that solubility is mainly due to ES form of the polymer backbone. However, solubility of the copolymers is lower than that of PANIs. A clear green solution of the copolymer can be easily spun- or drop-coated on a glass or metal substrate to get a coherent thin/thick film. It is well established that solubility of copolymer increases with increase in the feed concentration of *o*-toluidine [136]. Interestingly, an opposite trend has been observed in the present study. Solubility order for PANI, POT and copolymers is TIP-6 ~ PAT-73 > PAT-55 > PAT-37 > POT-6. In order to find out the solubility, constant known amount of each copolymer was added to 5 mL of chloroform, stirred for two minutes and filtered. The difference in the solubility is evident from the photographs of their solution as shown in Figure 7.2. Lower solubility of POT and copolymers containing higher fraction of *o*-toluidine may be due to their morphology and will be discussed in Section 7.10.
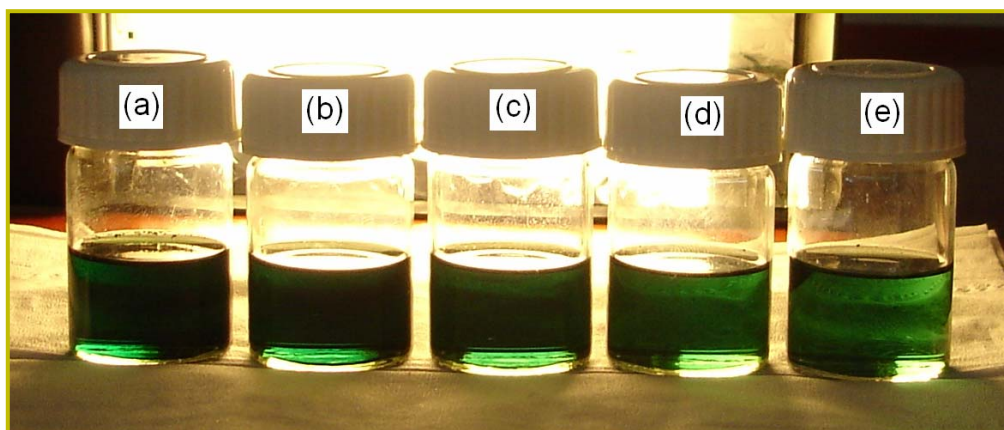
Figure 7.2. Photographs of solutions of copolymers in chloroform (a) TIP-6, (b) PAT-73, (c) PAT-55, (d) PAT-37 and (e) POT-6.

7.2 Elemental Analysis

The elemental composition (weight %) obtained from the elemental analysis was converted into molar compositions and sulfur was taken as reference (S = 1) to calculate the N/S ratio of a sample. N/S ratio obtained in this way was also used to find out the expected elemental composition and the extent of doping (%) of polymer samples.

(a) PANI-DBSA

The elemental compositions obtained from elemental analysis are in good agreement with the expected elemental composition (Table 7.1). Increase in the DBSA/aniline mole ratio from 5:1 to 7:1 does not affect the doping (40 % in both the cases) but by changing the mole ratio to 10:1, the doping is increased by 10 % (50 % doping). Doping in the range of 40 to 50 % always yields very good conductivity for PANI.

Table 7.1. Percentage yield, conductivity, experimental and calculated elemental composition of PANIs with different mole ratios of DBSA/aniline.

PANI	Yield (%)	Conductance $(1/R\ \Omega^{-1})$	C, H, N, S (experimental)	C, H, N, S (expected) Aniline unit	DBSA unit	Percentage doping
TIP-5	39	0.102	$C_{34}H_{43}N_{2.5}S$	$(C_6H_6N)_{2.5}$	$C_{18}H_{29}S$	40
TIP-6	45	0.096	$C_{33}H_{40}N_{2.5}S$	$(C_6H_6N)_{2.5}$	$C_{18}H_{29}S$	40
TIP-7	61	0.129	$C_{33}H_{42}N_2S$	$(C_6H_6N)_2$	$C_{18}H_{29}S$	50

(b) Poly(aniline-co-o-toluidine)

Elemental composition of the homo- and copolymers obtained by the C, H, N and S analysis are in good agreement with the expected values. Expected values were calculated taking into account the molar ratios of the monomers and N/S ratio obtained from the elemental analysis. Both expected and experimental elemental compositions are tabulated in Table 7.2. A close agreement between the experimental and calculated values qualitatively suggests that the ratio of the comonomer units in the polymer depends on the molar feed ratio of the monomers.

Table 7.2. Percentage yield, conductance, extent of doping (%) and experimental and expected elemental compositions of PANI, POT and PATs.

Sample	Yield (%)	Conductance* ($1/R \ \Omega^{-1}$)	Elemental composition	C, H, N, S (expected)		Percentage doping
				Polymer unit	DBSA unit	
TIP-6	45	2.05×10^{-2}	$C_{16}H_{14}N_{2.5}S$	$C_{15}H_{15}N_{2.5}$	$C_{18}H_{29}S$	40
PAT-73	44	1.54×10^{-3}	$C_{18}H_{17}N_{2.6}S$	$C_{16.5}H_{16.5}N_{2.6}$	$C_{18}H_{29}S$	39
PAT-55	57	2.33×10^{-4}	$C_{18}H_{17}N_{2.4}S$	$C_{15.6}H_{15.6}N_{2.4}$	$C_{18}H_{29}S$	42
PAT-37	46	1.10×10^{-4}	$C_{21}H_{21}N_{2.7}S$	$C_{18.1}H_{18.1}N_{2.7}$	$C_{18}H_{29}S$	37
POT-6	43	6.72×10^{-3}	$C_{17}H_{19}N_{2.6}S$	$C_{18.2}H_{18.2}N_{2.6}$	$C_{18}H_{29}S$	38

* Minimum conductance value obtained during the ongoing cathodic potential sweep in the first cycle.

Extent of doping in homopolymers as well as in copolymers is constant and is in the range of 37-42 %. A low doping has been expected for POT and copolymers having higher fraction of *o*-toluidine due to the steric hindrance caused by methyl group which disfavors the presence of bulky counter ions in the vicinity of −NH group of polymer backbone. Interestingly, results of elemental analysis rules out the above expectation and hence, it is assumed that doping in case of POT and copolymers is controlled by a conformational rearrangement of the polymer (e.g. from planar to twisted conformation). Su *et al.* [140] have reported that helical conformation of PANI was inverted when *o*-toluidine units were introduced into the polymer main chain. The copolymers in this case were synthesized by chemical oxidation of mixture of monomers using conventional ammonium persulfate as oxidant and chiral CSA as dopant. These results support the above assumption and, therefore, DBSA is considered as an efficient dopant for POT.

7.3 Polymerization Yield

For the calculation of yield we assume 100 % doping of the nitrogen atoms in the polymer backbone (1:1, **M/M** of monomer and DBSA) and the percentage yield was calculated using the equation:

$$\text{Percentage yield} = \frac{\text{Weight of homo- or copolymer}}{\text{Weight of } x\,\mathbf{M} \text{ monomer} + \text{Weight of } x\,\mathbf{M} \text{ DBSA}} \times 100$$

(a) Yield of PANI-DBSA

PANIs synthesized by the present method are obtained in an average yield (40–60 %; Table 7.1; Page 74). The reaction was carried out for a period of 28 hours because the yield obtained is optimal after this reaction period. During the separation and purification of PANI using acetone (Section 6.2.1; Page 67), a small amount of PANI remains associated with the acetone and, therefore, the reported yields of PANI are average values. Yield increases as the molar ratio of DBSA/aniline in the feed increases. For example, when the ratio of DBSA/aniline is changed from 5:1 to 10:1, yield increases from 39 to 61 %. This steep increase in the yield may be due to decreased pH and higher stability of the emulsion at higher DBSA concentration.

(b) Yield of Poly(aniline-co-o-toluidine)

Percentage yield of the homopolymers of aniline and *o*-toluidine and their copolymers lies in the range of 45-60 % (Table 7.2, Page 75). An optimal yield was obtained when the reaction was carried out for 28 h at the oxidant-to-monomer ratio of 2.5. All the homo- and copolymers were produced with the same yield except PAT-55 whose yield was ~10 % higher than the others. Su and coworkers [140] have reported highest yield for the copolymer containing equimolar feed ratios of aniline and *o*-toluidine, however, above or below this ratio, the percentage yield of the copolymer decreased. Huang and coworkers [136] reported that yield of copolymers of aniline and *o*-toluidine (10–13 %) is much lower than that of POT (34 %). The decrease in yield was attributed to the negative effect of oligoanilines and aniline radicals in the reaction mixture. 9–14 % yield was also observed by Wei *et al.* [126] for copolymers of aniline and *o*-toluidine. Relatively better yields obtained in the present case may be due to the effective protonation/complexation of DBSA with polymer main chain.

7.4 *In Situ* Electrical Conductivity

(a) Conductivity of PANI-DBSA

In situ resistance values of all PANIs synthesized by the present method are in the order of 10 Ω ($1/R = 0.1$; Table 7.1; Page 74), which is much higher than the ones reported in the literature [115, 142, 145, 149]. PANI-DBSA synthesized *via* gelation method has shown conductivity of the same order of magnitude but excess of dopant always associated with the polymer reduces the chemical purity of the polymer [106]. Conductance of PANI is proportional to the thickness of PANI film bridging the two bands, however, beyond certain thickness, conductivity is not much affected any more. Higher conductivities in the present case may be due to the bulky dopant DBSA and the preparative method chosen.

Figure 7.3 (Page 78) shows a plot of log R *vs* $E_{Ag/AgCl}$ for TIP-7 in an anodic and cathodic sweep in the second potential cycle. As the applied potential increases, log R remains unchanged until the offset potential for the first oxidation wave in the CV is reached (Figure 7.4, Page 78). Further increase in the potential causes a sharp decrease in log R (indicating a sharp increase in conductivity) until the offset of the second oxidation wave in the CV is reached. Resistance increases when the applied potential is further increased. During the cathodic sweep resistance values follow CV and the minimum value of resistance is almost the same as in the case of the anodic sweep. This indicates that stability of the PANI bridging the two bands is very good. A similar trend is observed for polyaniline synthesized electrochemically in non-aqueous solvents [132]. However, the minimum resistance during the cathodic sweep is higher than during the anodic sweep. It is also observed that conductivity of the PANI film improved after the first potential cycle. This may be due to the conformational changes in the chemically oxidized PANI bridging the two bands induced by the applied potential cycle. The higher potential limit in the conductivity measurements ($E_{Ag/AgCl} = 1.8$ V) slowly damages the film thereby reducing the conductivity after second potential cycle. Increase in the mole ratio of DBSA/aniline in the feed does not influence the conductivity of the film. CVs recorded after the conductivity measurements reveal that the conductivity is directly proportional to the anodic peak current. With an increasing amount of PANI bridging the two bands, the anodic peak response in CV is higher and thus measured conductivity is higher.

Our attempt to measure the resistance values of PANI in aqueous acids failed; the log R values were in the range of 5 and 6 for all applied potentials. Such different behavior of conductivity in aqueous and non-aqueous electrolyte solutions is due to the presence of

the long chain bulky dopant. This influence was later confirmed by cyclic voltammetry studies. Polar groups of this dopant are engaged in protonation of the nitrogen atoms whereas the non-polar aliphatic chain is extended to the environment leading to a repulsive interaction with aqueous electrolyte solution.
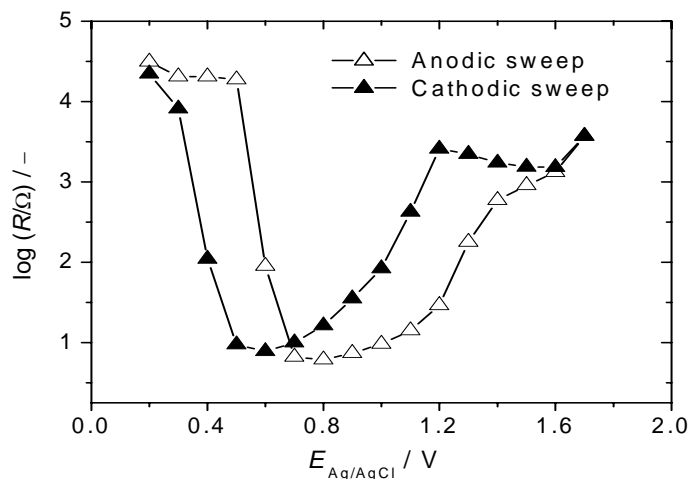
Figure 7.3. Plot of log R *vs* $E_{Ag/AgCl}$ of TIP-7 during an ongoing anodic followed by a cathodic potential sweep in the second cycle.
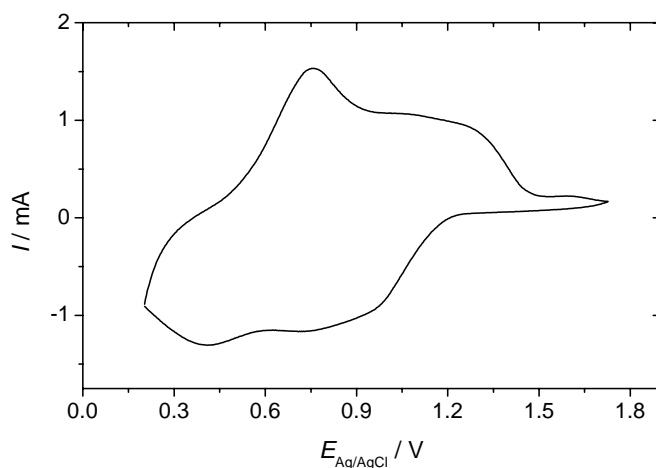
Figure 7.4. CV of TIP-7 modified gold double band electrode in acetonitrile containing 0.1 **M** Bu_4NBF_4 and 0.075 **M** HBF_4.

(b) Conductivity of Poly(aniline-co-o-toluidine)

Plots of log R *vs* applied potential for PANI (TIP-6), POT (POT-6) and copolymers (PAT-37 and PAT-73) are shown in Figure 7.5 (Page 80). *In situ* conductivity of POT

(minimum resistance observed during a potential sweep) is almost an order of magnitude lower than that of PANI. Such a decrease in conductivity for POT is due to the steric effect caused by methyl group of the polymer chain [126]. It can also be attributed to the decrease in conjugation length of the polymer backbone and to the variation in molecular conformation of polymer main chain [139]. The minimum resistance of the copolymers is in the range of 10^3–10^4 ohm ($1/R = 10^{-3}$–10^{-4} Ω^{-1}). When the concentration of o-toluidine in the feed increases, conductivity of the copolymer decreases (reflected from the respective increase in the resistance) indicating that more and more o-toluidine is incorporated in the copolymer. These observations are similar to the previously reported ones [126, 141]. Conductivity of POT after the first potential cycle, unlike PANI, did not show any improvement but rather decreased. This is due to the faster degradation of POT at the higher potential limit of the conductivity measurements. Conductance values obtained during the cathodic sweep of the first potential cycle are given in Table 7.2 (Page 75). A decrease in conductivity during cycling is also observed for copolymers containing higher concentration of o-toluidine in the feed.

The plot of log R as a function of applied potential (Figure 7.5; Page 80) can be correlated to the cyclic voltammogram (CV) recorded after the conductivity measurements (Figure 7.6; Page 80). During an ongoing positive potential sweep, a sharp increase in the conductivity is observed after a certain potential ($E_{Ag/AgCl} = 0.4$–0.6 V). The first oxidation wave in the CV is observed in the same potential region. A decrease in conductivity observed in the higher potential region ($E_{Ag/AgCl} = 0.8$–1.2 V) corresponds to the second oxidation wave of the CV. The variation of conductivity arising from the change in the applied potential in a reverse cathodic sweep also corresponds to the cathodic wave of the CV. Resistance values of PANI stay close to the minimum resistance in a potential range of $E_{Ag/AgCl} = 0.7$–1.2 V; i.e., the potential window for PANI is ~500 mV (during a positive going sweep). A potential window of similar magnitude was also observed for electrochemically synthesized PANI [150]. The potential window for POT is ~400 mV whereas in case of copolymers, it lies in the range of ~400–500 mV (Figure 7.5). Electrochemically synthesized POT shows very small potential window and the plot of resistance vs electrode potential is almost parabolic in shape [42]. The larger potential window observed for POT may be due to the different conformational arrangement of the polymer chain arising from the different synthetic approach and bulky dopant chosen.
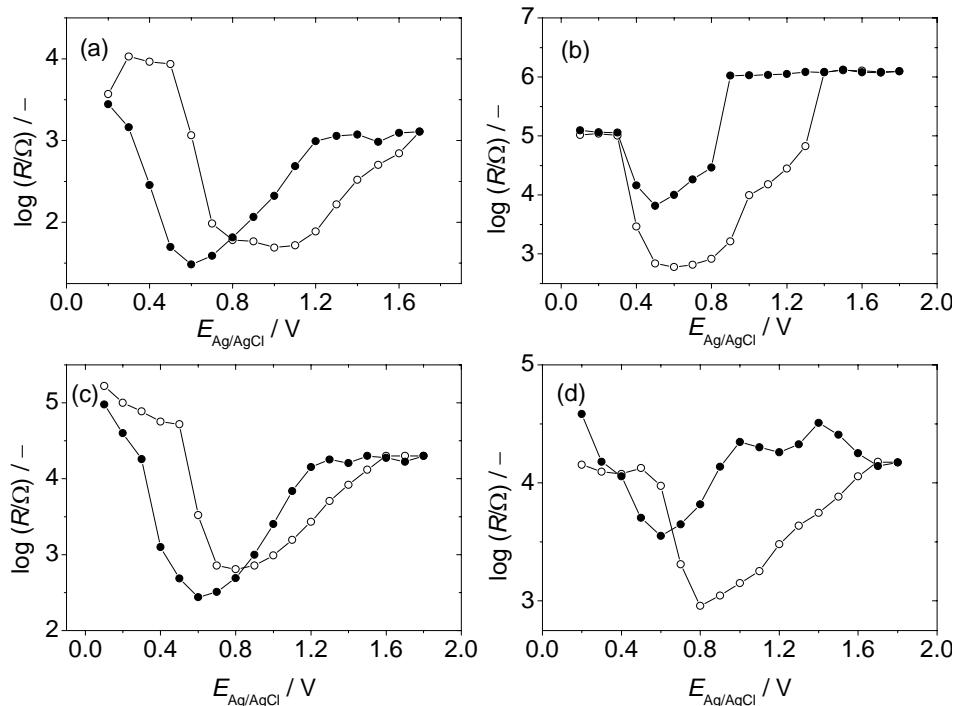
Figure 7.5. Plots of log R *vs* applied potential of (a) TIP-6, (b) POT-6, (c) PAT-73 and (d) PAT-37 during a ongoing anodic (—○—) followed by a cathodic (—●—) potential sweep in a second cycle.
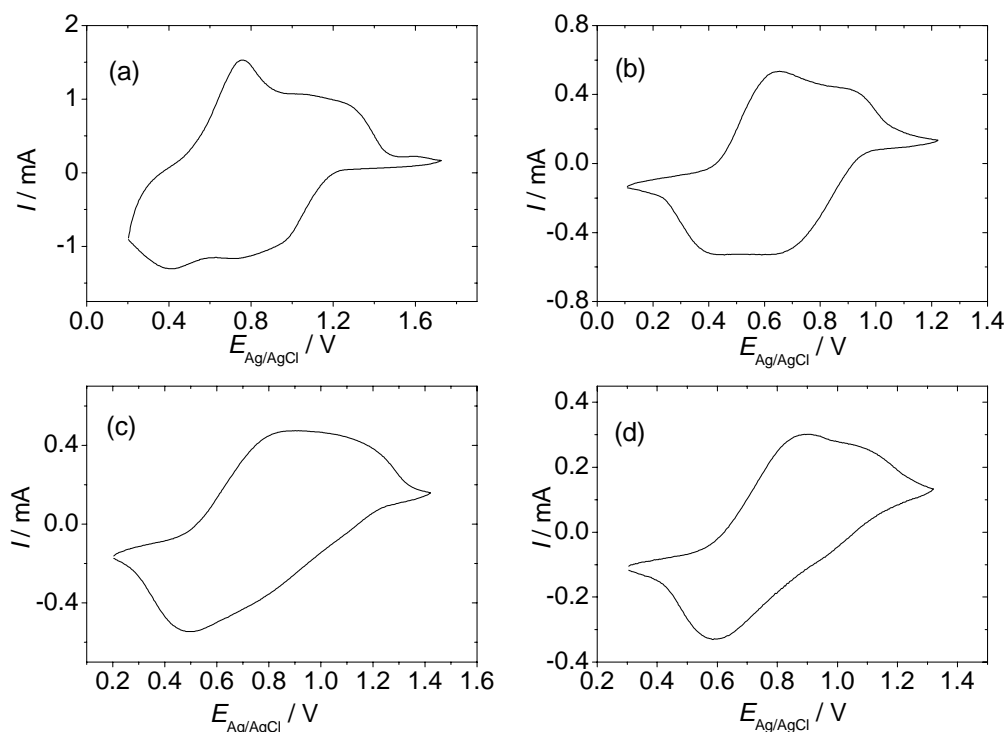

Figure 7.6. Cyclic voltammograms of (a) TIP-6, (b) POT-6, (c) PAT-73 and (d) PAT-37 modified gold double band electrode after the conductivity measurements recorded in acetonitrile containing 0.1 **M** Bu₄NBF₄ and 0.075 **M** HBF₄. Scan rate = 50 mV s⁻¹.

As in the case of PANIs, conductivity of the copolymer samples also depends on the quality of the film bridging the two gold strips and, thus, corresponds to the peak current of the first oxidation wave (in CV). However, above certain film thickness, conductivity of the copolymer is not much affected anymore. Similar to PANI, films processed from poly(aniline-*co-o*-toluidine)s also show very poor electrical conductivity in acidified aqueous electrolytes.

7.5 UV-Vis Spectroscopy

(a) UV-Vis Spectra of PANI-DBSA

Figure 7.7 (a and b; Page 82) shows absorption spectra of polyaniline with different molar ratios of DBSA to aniline in chloroform and in a 2:1 mixture of toluene+2-propanol. Polyaniline dissolved in chloroform or in a toluene+2-propanol mixture (2:1) shows three bands characteristic of emeraldine salt. A band at 350 nm arises from $\pi* \leftarrow \pi$ transition while the bands at 420 nm and 800 nm originate from the charged cationic species known as polarons [86]. In addition, a hump at around 735 nm is observed for TIP-5 and TIP-6 in chloroform with unknown cause. PANI dissolved in chloroform shows a hypsochromic shift when the mole ratio of DBSA in the feed is increased from 5:1 to 10:1 (Figure 7.7a; Page 82). Such a blue shift was observed by Yin and Ruckenstein [86] for PANIs codoped with HCl and DBSA. They suggested that an increase in the amount of HCl in the polymer increases the compact coil conformation of the polymer leading to a hypsochromic shift. Increase in the dopant ions favors the compact coil conformation and thus the absorption maximum is shifted to lower wavelengths. Such hypsochromic shift is not observed for PANI dissolved in a 2:1 mixture of toluene+2-propanol (Figure 7.7b; Page 82). However, interestingly the ratio of intensity of the band at 800 nm to the band at 350 nm is much higher for TIP-7 indicating a higher concentration of polaronic species generated from higher doping (Table 7.1, Page 74).

Figure 7.8a (Page 83) shows UV-Vis spectra of TIP-5 dissolved in a 2:1 mixture of toluene+2-propanol at different concentrations of PANI. At lower concentrations of the polymer in the solution, a new band characteristic of PANI-EB appears at ~650 nm and the low energy polaron band (760–820 nm) shows a bathochromic shift (> 50 nm). The band at 345 nm indicative of the extent of conjugation in the polymer backbone undergoes a blue shift with decreasing concentration of PANI. However, such changes were not observed for PANI dissolved in chloroform except for a small red shift of the low energy po-

laron band (~7 nm) (Figure 7.8b; Page 83). These observations reveal the interaction of a 2:1 mixture of toluene+2-propanol with the polymer. The possible interaction between PANI and solvent in this case is hydrogen bonding between −N atoms of PANI and −OH group of the solvent. Athawale and coworkers [146] observed such interactions for acrylic acid doped polyaniline dissolved in *m*-cresol and in NMP where hydrogen bonding deprotonates the polymer chain. The ratio of absorbances of the bands at 330–350 and 760–820 nm (A_{800}/A_{350}) reveals the extent of protonation of the polymer backbone and the influence of the solvent on protonation. When chloroform is used as a solvent, this ratio does not depend on the amount of PANI dissolved, whereas, in case of a 2:1 mixture of toluene+2-propanol, the ratio increases as the amount of PANI in the solution is increased. For example, the absorbance ratio of TIP-5 increases from 0.6 to 1.4 in 2:1 mixture of toluene+2-propanol but shows a constant value of 1.6 in chloroform. A constant ratio suggests that PANI dissolved in chloroform retains protonation, thereby retaining its electrical properties in solution. However, varying ratios of absorbance for PANI dissolved in 2:1 mixture of toluene+2-propanol proves its non-suitability for diluted solutions. Absorbance ratios of 1.1−1.2 were reported for polyaniline films on glass substrates and for PANI dispersions by Stejskal and Sapurina [151] without any further explanation.
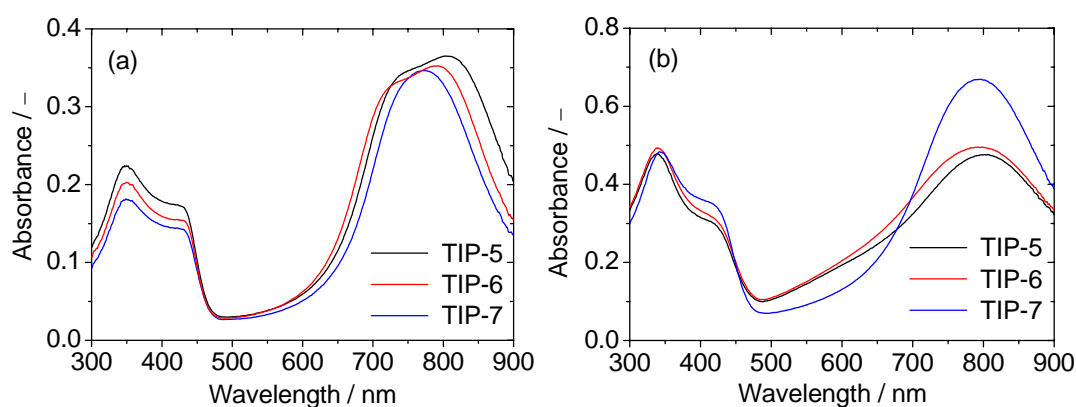

Figure 7.7. Electronic absorption spectra of PANI with different feed ratios of DBSA/aniline recorded in (a) CHCl₃ and (b) 2:1 toluene+2-propanol.

Figure 7.9 (Page 83) shows the plot of ratio of absorbances (A_{800}/A_{350}) as a function of feed ratio of DBSA to aniline. The absorbance ratio exhibits a linear increase with the feed ratio of DBSA to aniline when chloroform is used as solvent whereas a sharp increase is noticed when the feed ratio of DBSA to aniline is changed from 7 to 10 in case of 2:1 mixture of toluene+2-propanol. Higher values of the ratio of absorbances for chloroform
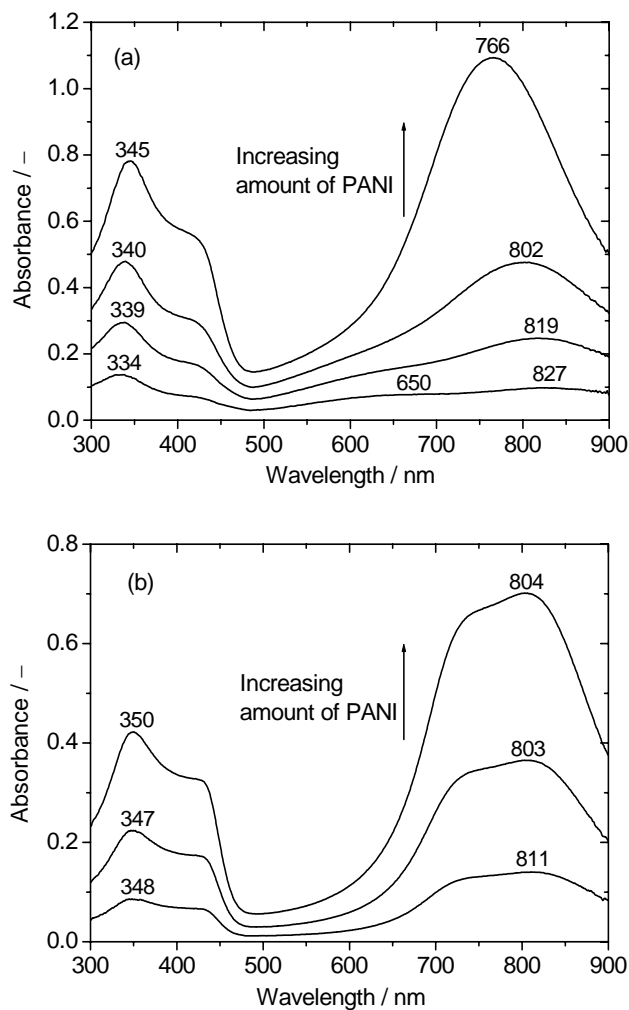
indicate the absence of solvent-solute interaction.

Figure 7.8. Solution state UV-Vis spectra of TIP-5 dissolved in (a) 2:1 mixture of toluene + 2-propanol and (b) chloroform.
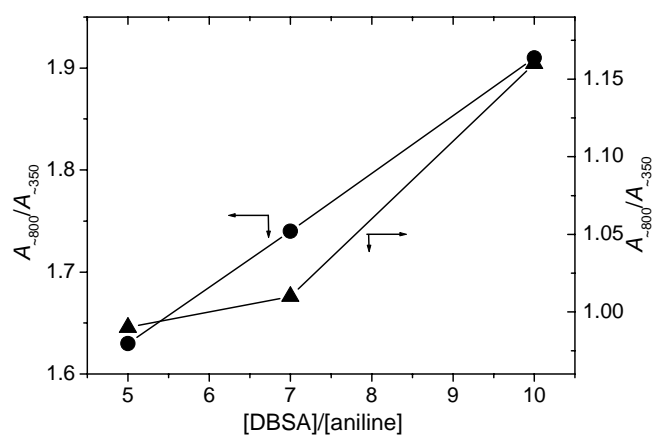

Figure 7.9. Plot of ratio of absorbances at ~800 to ~350 nm *vs* DBSA-to-aniline feed ratio. Solution state spectra of PANI were recorded in chloroform (—●—) and in 2:1 mixture of toluene+2-propanol (—▲—).

(b) UV-Vis Spectra of Poly(aniline-co-o-toluidine)

Electronic absorption spectra of homopolymers of aniline and *o*-toluidine along with copolymer containing equimolar fractions of the comonomers in the feed are shown in Figure 7.10. In chloroform, POT exhibits a band at ~800 nm originating from the polaronic species. In addition, a broad band observed at $\lambda_{max} \approx 385$ nm is probably due to overlapping of two bands originating from radical cations and $\pi* \leftarrow \pi$ transition. In a 2:1 mixture of toluene+2-propanol, these bands appear at ~790 and ~380 nm, respectively. UV-Vis spectra of copolymers in chloroform exhibit three bands in the region of 785–815, 415–425 and 350–355 nm. The λ_{max} values for homo- and copolymers obtained from their UV-Vis spectra in chloroform and a 2:1 mixture of toluene+2-propanol are summarized in Table 7.3 (Page 85).
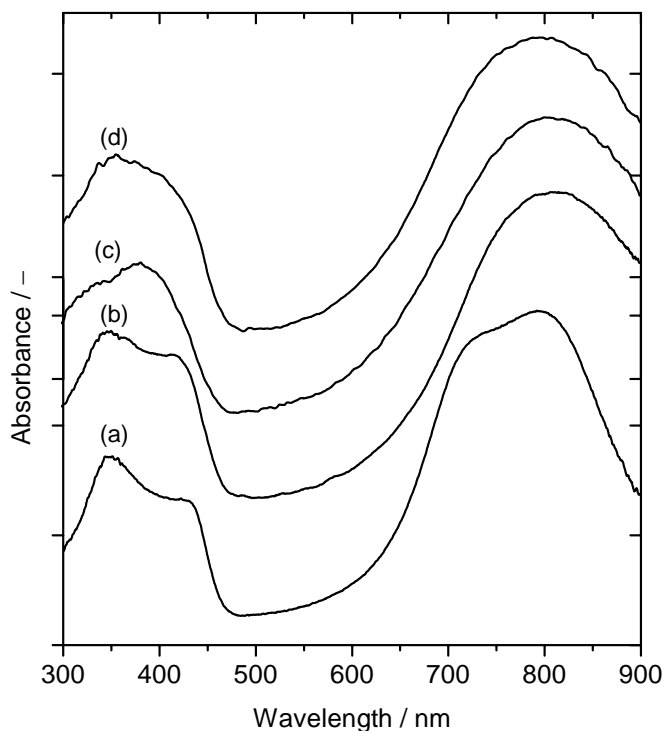

Figure 7.10. Electronic absorption spectra of (a) TIP-6 (PANI), (b) PAT-55, (c) POT-6 and (d) mechanical mixture of TIP-6 and POT-6 recorded in chloroform.

When the feed concentration of *o*-toluidine is increased from 0 to 0.005 **M**, the low energy polaron band registers a bathochromic shift from 790 to 815 nm. Position of this band maximum resembles that of POT when the concentration of *o*-toluidine is further increased. Such different behavior of PAT-55, which was also observed in polymerization yield, may be due to its morphology which is discussed later. Increase in the feed concen-

tration of *o*-toluidine does not influence the position of the ~420 and ~350 nm bands of the copolymers. A similar trend was observed for the spectra recorded in a 2:1 mixture of toluene+2-propanol. A UV-Vis spectrum of a mechanical mixture of PANI and POT was recorded in chloroform in order find out whether the copolymerization produced real copolymers or composites because reactivity of the comonomers is different. A band at 350 nm and an ill defined hump (due to the overlapping of the bands at 380 and 420 nm) is observed in the UV-Vis spectrum (Figure 7.10; Page 84) of the mixture which is essentially different in comparison with the copolymers (PATs) indicating that the materials produced are real copolymers.

Table 7.3. λ_{max} of the UV-Vis absorption bands of homo- and copolymers of aniline and *o*-toluidine recorded in chloroform and a 2:1 mixture of toluene+2-propanol.

Sample code	λ_{max} (nm)						
	Chloroform				2:1 mixture of toluene+2-propanol		
TIP-6	793	737*	425	350	799	409	337
PAT-73	797	755*	425	351	821	412	345
PAT-55	813	–	415	351	825	407	342
PAT-37	806	–	415	351	815	406	339
POT-6	802	–	–	384	790	–	349

* observed as a hump with unknown cause

As discussed in the preceding sections, position of the low energy polaron band (~800 nm) depends strongly on the nature of the solvent and its interaction with the polymer main chain. In a 2:1 mixture of toluene+2-propanol, with gradual increase in amount of PANI dissolved, this band is blue shifted by more than 50 nm but such a blue shift could not be seen for POT. The shift in PANI (at lower concentration) is attributed to the rearrangement of compact coil conformation to an extended coil conformation. The compact coil conformation is preferred at higher concentration of dissolved PANI due to the presence of more counter ions which compete over the interactions between −NH and −OH groups. Presence of the methyl groups on the polymer backbone, due to their steric hindrance, inhibits the interaction between −NH groups of polymer and −OH groups of 2-propanol and, therefore, POT does not exhibit the conformational rearrangement. A similar observation was reported for (+)-CSA doped PANI and POT dissolved in *m*-cresol [140].

Poly(aniline-*co-o*-toluidine)s when dissolved in a 2:1 mixture of toluene+2-

propanol also exhibit hypsochromic shift by 30–60 nm and the magnitude of shift depends on the fraction of *o*-toluidine in the feed. Electronic absorption spectra of PAT-55 dissolved in 2:1 mixture of toluene+2-propanol and chloroform are shown in Figure 7.11. Interestingly, the spectral changes (hypsochromic shift > 50 nm) observed for PAT-55 has more similarity to that of pure PANI and can be attributed to the close resemblance in the morphology of PANI (TIP-6) and PAT-55 which are discussed in section 7.10. An opposite behavior was observed for copolymers of aniline and *o*-toluidine doped with (+)-CSA where the spectral features of copolymers resemble POT [140].
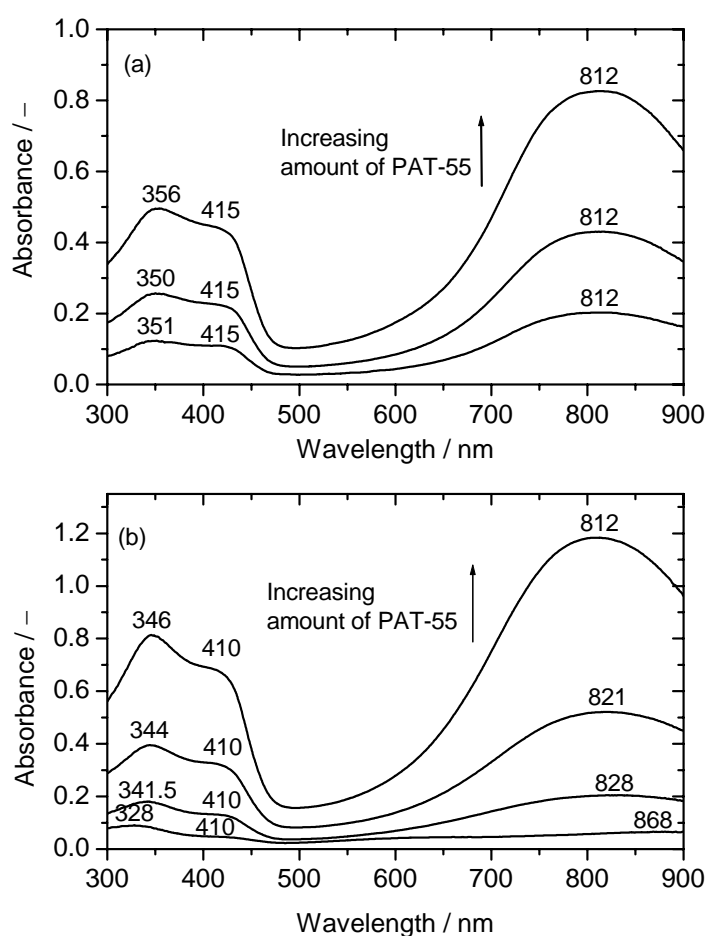

Figure 7.11. Electronic absorption spectra of PAT-55 recorded in (a) chloroform and (b) 2:1 mixture of toluene+2-propanol.

As in the case of PANI, copolymers dissolved in chloroform possess higher absorbance ratios ($A_{\sim800}/A_{\sim350}$) indicating that when dissolved in chloroform, copolymers retain the protonation. In a 2:1 mixture of toluene+2-propanol, the ratio of absorbances depends on the amount of polymer dissolved indicating interaction between the –NH group of

polymer and –OH group of the solvent. However, the absorbance ratios of POT depend neither on the nature of the solvent nor on the amount of the polymer dissolved, which, as mentioned earlier, confirms the absence of conformational rearrangements in this polymer. The ratio of absorbance is ~1.8 and ~1.6 for PANI and POT dissolved in chloroform, whereas, this ratio for copolymers lies in the range of 1.6–1.8. The absorbance ratio of co-polymers containing higher feed concentration of aniline is close to that of aniline while for those containing higher concentration of *o*-toluidine in the feed are close to that of POT. The higher absorbance ratios for POT and copolymers indicate that DBSA, even though a bulky dopant, can effectively dope the polymer backbone overcoming the steric hindrance exerted by methyl groups.

7.6 *In Situ* UV-Vis Spectroscopy

(a) In Situ UV-Vis Spectra of PANI-DBSA in Acidic Electrolyte

Figure 7.12 (Page 88) shows *in situ* UV-Vis spectra recorded in 1 **N** H_2SO_4 at different potentials successively shifted into anodic direction for TIP-7. An absorption band at 800 nm shows a blue shift with increase in the applied potential from $E_{SCE} = -0.2$ to 0.8 V. The gradual blue shift of this band is attributed to the formation of a compact coil structure due to the incorporation of SO_4^{2-} ions. At $E_{SCE} > 0.6$ V, a drastic blue shift is observed which corresponds to the conversion from emeraldine state to pernigraniline state. Dominis *et al.* [152] observed that the absorption maximum of redoped PANI in two different solvents is different. They have attributed this difference to the compact and extended coil conformation of the PANI where the compact coil form shows absorption maxima at higher energies.

Absorbance at 420 nm originates from radical cations showing a maximum value at $E_{SCE} = 0.2$ V indicating maximum concentration. At $E_{SCE} = 0.2$ V, the first oxidation wave peak in the CV has maximum peak current (Section 7.7; Figure 7.19a; Page 95). *In situ* spectral investigations reveal that polarons exists even at $E_{SCE} = -0.2$ V (identified with their 420 nm band) where PANI exists in a completely reduced leucoemeraldine state. Similar trends have been observed for PANI-H_2SO_4 synthesized electrochemically on an indium tin oxide coated glass electrode, however, no explanation has been given for such shifts [87]. Position of the band at 350 nm is influenced by the extent of conjugation in the polymer backbone. Increasing the applied potential from $E_{SCE} = -0.2$ to 0.8 V, this band shifts towards lower energy along with decrease in absorbance.
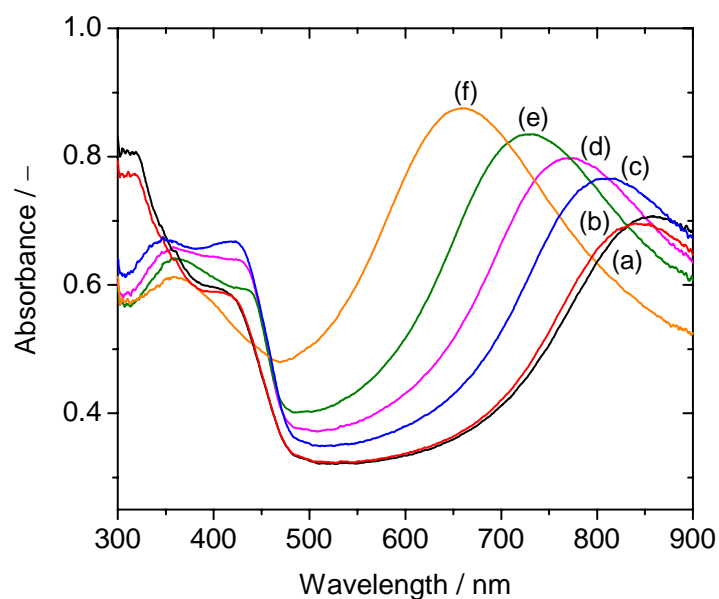
Figure 7.12. *In situ* electronic absorption spectra of PANI (TIP-7) recorded in ongoing anodic potential direction in 1 **N** H_2SO_4. E_{SCE} (V) = (a) −0.2, (b) 0, (c) 0.2, (d) 0.4, (e) 0.6 and (f) 0.8.

In situ electronic absorption spectra were also recorded in the cathodic direction to check the electrochromic reversibility of the polymer film. Figure 7.13 shows plots of λ_{max} and absorbance at λ_{max} *vs* applied potential. It is clear from the figure that PANI films have very good electrochromic reversibility. λ_{max} at 800 nm shows linear dependency with applied potential. This linear dependency improves as the molar ratio of DBSA/aniline in the feed is increased. It is also observed that increase in the concentration of DBSA in the feed improves the reversibility of the absorbance at λ_{max}. In the potential range of E_{SCE} = 0.1 to 0.9 V, PANI exist in emeraldine and pernigraniline oxidation states. There exists an isosbestic point at 460 nm in this potential range indicating a one-step transition from the emeraldine to the pernigraniline state (Figure 7.12) [153]. Recently, MacDiarmid and coworkers [154] carried out a detailed study with UV-Vis spectroscopy during interconversion of different oxidation states of the PANI, where they have observed two isosbestic points, which are attributed to the interconversion of all three oxidation states.
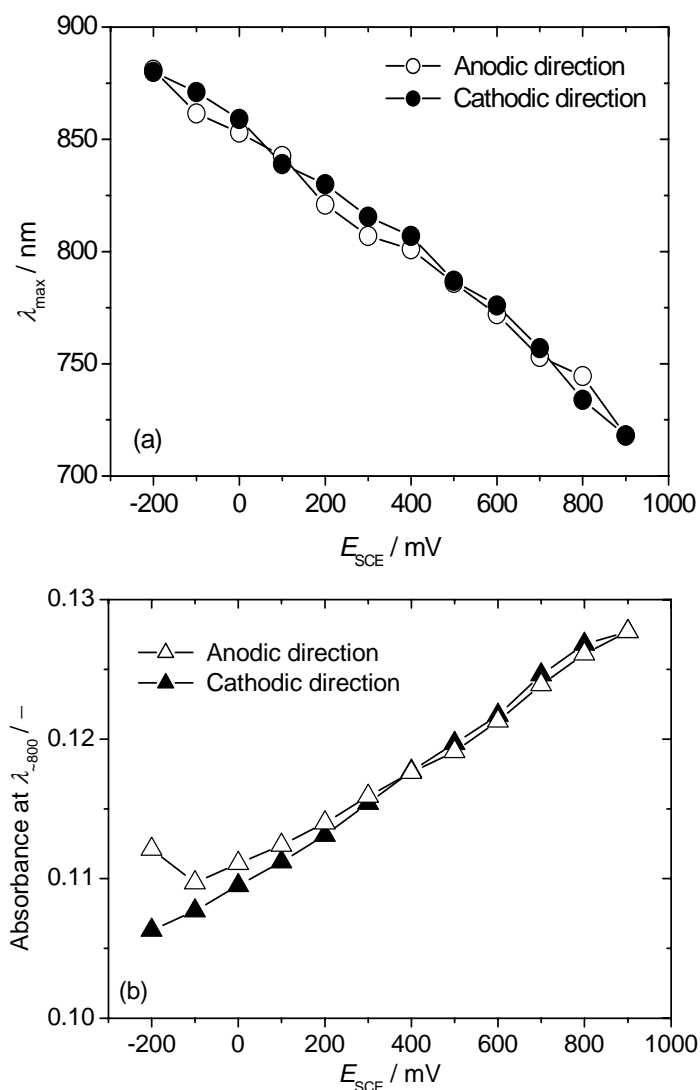
Figure 7.13. Plots of λ_{max} (a) and absorbance at λ_{max} (b) *vs* applied potential for PANI (TIP-7).

(b) In Situ UV-Vis Spectra of PANI-DBSA in Acid Free Electrolytes

It is well known that PANI synthesized either chemically or electrochemically in presence of mineral acids does not exhibit redox activity at pH > 4 [155]. However, the UV-Vis response of the chemically synthesized PANI doped with bulky organic dopant as a function of applied potential in acid free electrolytes has not been reported. Figure 7.14 shows the *in situ* UV-Vis spectra of a drop-coated film of TIP-5 as a function of applied potential successively shifted into anodic direction as recorded in 0.1 **M** KCl.
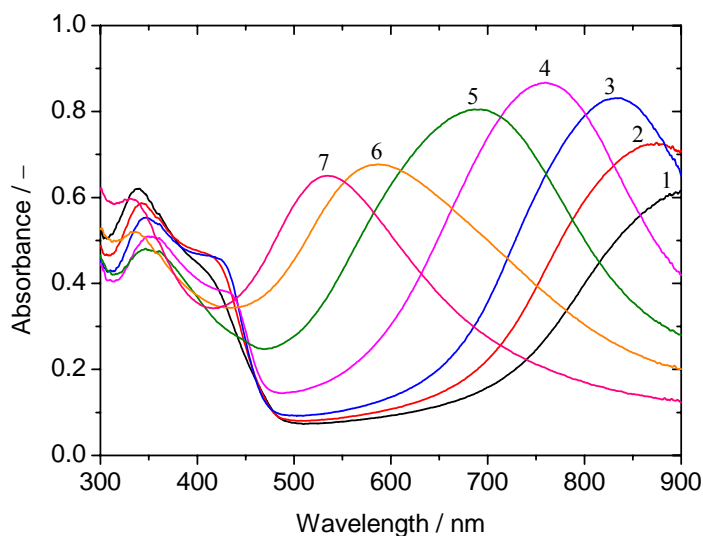
Figure 7.14. *In situ* UV-Vis spectra of drop-coated film of TIP-5 recorded in 0.1 **M** KCl as a function of applied potential successively shifting to anodic direction. E_{SCE} (V): (1) −0.2, (2) 0, (3) 0.2, (4) 0.4, (5) 0.5, (6) 0.6 and (7) 0.8.

The low energy band at ~800 nm shows a blue shift when the applied potential is increased from E_{SCE} = −0.2 to 0.8 V. The absorbance increases up to E_{SCE} = 0.4 V and then decreases. The rapid blue shift of this band at E_{SCE} > 0.4 V is attributed to the emeraldine-to-pernigraniline transformation. Such changes were also observed for PANI films in 0.5 **M** H_2SO_4 but the oxidative transformation is observed at E_{SCE} > 0.6 V (see preceding paragraphs). The band at ~400 nm exhibit maximum absorbance for E_{SCE} = 0.1 to 0.2 V indicating maximum protonation in this potential range [156]. A decrease in the absorbance and a red shift is observed for the band at ~350 nm when the potential is increased from E_{SCE} = −0.2 to 0.5 V indicating decreased conjugation caused by the protonation, an opposite trend is observed for E_{SCE} > 0.5 V. *In situ* UV-Vis spectra of PANI-DBSA films as a function of applied potential were also recorded during a cathodic sweep to complete a potential cycle. The spectrum shows only two bands at 330 nm and at 520–600 nm at all applied potentials. During an electrochemical oxidation, counter ions enter the PANI film whereas they are expelled from the film during reduction [157]. The insertion of Cl^- ions into the film during an anodic sweep is a slow process due to the repelling nature of long hydrophobic chain of DBSA and thus, UV-Vis responses of PANI film recorded in KCl are similar to those in H_2SO_4.

In situ UV-Vis spectra measured in another acid free electrolyte solution (Na_2SO_4

in this case) containing relatively larger counter ions (SO_4^{2-}) reveal that anion exchange rate between PANI-DBSA and the electrolyte is influenced by the size of the anions. When larger anions (SO_4^{2-}) are present in the solution, the bands corresponding to polaron transitions reappear during the negative going potential sweep (Figure 7.15). It is clear from the figure that at $E_{SCE} < 0.4$ V, bands corresponding to protonated PANI-ES (~800 nm) are broad and overlapping with the band corresponding to PANI-EB (~600 nm). Unlike in acidic electrolytes, electrochromic as well as electrochemical reversibility in terms of position and absorbance of the low energy band could be observed neither in KCl nor in Na$_2$SO$_4$ solution. The emeraldine-to-pernigraniline transformation during the anodic sweep in 0.3 **M** Na$_2$SO$_4$ is positively shifted to $E_{SCE} > 0.5$ V when compared to that in 0.1 **M** KCl. A PANI-DBSA film cycled in neutral electrolyte was washed with water, re-immersed in 0.5 **M** H$_2$SO$_4$ and cycled again to check for possible degradation/structural changes in neutral electrolytes. The UV-Vis response of the PANI film re-immersed in acid is similar to the one recorded for the fresh PANI film indicating the absence of structural modifications.
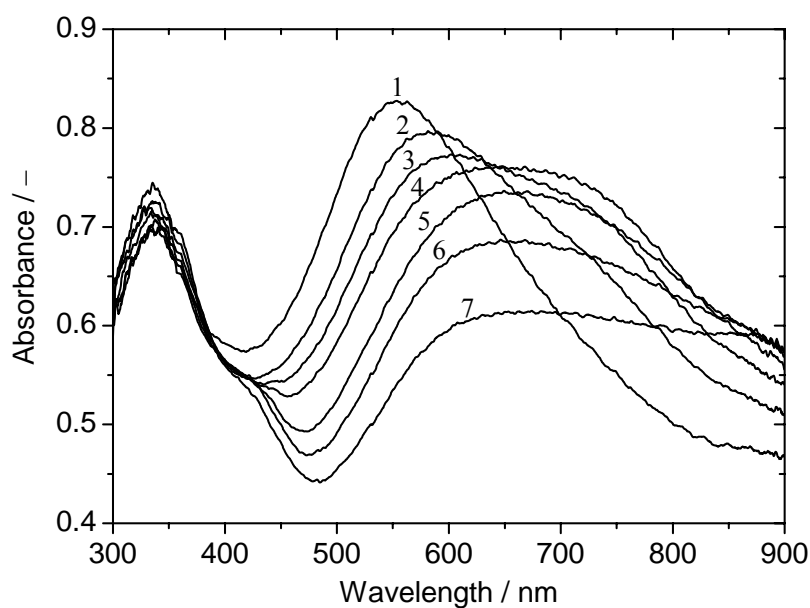

Figure 7.15. *In situ* UV-Vis spectra of drop-coated film of TIP-6 recorded in 0.3 **M** Na$_2$SO$_4$ as a function of applied potential successively shifting to cathodic direction. E_{SCE} (V): (1) 0.8, (2) 0.4, (3) 0.3, (4) 0.2, (5) 0, (6) −0.1 and (7) −0.2.

(c) In Situ UV-Vis Spectra of Poly(aniline-co-o-toluidine) in Acidic Electrolyte

UV-Vis spectral responses of POT to the applied potential is similar to that of PANI except for the fact that applied potential at which interconversion of the oxidation states are taking place has been shifted. Electronic absorption spectra of POT coated ITO-glass sheets in 0.5 **M** H_2SO_4 are shown in Figure 7.16. The emeraldine-to-pernigraniline transformation, as reflected from the steep blue shift of the low energy polaron band (~800 nm), is observed at $E_{SCE} \geq 0.5$ V for POT ($E_{SCE} \geq 0.7$ V for PANI). At $E_{SCE} \geq 0.6$ V, absorbance of this band decreases indicating irreversible changes, possibly due to degradation of the polymer at this potential. Interestingly, the broad overlapping band at ~385 nm observed in the solution state spectrum of POT, splits into two bands during an ongoing potential sweep. The high energy polaron band originating from the radical cations exhibit maximum absorbance at $E_{SCE} = 0.2$ V for PANI, whereas its absorbance increases up to $E_{SCE} = $ ~0.4 V in case of POT. This is in accordance with the first oxidation peak potential observed in the CV of POT which is discussed later. Similar to PANI, UV-Vis responses of POT film follows its CV profile. At $E_{SCE} < 0.2$ V, UV-Vis responses, characteristic of leucoemeraldine, have been observed (Figure 7.16). However, the band corresponding to radical cations is present even at $E_{SCE} = -0.2$ V, as in the case of PANI, indicating the presence of charged species in the reduced state. Similar results were reported by Yang *et al.* [138] for the electrochemically synthesized HCl doped POT on ITO-glass electrodes.
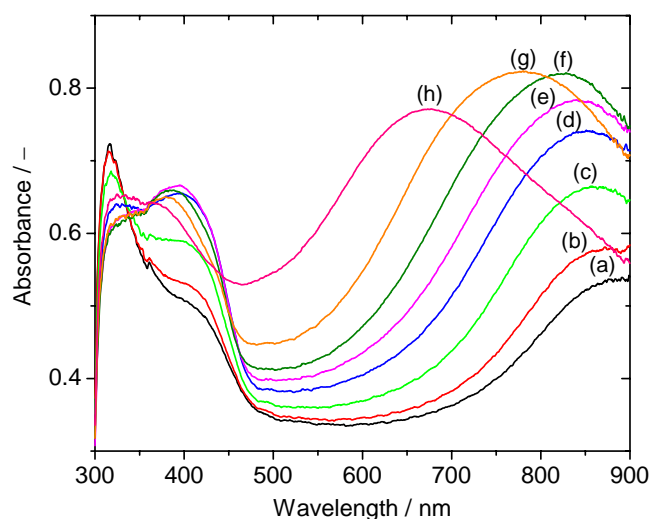

Figure 7.16. *In situ* UV-Vis spectra of POT-6 coated ITO-glass sheets recorded in 0.5 **M** H_2SO_4 at successively shifting positive potentials. E_{SCE} (V): (a) −0.2, (b) 0.1, (c) 0.2, (d) 0.3, (e) 0.4, (f) 0.5, (g) 0.6 and (h) 0.7.

In situ spectroelectrochemical measurements were also carried out in cathodic direction soon after the anodic sweep to check the electrochromic reversibility and electrochemical stability of the material. Figure 17.17a shows a plot of wavelength at band maximum *vs* applied potential. Overlapping lines in the figure indicates that POT synthesized by the present method possesses good electrochromic reversibility. However, a hysteresis is formed in Figure 7.17b, where absorbance at λ_{max} is plotted *vs* applied potential in a potential cycle, indicating that POT, in the potential range applied (E_{SCE} = −0.2 to 0.8 V), is electrochemically unstable. It is also clear from Figure 7.17b that absorbance values are higher during the cathodic sweep than the anodic sweep which may be due to the dissolved degraded species produced at higher positive potential.
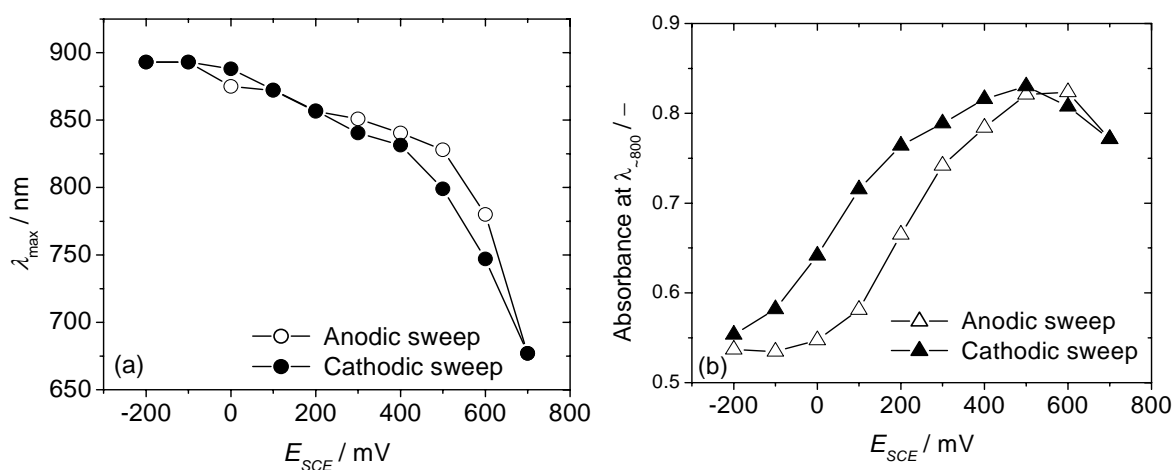

Figure 7.17. Plots of (a) λ_{max} and absorbance at (b) λ_{max} *vs* applied potential for POT-6.

In the applied potential range, UV-Vis spectral responses of copolymer films are similar to that of POT. However, E_{SCE} at which emeraldine-to-pernigraniline transformation is taking place depends on the fraction of *o*-toluidine in the copolymer. This transformation takes place at lower positive potential (E_{SCE} = 0.4–0.5 V) for the copolymers generated from higher concentration of *o*-toluidine in the feed (≥ 0.005 **M**), whereas, it occurs at $E_{SCE} \geq 0.6$ V for the copolymers with the lower feed concentration of *o*-toluidine (≤ 0.005 **M**). Likewise, E_{SCE} at which highest concentration of the radical cations is observed ($A_{\sim420}$) also depends on the *o*-toluidine content of the copolymer. All these observations clearly indicate that the spectral responses of copolymers containing a higher mole fraction of aniline in the feed are similar to that of PANI whereas copolymers containing higher mole fraction of *o*-toluidine behaves like POT. Like PANI and POT, copolymers also exhibit

good electrochromic reversibility (overlapping lines in Figure 7.18a). However, electro-chemical stability of the copolymer films in the applied potential range (E_{SCE} = –0.2 to 0.8 V) is not very good as indicated by the hysteresis in the plot of absorbance at ~800 nm *vs* E_{SCE} (Figure 7.18b).
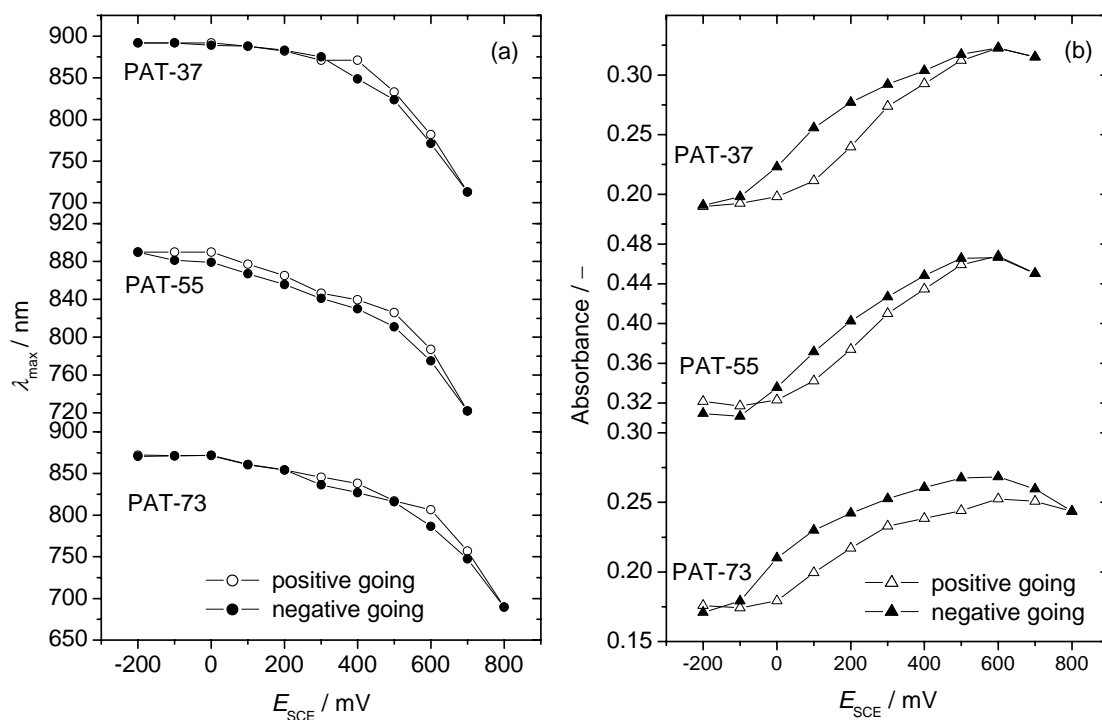

Figure 7.18. Plots of (a) λ_{max} and (b) absorbance of low energy polaron band as a function of applied potential for the copolymers containing different mole fractions of the comonomers in the feed.

7.7 Cyclic Voltammetry

(a) Cyclic Voltammetry of PANI-DBSA in Acidified Electrolytes

Representative CVs of TIP-5 in three different aqueous mineral acids are shown in Figure 7.19a. There are two pairs of redox peaks almost similar to the ones observed with PANI prepared electrochemically in aqueous acids. A first oxidation wave around E_{SCE} = 0.2 V is assigned to the leucoemeraldine-to-emeraldine transition and the second oxidation wave at around E_{SCE} = 0.8 V is due to transition from emeraldine to pernigraniline state.

During the first 20 cycles, the second oxidation wave shifts to more negative potentials and a dramatic decrease in the peak current is observed. A new oxidation wave starts to appear at E_{SCE} = 0.5 V and its current density gradually increases. In case of HCl, the new band grows much faster than with the other two acids. This is attributed to a kinetic

effect i.e., slow exchange of anions in the acid and the bulky dopant anions present in the polymer film. Thus the two oxidation waves in the region of $E_{SCE} = 0.5$ to 0.8 V may originate from two different counter ions in the system. Dominis *et al.* [152] observed that PANI redoped with DBSA does not show distinct redox waves. They quote that the surfactant-like nature of the dopant hinders the charge transfer due to poor wettability of the polymer by the aqueous electrolyte. A hump observed in the region of 0.3 to 0.5 V arises from products of overoxidation [89]. The cathodic part of the CV exhibits complicated features; the waves are broad and overlapping [158]. It is also observed that anodic peak currents are relatively higher than the cathodic ones. Jiang and Dong [35] have observed the same behavior for soluble polyaniline synthesized by the treatment of emeraldine base with boiling 2 **M** NaOH. They conclude that the rate of proton elimination in the anodic process is greater than that of the proton addition reaction in the cathodic process leading to higher and sharper peak currents in the anodic process.
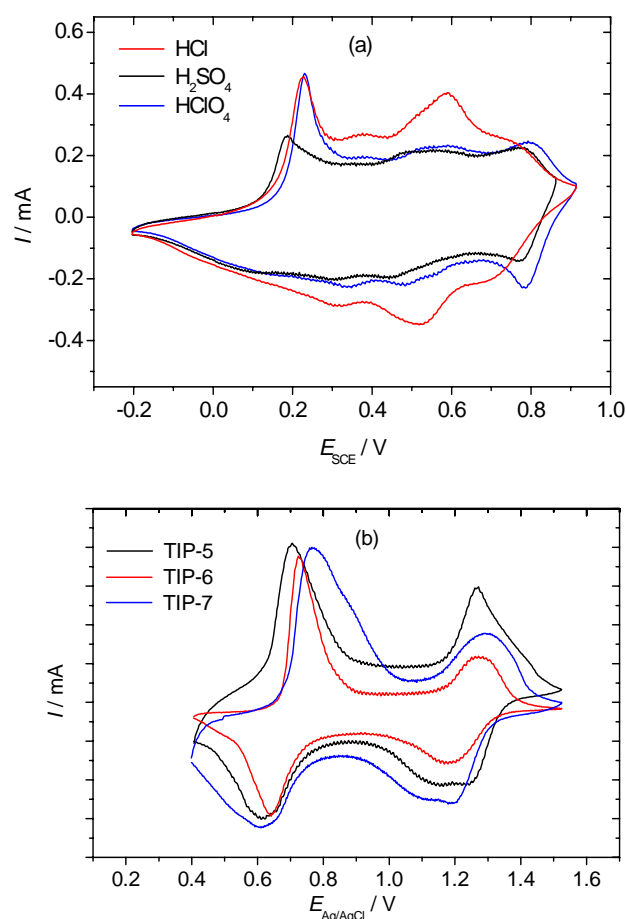

Figure 7.19. CVs of (a) TIP-5 coated GCE electrodes in three different acids at a scan rate of 50 mV s^{-1} and (b) PANIs with different mole ratios of DBSA/aniline coated on a platinum sheet electrode at a scan rate of 50 mV s^{-1} recorded in acetonitrile containing 0.1 **M** Bu$_4$NBF$_4$ and 0.075 **M** HBF$_4$.

Cyclic voltammograms of PANI in acetonitrile containing 0.1 **M** Bu$_4$NBF$_4$ + 0.075 **M** HBF$_4$ with different molar ratios of DBSA/aniline in the feed are shown in Figure 7.19b. CVs show two pairs of well-defined redox waves similar to the ones synthesized electrochemically in aqueous acids [158]. Electroactivity of PANI in non-aqueous solvents is very good when compared to aqueous electrolytes even though they have low pH. As mentioned earlier, this difference arises from the poor wettability of the PANI film in aqueous media. CVs are reproducible for several cycles indicating absence of any free monomers or oligomers in the PANI. When cycled up to $E_{Ag/AgCl}$ = 2.0 V overoxidation takes place, which is reflected by gradual decrease in the peak current. Increase in the amount of DBSA in the feed shifts the position of the first oxidation wave to more positive potentials (Figure 7.19b; Page 95). As mentioned earlier, an increasing amount of dopant in the polymer leads to the formation of compact coil structures, thereby, shifting the position of the oxidation wave to more positive potentials. Figure 7.20 shows plots of anodic and cathodic peak currents *vs* square root of the scan rate. The plots yield straight lines indicating that the electrochemical processes are diffusion controlled [35]. Normally, in ideal diffusion controlled systems, the intercept of the plot is zero, but in the case of conducting polymers contributions such as double layer charging disturb the concept of zero intercept. Plots of current/square root of the scan rate *vs* $E_{Ag/AgCl}$ (not shown here) yield identical values of current/square root of scan rate at the peak maxima confirming the diffusion controlled process. The straight lines in Figure 7.20 also indicate that electrochemical behavior of PANI synthesized by the present method is similar to that of electrochemically synthesized PANI.
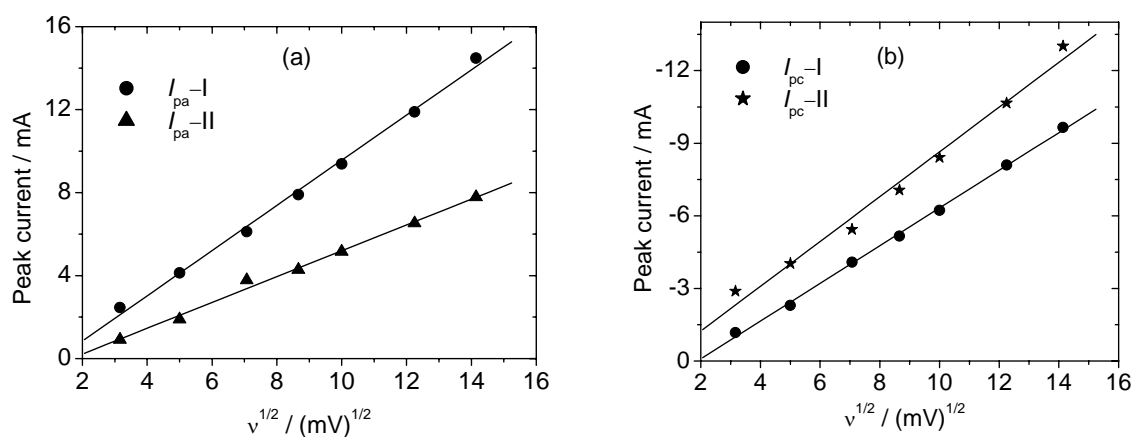

Figure 7.20. Plots of (a) anodic (I_{pa}) and (b) cathodic (I_{pc}) peak currents *vs* square root of the scan rate [$(v)^{1/2}$].

(b) Cyclic Voltammetry of Poly(aniline-co-o-toluidine) in Acidified Electrolytes

Cyclic voltammograms of POT-6 drop-coated on a glassy carbon electrode and recorded in three different (1 **N**) aqueous mineral acids are shown in Figure 7.21a (Page 98). CVs in all three mineral acids show two redox processes corresponding to leucoemeraldine-to-emeraldine and emeraldine-to-pernigraniline transformations. It is clear from Figure 7.21a that the first oxidation wave of POT ($E_{ox, 1}$), when compared to PANI, has shifted to more positive potential, whereas, the second oxidation wave ($E_{ox, 2}$) has shifted to lower positive potentials. However, the magnitude of cathodic shift in the $E_{ox, 2}$ is much smaller compared to that of anodic shift in the $E_{ox, 1}$. The anodic shift of $E_{ox, 1}$ is due to larger steric hindrance associated with the double bond of the radical cation which prevents free rotation along C–N–C chain of the polymer. The instability of the radical cations in POT due to the steric factor shifts the $E_{ox, 2}$ in cathodic direction. Similar trends were observed by Probst and Holze [42] for electrochemically synthesized POT in $HClO_4$. Hence, the electrochemical behavior of chemically synthesized POT using the present protocol is similar to that of electrochemically synthesized one. However, the lower magnitude of the cathodic shift observed for the second oxidation wave may be due to the sterically favorable molecular conformation of the polymer synthesized using present protocol which leads to the improved stability of the radical cations.

The oxidation potential of POT, particularly $E_{ox, 2}$, is strongly influenced by the counter ions present in the electrolyte. In HCl and H_2SO_4, $E_{ox, 2}$ appears at $E_{SCE} = 0.81$ V whereas it appears at $E_{SCE} = 0.63$ V in $HClO_4$. During the first 20 cycles, $E_{ox, 2}$ of POT in $HClO_4$ shifts to more negative potentials and a gradual increase in the peak current is observed (Figure 7.21b; Page 98). In HCl and H_2SO_4 the cathodic shift is of very low magnitude and the peak current shows gradual decrease. With further increase in the number of cycles, more reproducible CVs are obtained. These observations suggest that in $HClO_4$, the radical cations formed above $E_{ox, 1}$ are not stable which may be due to the conformational rearrangement taking place in this electrolyte. Interestingly, unlike PANI, no new oxidation wave appears during cycling indicating faster exchange of the anions in the acid and the bulky dopant anions present in the polymer film.
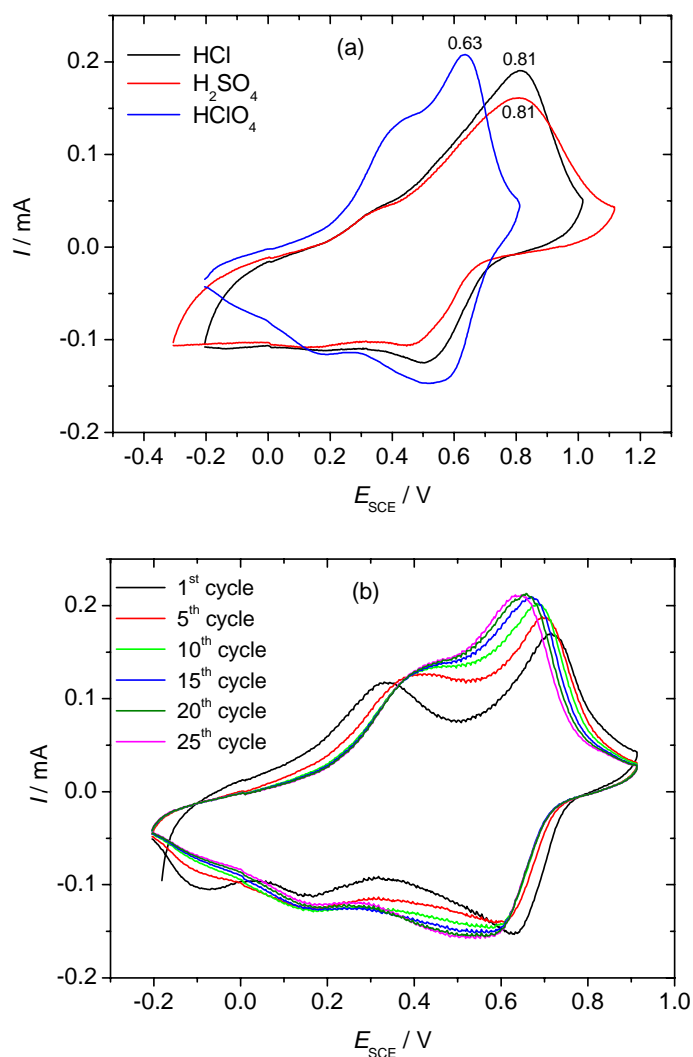
Figure 7.21. Cyclic voltammograms of POT drop-coated glassy carbon electrode recorded in (a) three different mineral acids (1 **N**; 30th cycle) and (b) 1 **N** HClO$_4$ at progressively increasing cycle number. Scan rate = 50 mV s^{-1}.

Cyclic voltammograms recorded in 1 **N** HClO$_4$ of homo- and copolymers with different mole fractions of the comonomers in the feed are shown in Figure 7.22 (Page 99) and their oxidation potentials are given in Table 7.4 (Page 100). Electrochemical responses of the copolymers are strongly influenced by the mole fraction of the comonomers in the feed. The value of $E_{ox, 1}$ of the copolymers was found to fall in between the values of PANI and POT. When the feed concentration of *o*-toluidine is increased, $E_{ox, 1}$ of the copolymer gradually shifts towards the $E_{ox, 1}$ of POT. Copolymers containing higher mole fraction of aniline in the feed exhibit two oxidation waves in the region of E_{SCE} = 0.6 to 0.8 V (Figure 7.22; Page 99) indicating their resemblance to PANI. Similarly copolymers with higher

mole fraction of *o*-toluidine in the feed resemble POT. The potential window of POT ($E_{ox, 2}$ − $E_{ox, 1}$; high conductivity range) is ~330 mV smaller than that of PANI (Table 7.4; Page 100). Copolymerization not only improves the conductivity of POT but also improves the potential window. As mentioned in the previous paragraph for POT, CVs of the copolymers recorded in 1 **N** HCl and H$_2$SO$_4$ do not show broad variation in the position of $E_{ox, 2}$ thereby not showing any conformational rearrangement which destabilizes the radical cations (Figure 7.23; Page 100). As in the case of PANI, electrochemical responses of POT and poly(aniline-*co*-*o*-toluidine)s are not very good due to poor wetting property of the bulky counter ions. Presence of single redox pair in the copolymers for each redox process suggests formation of real copolymers and not composites which otherwise would have resulted in separate redox pairs for PANI and POT [126, 140]. This indicates that expected copolymers are produced from the present protocol using benzoyl peroxide as the oxidant and DBSA as the dopant.
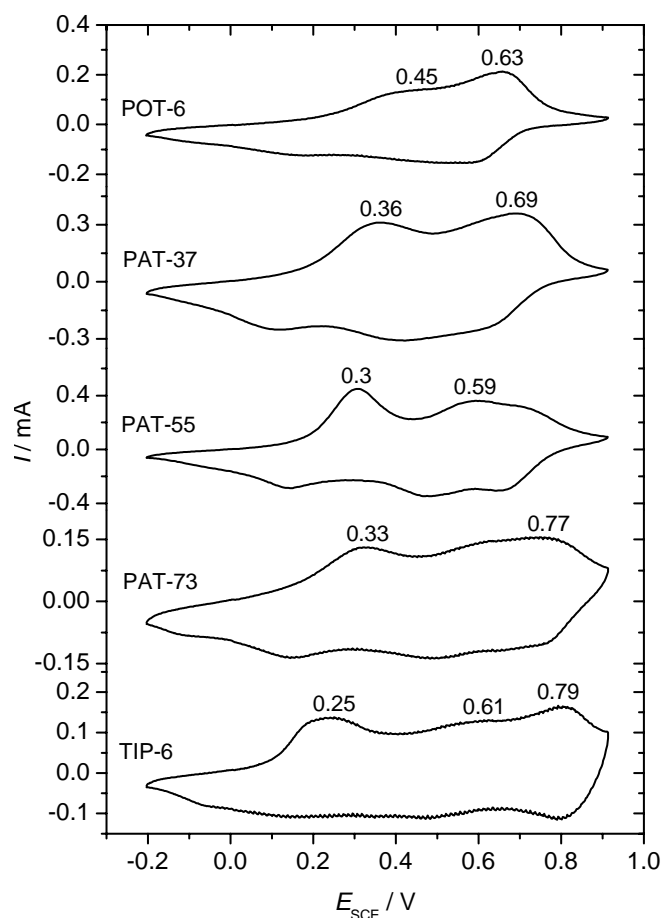

Figure 7.22. Cyclic voltammograms of homo- and copolymers recorded in 1 **N** HClO$_4$. Solutions of the polymers were drop-coated on glassy carbon working electrode; scan rate = 50 mV s^{-1}; 30th cycle.

Table 7.4. Oxidation potentials of homo- and copolymers obtained from their respective CVs recorded in HClO$_4$; scan rate 50 mV s^{-1} (*vs* SCE reference).

Sample code	$E_{ox, 1}$ (V)	$E_{ox, 2}$ (V)		ΔE (mV)
TIP-6	0.25	0.61	0.79	540
PAT-73	0.33	0.63	0.77	440
PAT-55	0.30	0.59	0.69	390
PAT-37	0.36	–	0.69	300
POT-6	0.45	–	0.66	210
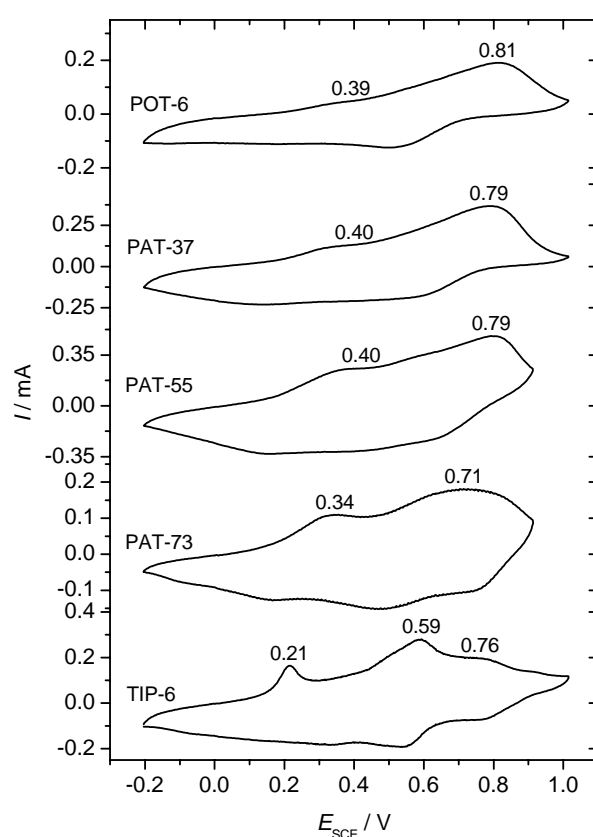
Figure 7.23. Cyclic voltammograms of homo- and copolymers recorded in 1 **N** HCl. Solutions of the polymers were drop-coated on glassy carbon working electrode; scan rate = 50 mV s^{-1}; 30th cycle.

Generally, the first oxidation peak in the CV of electrochemically synthesized PANI, POT or copolymers is sharp and its peak current is much higher than the second oxidation peak [42, 126, 148]. However, homopolymers as well as copolymers synthesized by the present protocol exhibit an opposite behavior, i.e., peak current of the second oxidation peak is much higher than the first one. In case of PANI-DBSA, such a trend is ob-

served only in the first 10 cycles. During an electrochemical reduction, counter ions are expelled from the polymer film whereas their insertion takes place during oxidation. Emeraldine state is the inherent oxidation state of chemically synthesized polymer and is further stabilized by a stable chain conformation. Due to the strong complexation of polar head group of DBSA with amine/imine moiety of the polymer backbone, the emeraldine-to-leucoemeraldine transformation is much slower during potential cycling. *In situ* UV-Vis spectroscopy also reveals the presence of radical cations at the applied potential where PANI or POT is in the completely reduced state. These facts lead to higher peak current observed for the second oxidation potential. Su and coworkers [140] have observed a similar trend for POT and copolymers of aniline and toluidine synthesized using 2,3-dichloro-5,6-dicyanobenzoquinone as oxidant and (+)-CSA as dopant but gave no explanation for the observed trend. Wei *et al.* [126] have reported that CVs of chemically prepared poly(aniline-*co*-*o*-toluidine)s (dissolved in NMP and drop-coated on an electrode surface) are identical to those of electrochemically synthesized ones, however, no detailed discussion on the CVs has been given.

Cyclic voltammograms of homo- and copolymers of aniline and *o*-toluidine in non-aqueous solution are shown in Figure 7.24 (Page 102). As in case of PANI, POT and copolymers exhibit excellent electrochemical responses in acetonitrile containing 0.1 **M** Bu_4NBF_4+0.075 **M** HBF_4. POT and copolymers exhibit two pairs of redox waves which are assigned to the interconversion of three oxidation states of the polymer backbone. The electrochemical response of POT in acidified non-aqueous electrolyte is similar to those synthesized electrochemically [42, 126]. Peak current of the first oxidation wave is much higher than the second wave indicating that interconversion of all the three oxidation states takes place efficiently in non-aqueous electrolytes. Irrespective of the thickness of the polymer film, peak currents in the CV of PANI are much higher than that of POT and copolymers which is an indirect proof of higher conductivity of the PANI. As in the case of aqueous acidic electrolytes, copolymers exhibit single pair of peaks for each transformation indicating formation of expected real copolymers. It is further supported by the CV of a mechanical mixture of PANI and POT (Figure 7.24; Page 102), recorded under similar conditions, which exhibit two oxidation waves in the higher positive potential region (Table 7.5; Page 103).

The potential window where polymer backbone stays in conducting emeraldine state follows a similar trend as observed in the case of aqueous electrolytes. This potential window gradually narrows with increase in the mole fraction of *o*-toluidine in the feed.

This indicates that the amount of *o*-toluidine units incorporated in the polymer backbone strongly depends on its feed concentration. The values of first and second oxidation potentials ($E_{ox, 1}$ and $E_{ox, 2}$) along with the potential window (where polymer exists in emeraldine state) are given in Table 7.5 (Page 103). The change in the value of $E_{ox, 1}$ and $E_{ox, 2}$ of copolymers follows a trend similar to the one observed in aqueous electrolytes. Because of the lower positive potential of $E_{ox, 2}$ of POT and copolymers, overoxidation takes place when cycled up to $E_{Ag/AgCl} = 1.5$ V leading to degradation of the polymer film which is reflected by the decrease in the peak current of their CVs during progressive cycling. The magnitude of decrease is much faster in the copolymers containing higher fraction of *o*-toluidine units. As in the case of PANI, plots of square root of scan rate *vs* peak current of POT and poly(aniline-*co*-*o*-toluidine)s yield straight lines indicating that the electrochemical processes are diffusion controlled.

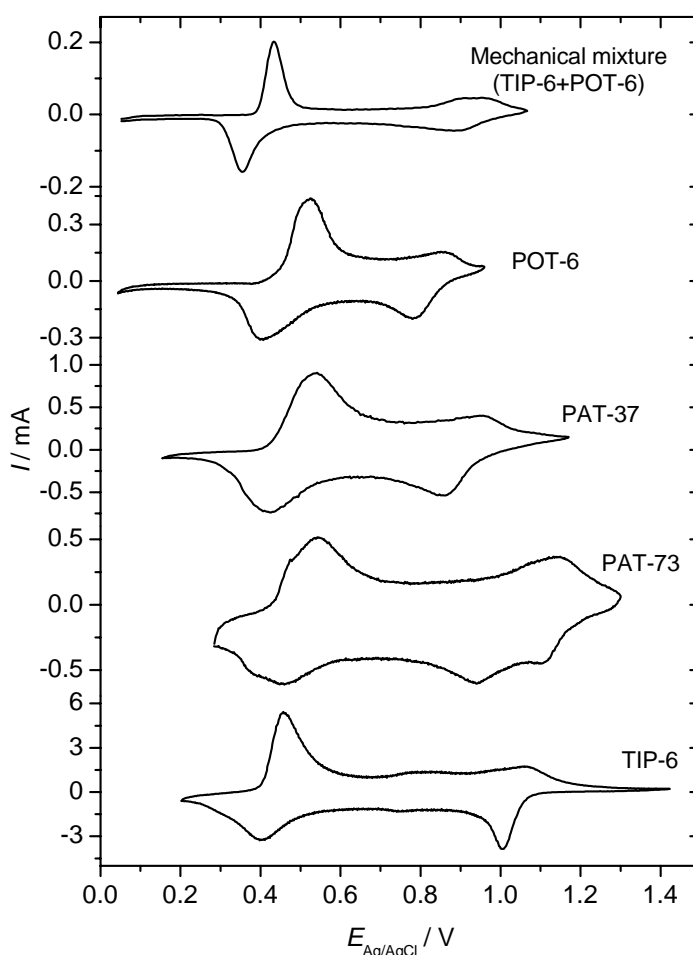**Figure 7.24.** Cyclic voltammograms of homo- and copolymers recorded in acetonitrile containing 0.1 **M** Bu$_4$NBF$_4$+0.075 **M** HBF$_4$. Solutions of the polymers were drop-coated on a platinum foil working electrode; scan rate = 50 mV s^{-1}; 5th cycle.

Table 7.5. Oxidation potentials of homo- and copolymers obtained from their respective CVs recorded in acetonitrile containing 0.1 **M** Bu$_4$NBF$_4$ and 0.075 **M** HBF$_4$; scan rate 50 mV s^{-1} (*vs* Ag/AgCl reference).

Sample code	$E_{\text{ox, 1}}$ (V)	$E_{\text{ox, 2}}$ (V)		ΔE (mV)
TIP-6	0.45	–	1.06	610
PAT-73	0.54	–	1.15	610
PAT-37	0.54	–	0.96	420
POT-6	0.52	–	0.85	330
Mechanical mixture of TIP-6 and POT-6	0.44	0.91	0.96	–

7.8 Infrared Spectroscopy

There are a handful of previously published reports discussing the infrared spectroscopy of both chemically and electrochemically synthesized PANI [84, 124] and POT [126, 139, 159] doped with various mineral as well as functionalized organic acids. Figure 7.25 (Page 105) shows FTIR spectra of homo- and copolymers synthesized using the present protocol. The vibrational frequencies of the major infrared bands and their assignments are summarized in Table 7.6 (Page 104). In general, with some exceptions, the spectral characteristics of the copolymers show greater similarity to the IR spectrum of POT [126].

The band at 1461 cm^{-1} of PANI attributed to the aromatic ring C–C stretching mode is blue shifted to 1484 cm^{-1} for POT, whereas, this mode for copolymers appear in the range of 1478–1486 cm^{-1}. When the feed composition of *o*-toluidine in the copolymer increases, this band exhibits a blue shift indicating incorporation of more and more *o*-toluidine moieties into the polymer backbone. The out-of-plane –NH bending vibration of PANI at 1296 cm^{-1} is absent in the IR spectrum of POT due to the steric hindrance arising from the methyl group. In the case of copolymers, intensity of this band diminishes with increase in the mole fraction of *o*-toluidine in the feed (Figure 7.25; Page 105). A new band at 1240 cm^{-1} of weak-to-medium intensity corresponding to benzoid C–N stretching appears only in the copolymers and its intensity decreases with increase in mole fraction of *o*-toluidine in the feed. However, the band at 1216 cm^{-1} corresponding to C–N stretching of benzoid-quinoid-benzoid triad sequence exhibits an opposite trend indicating that numbers of quinoid segments in POT are higher than those in PANI (Figure 7.25). The band at

$1240 \ \text{cm}^{-1}$ is not observed in the IR spectrum of a mechanical mixture of PANI and POT. Appearance of the new bands clearly indicates the formation of copolymers which was previously confirmed by cyclic voltammetry and UV-Vis spectroscopy.

Table 7.6. Major IR bands and their assignments for homo- and copolymers of aniline and *o*-toluidine.

Wavenumbers (cm^{-1})			Band assignments* [124, 159–161]
TIP-6	POT-6	Copolymers	
3439	–	–	Asymmetric $-NH_2^+$ stretching
–	3026	–	−CH stretching (−CH$_3$ group)
–	2954	2952 (w)	Assymmetric −CH stretching (DBSA)
2924	2922	2922	Aromatic −CH stretching
2854	2852	2852	Symmetric −CH$_2$− stretching (DBSA)
1552	1558	1555–1560	Aromatic C−C stretching (B)
1461	1486	1475–1490	Aromatic C−C stretching (Q)
1387	1382	1382	Out-of-plane −CH bending of −CH$_3$ group
1296	–	1295–1305	Out-of-plane −NH bending
–	–	1240–1245	Asymmetric C−N stretching (B) or C=C stretching
–	1212	1216	C−N stretching in QBQ, QBB, BBQ
–	1165	1132–1152	−CH$_3$ rocking (*o*-toluidine unit)
1111	1110	1110–1122	−CH in-plane bending (1,4-disubstituted ring)
1022	1032	1032	S=O stretching (DBSA)
–	1008	1006	−CH$_3$ bending
877	882	880	Ring breathing mode of ES (Q) / Out-of-plane −CH− bending of 1,2,4-trisubstituted ring
–	828	824	Out-of-plane −CH− bending of 1,2,4-trisubstituted ring
787	–	804-810	−CH out-of-plane bending (1,4-disubstituted ring)
–	686	686	S=O stretching (DBSA)

* B = Benzoid segment, Q = Quinoid segment; (w) = weak band

A strong band at $1152 \ \text{cm}^{-1}$ which is attributed to the −CH$_3$ rocking mode of POT decreases in intensity and exhibits red shift with increase in the mole fraction of aniline in the feed (Figure 7.25; Page 105). For example, at the feed ratio of 3:7 (aniline-to-*o*-toluidine) it appears at $1152 \ \text{cm}^{-1}$, whereas, at 7:3 ratio, it shifts to $1138 \ \text{cm}^{-1}$ (weak broad band). The −CH out-of-plane bending mode characteristic of 1,2,4-trisubstituted aromatic ring of POT appears as two strong bands at 882 and $828 \ \text{cm}^{-1}$, whereas, in case of PANI

(1,4-disubstituted benzene ring), it appears as a strong band at 787 cm^{-1} [160]. In the case of copolymers, bending modes characteristic of both tri- and disubstituted rings are present, however, the intensity of the bands due to trisubstituted ring increases and disubstituted ring decreases as the mole fraction of *o*-toluidine in the feed is increased and *vice versa*. Similar results have been reported by Huang and coworkers [136] for copolymers prepared *via* homogeneous solution polymerization using ammonium persulfate as oxidant and HCl as dopant. The band at 787 cm^{-1} corresponding to the *p*-disubstituted benzene ring in the PANI exhibits gradual blue shift as the molar fraction of *o*-toluidine in the feed is increased. When the mole ratio of aniline to *o*-toluidine in the feed is 7:3, this band appears at 804 cm^{-1}, whereas, changing the feed ratio to 3:7 shifts this band to 810 cm^{-1}.
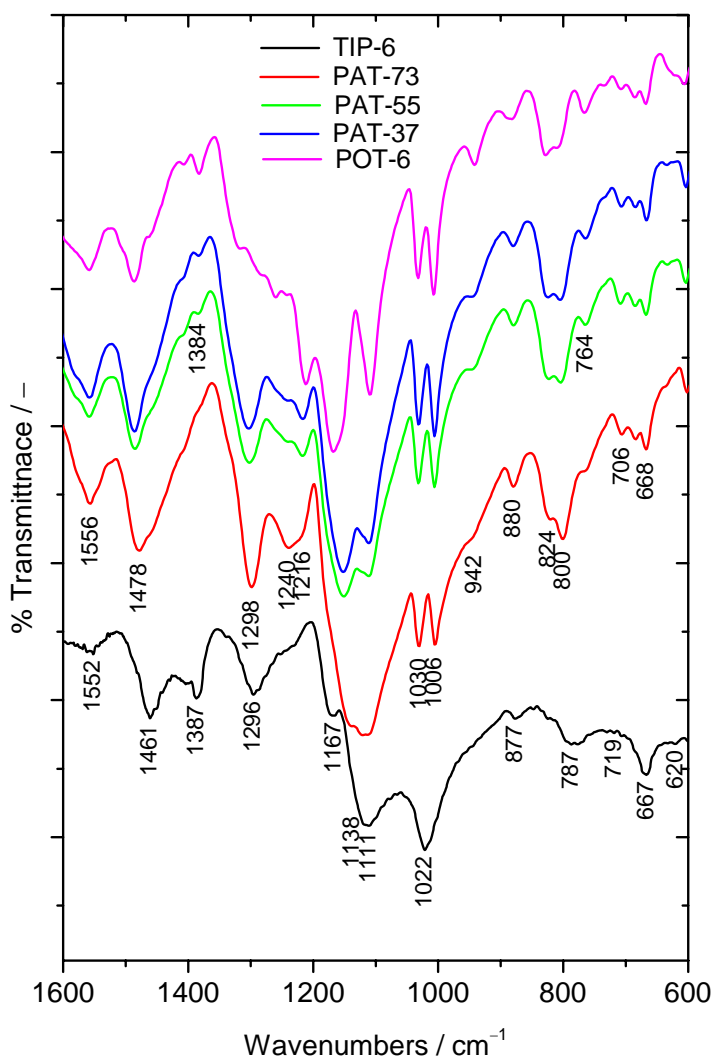

Figure 7.25. FTIR spectra of PANI, POT and copolymers having different aniline-to-*o*-toluidine feed ratios.

The band at 1022 cm^{-1} corresponding to S=O stretching mode of the SO$_3$ group of DBSA splits into two bands in the case of POT and copolymers. Such a splitting is even observed in the copolymer with 7:3 molar composition of aniline to *o*-toluidine.

7.9 Raman Spectroscopy

In this dissertation, Raman spectroscopy is used to gain structural information as well as data pertaining to the metal-to-insulator transition in conducting polyaniline and its copolymers taking place during electrochemically induced redox transformations. In case of PANI-DBSA, pre-resonance enhancement of Raman signals [25, 26] is effective because the laser excitation wavelength used ($\lambda_0 = 476.5$ nm) matches the longer wavelength wing of the absorption band centered at 420–430 nm of PANI. In case of copolymers, above mentioned laser excitation wavelength did not show effective pre-resonance enhancement. Also, the spectra recorded at this laser excitation were not well resolved. Therefore, *in situ* Raman spectra of copolymers were recorded using a green laser excitation wavelength ($\lambda_0 = 514.5$ nm). This laser excitation falls in the shorter wavelength wing of the absorption band centered at 570–650 nm (position depends on applied potential) originating from the pernigraniline oxidation state of polymer backbone which exists at $E_{SCE} > 0.5$ V and pre-resonance enhancement is effective only beyond this potential. Hence, the term 'pre-resonance enhancement' is not included in the subtitle discussing the Raman spectroscopy of copolymers.

(a) In Situ Pre-resonance Raman Spectroscopy of PANI-DBSA

As said above, pre-resonance enhancement is effective for the PANI films. *In situ* UV-Vis spectra reveal that during an anodic potential sweep, absorbance of the band at 430 nm increases, passes through a maximum and then decreases as shown in the inset of Figure 7.26 (Page 107). Frequencies of the major Raman bands and their assignments are summarized in Table 7.7 (Page 107). At $E_{SCE} = -0.2$ V, the Raman spectrum shows two strong peaks at 1628 and 1194 cm^{-1} assigned to benzoid ring modes. Intensity of almost all the peaks increases when the applied potential is raised up to $E_{SCE} = 0.2$ V, beyond this value scattered light intensity decreases with further positive going electrode potential. This trend of potential dependent pre-resonance enhancement is very similar to the plot of absorbance at 430 nm *vs* applied potential (inset of Figure 7.26).
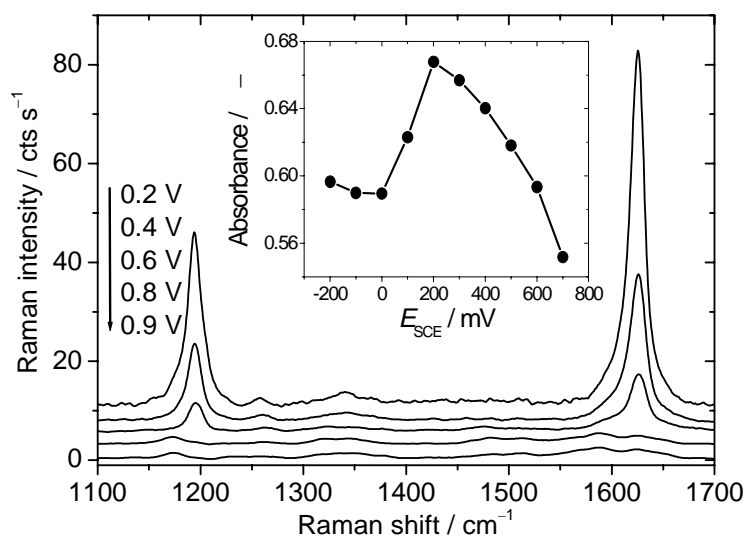
Figure 7.26. *In situ* pre-resonance Raman spectra of PANI (TIP-7) recorded in 1 **N** H_2SO_4 using $\lambda_0 = 476.5$ nm laser excitation at various applied electrode potentials. Inset: Plot of the absorbance at 430 nm against applied potential obtained from *in situ* electronic absorption spectra.

Table 7.7. Major Raman bands and their assignments for PANI, POT and poly(aniline-*co-o*-toluidine) films recorded in 1 **N** H_2SO_4.

Raman frequency (cm^{-1})			State*	Band assignments [90, 162]
PANI	POT	Copolymers		
1626–1630	1627–1632	1627–1632	B	C–C ring stretching
1585–1600	1589–1603	1590–1605	Q	C–C ring stretching
1506–1516	1490–1510	1510–1520	Q	C=N stretching
1480–1486		1490–1500	Q	C=N stretching
	1365–1370	1360–1365	SQR	C–C stretching + C–H bending
1339–1349	1330–1335	1330–1350	SQR	C–N$^+$ stretching
1257–1266	1260–1270	1260–1265	B	C–N stretching
	1250–1255	1250–1255		C–C twisting of methyl group
1228	1226	1226–1230	Q	C–N stretching
1190–1197	1200–1210	1190–1200	B	C–H in-plane bending
1171–1174	1160–1170	1165–1175	Q	C–H in-plane bending
	1110–1125	1110–1125		C–C stretching of methyl group
1008–1015	1010–1015	1005–1020		May be DBSA
885	887–900	880–900	B	In-plane ring deformation
830–836	820–830	811–820	Q	In-plane ring deformation
800–815	800	775–800	Q	C–H out-of-plane bending
	763	755–765	Q	Imine deformation
712–724	720–730	710–720	B	Out-of-plane ring deformation
685–698			SQR	Out-of-plane ring deformation
630	630–640	630–640	B	In-plane ring deformation
		600–610	B	Ring deformation
	585–600	580–595	B	Ring deformation
511–526	520–530	520–530		Out-of-plane C–N–C torsion
412–420	450–460	450–460	Q	Out-of-plane C–H wag

*: B = benzoid ring, Q = quinoid ring and SQR = semiquinone radical

Particularly, intensity of 1628 and 1194 cm^{-1} bands bleaches almost by two orders of magnitude at higher positive potentials [163] (Figure 7.26; Page 107). During an anodic sweep, a new band appears in the range of 680–690 cm^{-1} at E_{SCE} = 0.1 V and disappears at E_{SCE} = 0.6 V. Liu *et al.* [90] assigned this band to an out-of-plane ring deformation of the quinoid ring. As the band exists only in the potential region of the emeraldine state of PANI, it may be due to the semiquinone radical and not the quinoid ring. Two bands at 980 and 1005 cm^{-1} of weak-to-medium intensity are caused by internal modes of the sulfate anion; the band at 980 cm^{-1} is present at all applied potentials [163]. Two bands due to the dopant, DBSA appear at 1040–1057 (at all applied potentials) and 1120 cm^{-1} which are assigned to C–S stretching and S=O out-of-plane bending modes, respectively [94].

A band at 1345 cm^{-1} is assigned to the C–N stretching vibration of the semiquinone radical state (Table 7.7; Page 107); this band exists even at E_{SCE} = −0.2 V indicating that some radical cations are still present in leucoemeraldine state which is also confirmed by *in situ* UV-Vis spectroscopy. At higher positive potentials, a new band at 1327 cm^{-1} appears and the intensity of this band increases, whereas, intensity of the band at 1345 cm^{-1} decreases as the potential is increased in positive direction. New bands start to appear in the region of 1480–1520 cm^{-1} at E_{SCE} ≥ 0.6 V. At E_{SCE} > 0.6 V, PANI exists mainly in pernigraniline state where the polymer backbone has more quinoid segments. Figure 7.27 (Page 109) shows *in situ* pre-resonance Raman spectra of PANI at different applied potentials. The new bands in the region of 1480–1520 cm^{-1} and at 1590 cm^{-1} are caused by modes of quinoid structure. The band at 1590 cm^{-1} shows a red shift when the applied potential is increased from E_{SCE} = 0.6 to 0.8 V. Hugot-Le Goff and Bernard [91] stated that there should be three C–C ring stretching modes (1550, 1575 and 1585 cm^{-1}) and two C=N stretching modes (1485 and 1500–1515 cm^{-1}) for quinoid rings. They have also observed that C–C ring stretching modes are sensitive to the applied potential and pH of the medium and the multiplicity in C=N stretching arises from the difference in protonation and charge localization on the imine sites. The low frequency shift observed in the present study may be due to weakening of the C=N bond strength at higher potential where the next step is overoxidation. The new bands assigned to quinoid ring at higher potential clearly indicate the transformation from conducting emeraldine state to non-conducting pernigraniline state and thus *in situ* Raman spectroscopy has been used successfully to monitor the conductor-to-insulator transition.
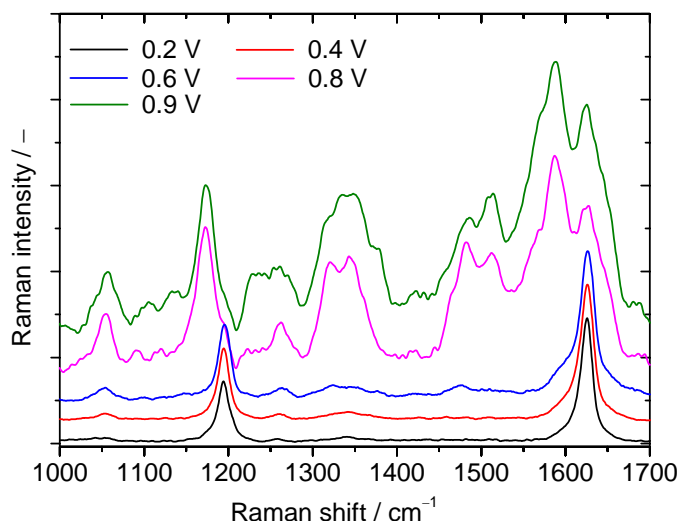
Figure 7.27. *In situ* pre-resonance Raman spectra of PANI (TIP-7) recorded in 1 **N** H_2SO_4 using $\lambda_0 = 476.5$ nm laser excitation at various applied electrode potentials (stacked for better visibility).

(b) In Situ Raman Spectroscopy of Poly(aniline-co-o-toluidine)s

It has already been mentioned that Raman spectra of POT and copolymers were recorded using green laser excitation wavelength ($\lambda_0 = 514.5$ nm). A Raman spectrum of PANI was also recorded using this laser excitation in order to make a fair comparison between the spectra of PANI and copolymers. Major Raman bands and their assignments along with those of PANI are summarized in Table 7.7 (Page 107). As films of POT and copolymers show resonance enhancement at $E_{SCE} > 0.5$ V, Raman spectra of homo- and copolymers recorded at a constant applied potential of $E_{SCE} = 0.8$ V (Figure 7.28; Page 110) are compared to study the influence of *o*-toluidine fraction on the molecular structure. It is important to note that at this applied potential, the dominant oxidation state is pernigraniline and, therefore, bands mainly due to quinoid rings are present in the Raman spectra.

A Raman spectrum of POT exhibits all the bands which are observed in the spectrum of PANI with a small shift in their position. *In situ* Raman spectra of PANI, POT and copolymers with different mole fraction of the comonomers in the feed are displayed in Figure 7.28. As mentioned in the preceding section, the multiplicity of quinoid C–C stretching vibration (1515, 1563 and 1589 cm^{-1}), which is sensitive to the applied potential, is visible in the Raman spectra of all the polymers and more clearly in the spectrum of PANI. PANI exhibits a strong band at ~1345 cm^{-1} due to the C–N stretching mode of the semiquinone radical cation which splits into a new band at 1327 cm^{-1} at higher applied po-

tentials [162]. Interestingly, this band further splits into three well-resolved bands in the case of POT (Figure 7.28) and the third band appears at ~1365 cm^{-1}. The multiplicity of the band due to semiquinone radicals in the Raman spectra of all the copolymers is similar to that of POT.
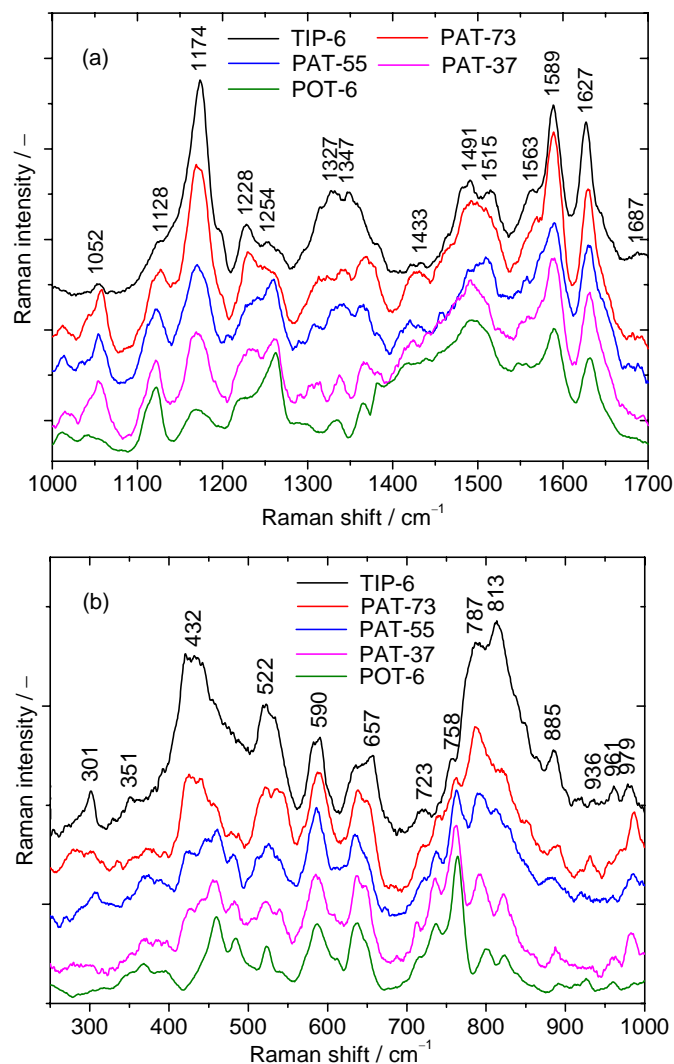

Figure 7.28. *In situ* Raman spectra of films of PANI (TIP-6), POT and copolymers with 7:3, 5:5 and 3:7 molar ratios of aniline to *o*-toluidine in the feed recorded in 1 **N** H$_2$SO$_4$. (a) and (b) stands for two different regions of Raman shift. E_{SCE} = 0.8 V; λ_0 = 514.5 nm; laser power = 100 mW at the sample. Spectra are stacked for better visibility.

The influence of the comonomer feed ratios on the structure of polymer can be observed in the region of 1226–1260 cm^{-1}. The strong band at 1228 cm^{-1} in the Raman spectrum of PANI originates from the C–N stretching of quinoid ring and shows gradual decrease in the intensity with increase in the mole fraction of *o*-toluidine in the feed. The

band at 1254 cm^{-1} due to C–C twisting of methyl group increases in intensity with an increase in the feed concentration of *o*-toluidine. Another characteristic band of POT appears at 1128 cm^{-1} which is assigned to the C–C twist of the methyl side group [43]. Intensity of this band increases with increase in the feed ratio of *o*-toluidine which confirms that more and more *o*-toluidine units have entered into the polymer chain. A band at 813 cm^{-1} in the spectrum of PANI assigned to out-of-plane C–H bending mode of quinoid ring, show gradual decrease in its intensity in the spectra of copolymers. There are three bands in the region of 730–830 cm^{-1} in the spectra of PANI, whereas, two new bands appear in the same region in the case of POT and copolymers. These bands mainly arise from the quinoid segments of the polymer backbone and they are well resolved in the case of POT and copolymers. Such better resolution in POT and copolymers may be due to the applied potential (E_{SCE} = 0.8 V) where they predominantly exist in pernigraniline oxidation state.

In situ Raman spectra of PANI-DBSA (TIP-6) as a function of applied potential is also recorded using green excitation wavelength. The spectral changes observed during an ongoing stepwise positive potential sweep are almost similar to the one recorded using 476.5 nm blue excitation wavelength. However, with the 514.5 nm green excitation wavelength, bands due to the quinoid stretching vibrations appear as strong bands. Both in POT and copolymers, spectral behaviors of the bands at 1628, 1590, 1195 and 1173 cm^{-1} are similar to those of PANI (Figure 7.28; Page 110) except for the fact that appearance or bleaching of the bands takes place at lower potential with an increase in the *o*-toluidine fraction in copolymer.

In the case of POT, intensity of the band at 1510 cm^{-1} attributed to C–N stretching vibration, exhibit sharp increase when E_{SCE} > 0.2 V. As reported by Hugot-Le Goff and Bernard [91], this band is sensitive to the applied potential and transformation of any smaller segments of the polymer leads to increase in the intensity of this band. In copolymers, this band appears at relatively higher potentials and is strongly influenced by the mole fraction of the comonomers in the feed. For example, in the case of PAT-55, it appears at 1519 cm^{-1} at E_{SCE} > 0.5 V and is red shifted to 1509 cm^{-1} with further increase in the applied potential (Figure 7.29; Page 112). Intensity of the band at 1114 cm^{-1} due the methyl group increases with increase in the applied potential and is blue shifted to 1122 cm^{-1}. As discussed in the UV-Vis spectroscopy and cyclic voltammetry, application of potential to a chemically synthesized POT film induces a conformational change which is responsible for the blue shift of the band at 1114 cm^{-1}. Similar trend is observed in the case

of copolymers. The bands in the region of 1140–1350 cm^{-1} are well resolved at $E_{SCE} > 0.4$ V and a new band appears at 1020 cm^{-1}. Further increase in the applied potential shifts this band to 1012 cm^{-1}.

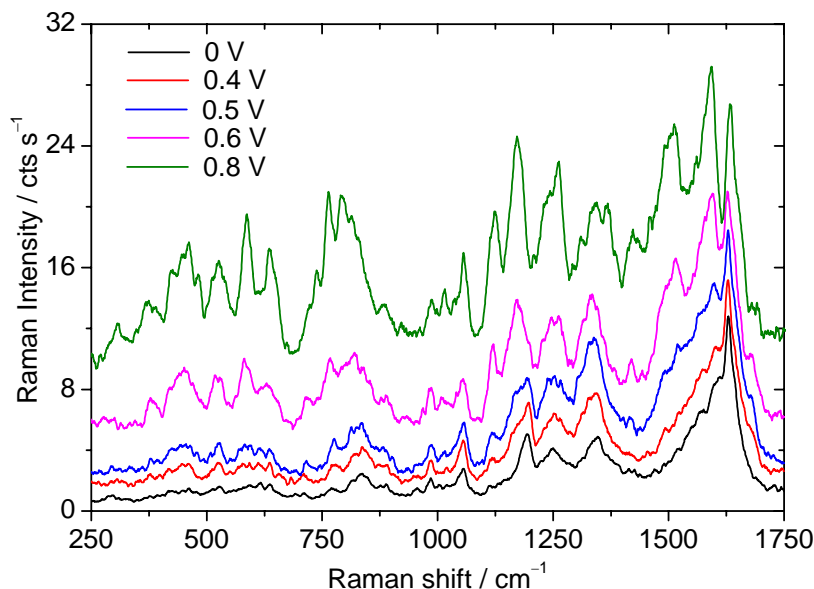**Figure 7.29.** *In situ* Raman spectra of PAT-55 drop-coated film in 1 **N** H$_2$SO$_4$ recorded at various applied potentials progressively shifted in positive direction. λ_0 = 514.5 nm; laser power = 100 mW at the sample.

The main idea of carrying out the *in situ* Raman spectroscopy is to monitor the oxidative transformation induced by electrochemical changes. From the above discussions it is clear that the bands at 1630 and 1590 cm^{-1} originate from the benzoid and quinoid segments in the polymer backbone, respectively. It is well known that higher numbers of benzoid segments are present in protonated emeraldine state and concentrations of quinoid segments are higher in pernigraniline state. Gradual stepwise increase in the applied potential decreases the intensity of benzoid band, whereas quinoid band intensity increases. A steep change in their intensity ratios indicates emeraldine-to-pernigraniline transformation. Hence, a plot of ratio of band intensity of 1630 to 1590 cm^{-1} *vs* applied potential will help us to monitor the emeraldine-to-pernigraniline transformation. Such plots for PANI (TIP-6), POT and copolymer containing 7:3, 5:5 and 3:7 mole ratios of aniline to *o*-toluidine are shown in Figure 7.30 (Page 113). The plots indicate that the offset of oxidative transformation appears at progressively decreasing positive potentials as the fraction of *o*-toluidine in the feed is increased.
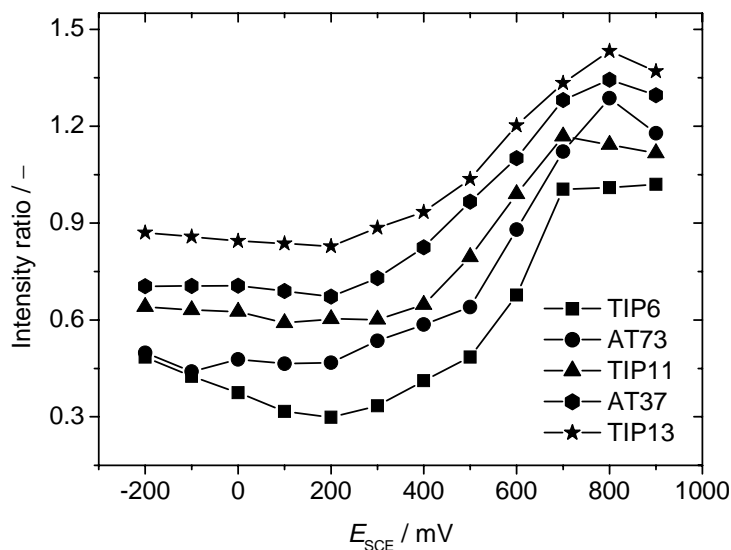
Figure 7.30. Plot of intensity ratio of bands at 1630 and 1595 cm^{-1} (I_{1595}/I_{1630}) as a function of applied potential.

A similar concept can also be applied for the bands at 1195–1200 and 1175 cm^{-1} which have their origin in benzoid and quinoid segments, respectively. In this case, stepwise increase in the applied potential decreases the intensity of 1195–1200 cm^{-1} band, whereas, it increases the intensity of the band at 1175 cm^{-1}. A plot of intensity of both these bands as a function of applied potential will give more precise information about the metal-to-insulator transition. The potential at which both plots intersect can be taken as the equilibrium potential above which pernigraniline is the predominant oxidation state and below this potential emeraldine state dominates. Plots of intensity of 1200 and 1175 cm^{-1} bands *vs* applied potential for PANI, POT and copolymer with 7:3 and 3:7 mole ratios of aniline to *o*-toluidine are shown in Figure 7.31 (Page 114). It is clear from the figure that the metal-to-insulator transition is induced at much lower potential when higher fraction of *o*-toluidine is present in the copolymers which is also confirmed by the *in situ* UV-Vis and cyclic voltammetry investigations. Bartonek and coworkers [92] have applied resonance Raman spectroscopy to trace the metal-to-insulator transition in electrochemically synthesized PANI as a function of pH. However, they have plotted the ratio of the intensities of the bands at 1170 and 1196 cm^{-1} as a function of pH to find out the pH at which ES-to-EB transformation is taking place. It is to be noted that a small increase in the intensity of the bands at 1200 cm^{-1} at $E_{SCE} > 0.6$ V, which is not a normal trend for aniline based poly-

mers, is due to the effective resonance enhancement at these potentials.

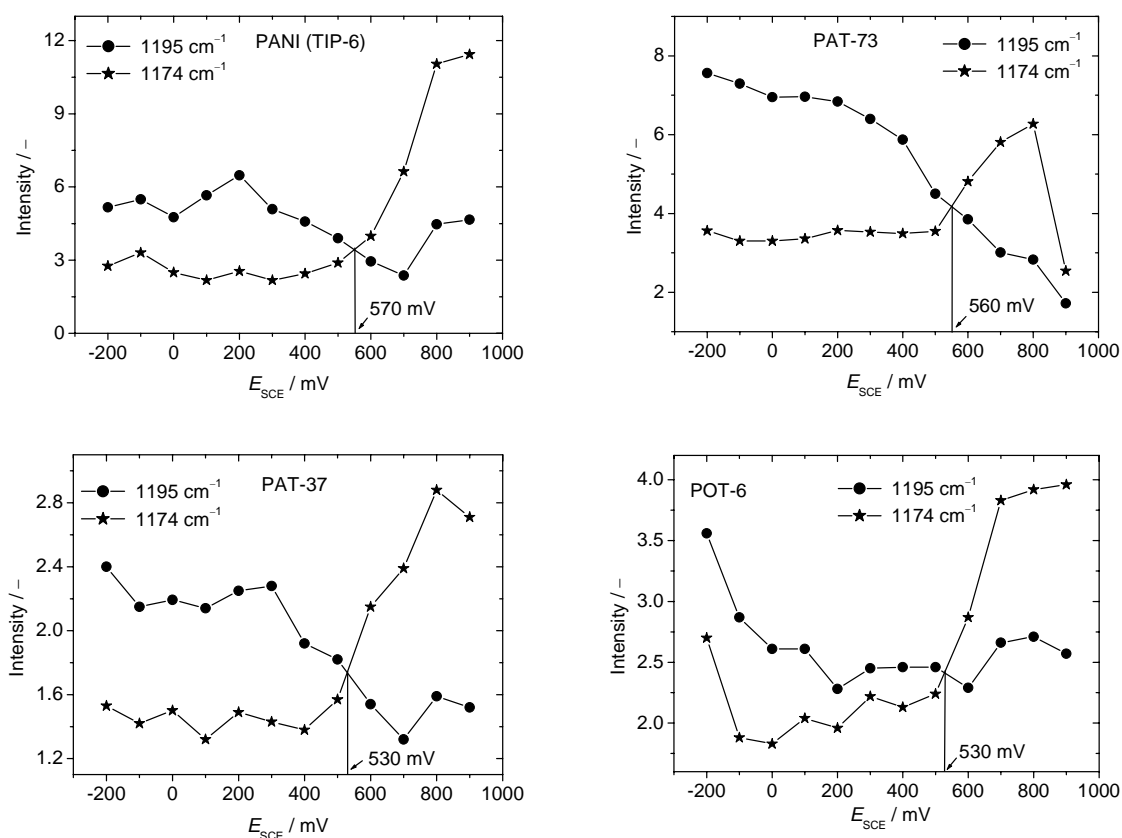**Figure 7.31.** Plots of intensity of bands at ~1195 cm^{-1} (benzoid vibration) and ~1174 cm^{-1} (quinoid vibration) as a function of applied potential for PANI (TIP-6), POT and copolymers with 7:3 and 3:7 mole ratios of aniline to *o*-toluidine in the feed.

7.10 Scanning Electron Microscopy

(a) SEM of PANI-DBSA

Morphological investigations were carried out using scanning electron microscopy (SEM) to study the influence of amount of DBSA in the feed on morphology. It is well known that morphology of PANI is influenced by the method of synthesis and the oxidizing agent employed [164]. SEM micrographs recorded at lower resolution for all the samples show porous film and smooth film morphology for the surface open to environment and the surface in contact with glass substrate during evaporation of the solvent, respectively. The size of the pores varies from 20–150 μm and they arise when evaporation of the solvent is carried out during synthesis. SEM pictures reveal that PANI flakes are formed

during layer-by-layer stacking of the polymer. High-resolution SEM micrographs reveal that morphology of PANI is strongly influenced by the mole ratio of DBSA/aniline in the feed. Figure 7.32 shows SEM images of PANI-DBSA flakes at different molar ratios of DBSA/aniline in the feed. TIP-5 (DBSA/aniline is 5:1) exhibit fibrillar morphology (Figure 7.32a) where the fibers are approximately 8 μm in length and 1 μm in width. When the ratio of DBSA to aniline is increased to 7:1 (TIP-6) and 10:1 (TIP-7), morphology changes to porous network type (Figure 7.32b) and compact film type (Figure 7.32c), respectively. Cross sectional view shows porous network type of morphology (Figure 7.32d). SEM images of PANI-DBSA synthesized *via* gelation also exhibit a stacked layer-by-layer morphology and the surface of the gel exhibit fibrillar morphology [106]. The change in the morphology due to change in the mole ratio of DBSA to aniline may be caused by a change in conformation of the polymer. At higher DBSA to aniline mole ratios, PANI prefers compact film morphology.
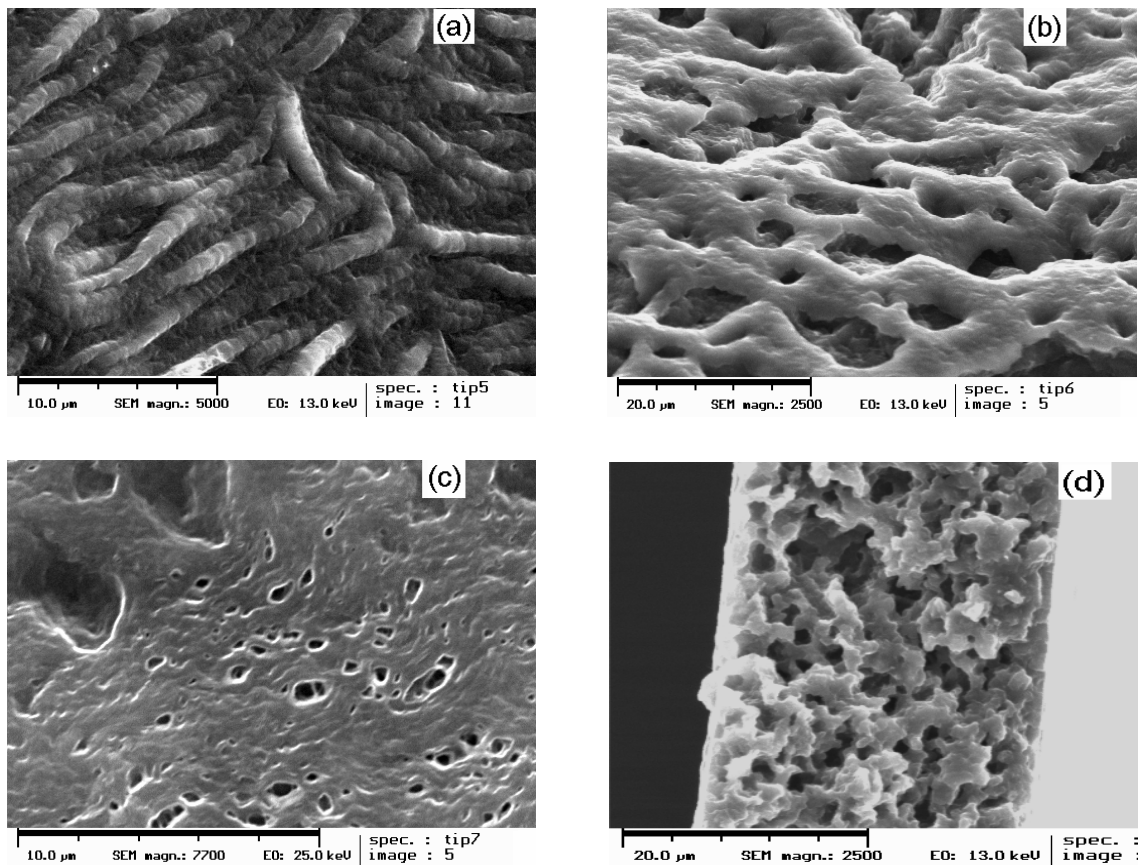

Figure 7.32. SEM micrographs of PANI-DBSA at (a) 5:1, (b) 7:1 and (c) 10:1 feed ratios of DBSA to PANI. (d) Cross sectional view of image 'b'.

(b) SEM of Poly(aniline-co-o-toluidine)s

As mentioned in the preceding section, morphology of aniline based polymers is strongly influenced by the nature of dopant and oxidant used and the synthetic approach employed. SEM image of PANI (TIP-6) shows highly ordered network type morphology (Figure 7.32b and d; Page 115). Reaction conditions employed for the synthesis of POT and copolymers were similar to that of TIP-6.

SEM images of POT recorded at two different resolutions are shown in Figure 7.33. Flakes of POT exhibit relatively smoother surface without any pores. Even the larger pores arising from the solvent evaporation are also absent. As in the case of PANI, flakes of POT are formed through layer-by-layer stacking. It is clear from Figure 7.33c that POT flakes are formed through a random 3D growth of the polymer. The lower solubility of POT-DBSA, which is quite opposite to the one observed in literature, may be due to the absence of any free volumes in it. Cross-sectional view (Figure 7.33b) of a polymer flake also reveals similar compact morphology for POT.
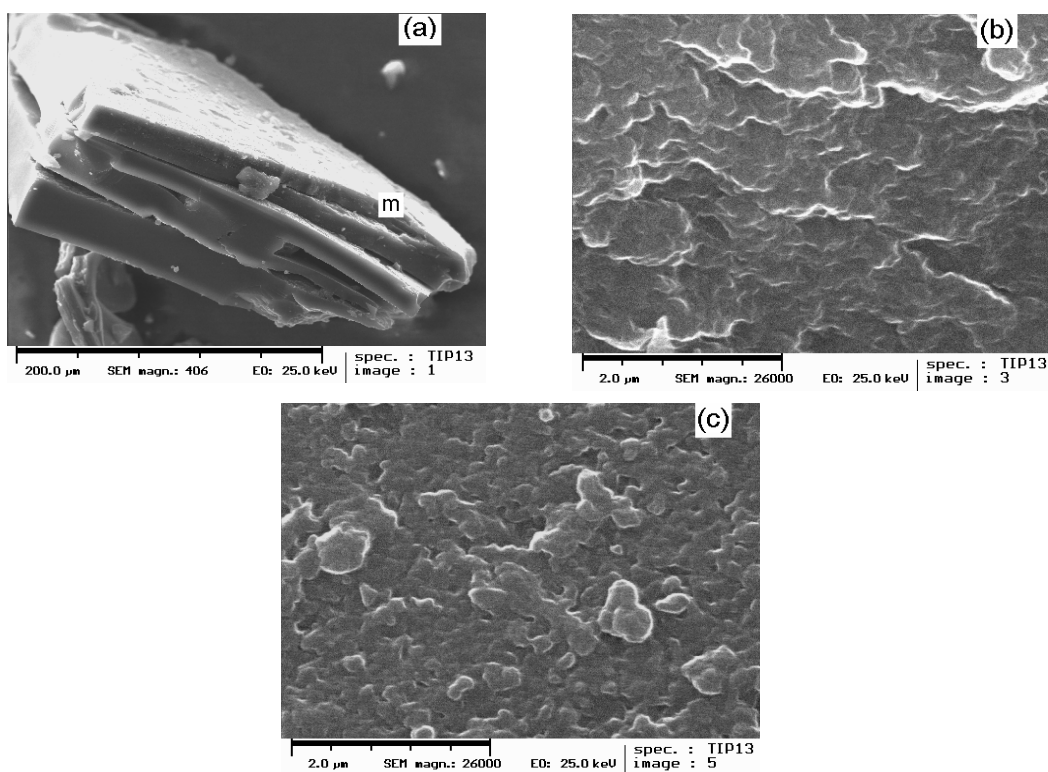

Figure 7.33. SEM micrographs of POT flakes recorded at (a) lower magnification (200 μm), (b) magnified portion of the cross-section marked as 'm' and (c) surface of the flake at higher magnification (2 μm).

Morphology of the poly(aniline-*co-o*-toluidine)s is not greatly affected by the molar ratio of comonomers in the feed with an exception. The bulk morphology of copolymer

containing 3:7 ratio of aniline-to-*o*-toluidine shows slight similarity to POT (Figure 7.34a and b). It still exhibits a compact morphology, but the smooth surface in POT gets slightly roughened. The only influence of aniline in the feed is the generation of free volumes. However, we can not conclude that increase in the amount of aniline in the feed increases the free volumes in copolymer flakes. SEM micrograph of the PAT-73 is similar to that of PAT-37 except for the fact that its surface is smoother than that of PAT-37 (Figure 7.34c and d).
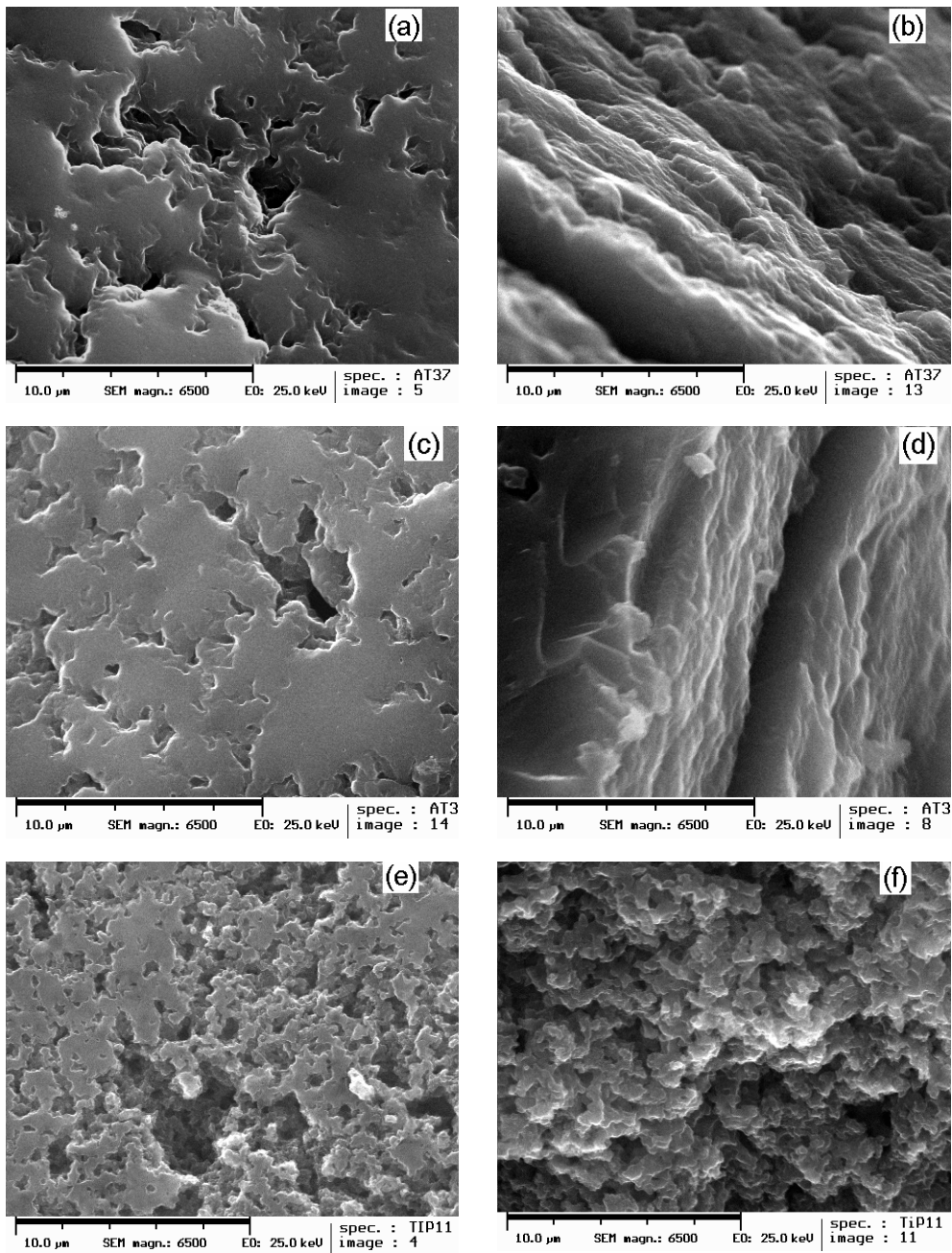

Figure 7.34. SEM micrographs of (a) PAT-37, (b) cross-section of 'a', (c) PAT-73, (d) cross-section of 'c', (e) PAT-55 and (f) cross-section of 'e'.

117

A surprising change in the morphology is observed for the copolymer containing equimolar fractions of aniline and *o*-toluidine (PAT-55). Its morphology is somewhat similar to the morphology of PANI. Large numbers of free volumes are generated and more regular growth of the polymer is seen (Figure 7.34e; Page 117). However, the cross-sectional view of SEM micrograph of PAT-55 (Figure 7.34f) does not show any porous network pattern as in PANI. Such a dramatic change in the morphology arises either due to the formation of composite material where PANI and POT are present as homopolymers or the conformational rearrangement of polymer chain due to self assembling. Formation of composites in the present case is simply ruled out because all the spectroscopic and cyclic voltammetry investigations confirm the formation of real copolymer. Therefore, the concept of conformational rearrangement can be adopted to explain the special properties of this copolymer.

7.11 Transmission Electron Microscopy of PANI-DBSA

Figure 7.35 (Page 119) shows TEM images of PANI-DBSA at different feed ratios of DBSA to aniline. It is clear from the figures that the PANI particles are basically spherical in shape and their size is strongly influenced by the feed ratio of DBSA to aniline. When the ratio is 5, particles are organized in a way normally exhibited by monolayers and the average particle size lies in the range of 1−7 nm. Increasing the feed ratio to 7 and then to 10, increases the average particle size to 8.5−15 nm and then to 20−30 nm, respectively. The feed ratio of DBSA to aniline also influences the aggregation tendency of the PANI particles. In TIP-6 and TIP-7 where the feed ratio is 7 and 10, respectively, the agglomeration tendency is higher leading to the formation of a group of spherical particles overlapping each other. Yang and coworkers [165] have reported that TEM images of PANI-DBSA directly cast from the emulsion show entangled fibers of 1 μm width and a length of 1 mm. Nanocomposites of PANI-CSA and acrylic acid show rice grain-shaped particles with 70 nm width and 120 nm length, whereas, electrochemically synthesized PANI-CSA exhibits agglomerated irregular shaped particles [166, 167]. The tendency of aggregation monitored in TEM images could be correlated to the bulk morphology (SEM) of the polymers. The well organized particles observed in the Figure 7.35a for TIP-5 leads to more ordered fibrillar morphology (Figure 7.32a; Page 115). Increasing tendency of aggregation as reflected from the TEM images of TIP-6 and TIP-7 (Figure 7.35b and c) leads to the

formation of porous (Figure 7.32b; Page 115) and compact (Figure 7.32c; Page 115) poly-mer flakes, respectively.
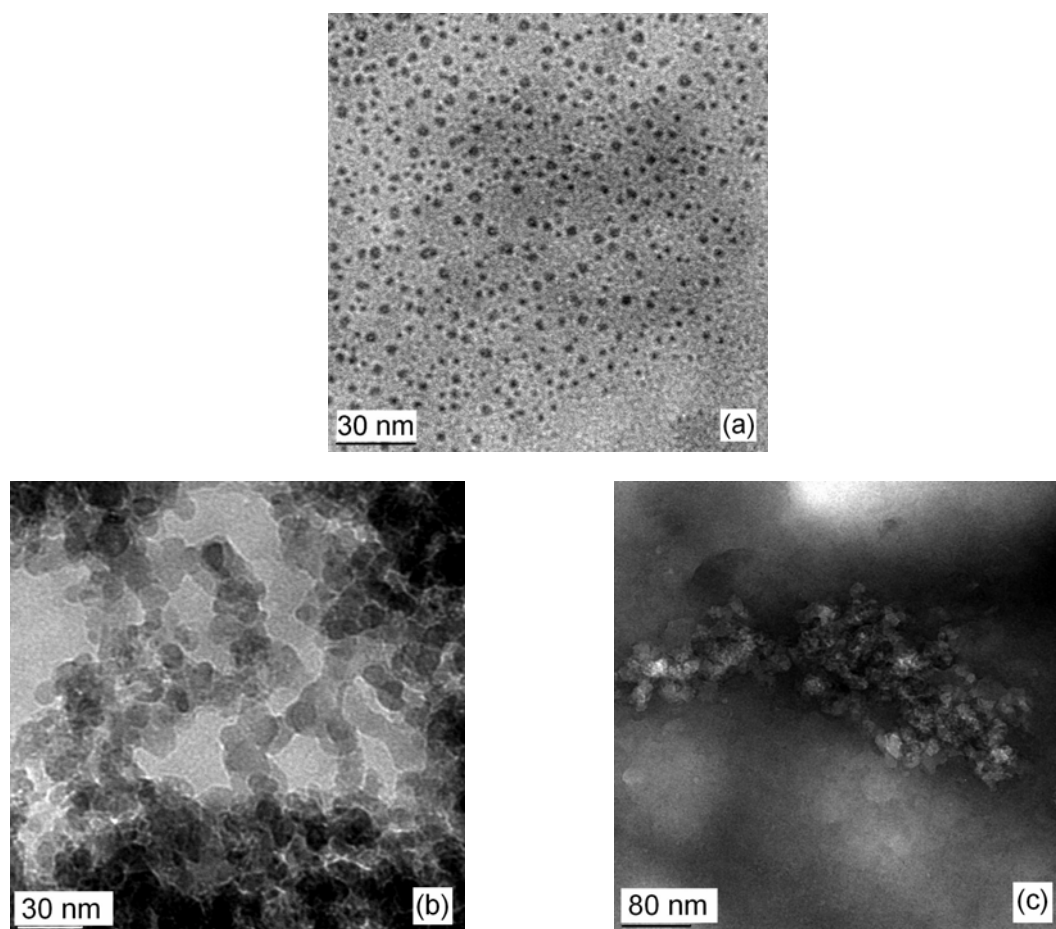
Figure 7.35. Transmission electron microscope images of (a) TIP-5, (b) TIP-6 and (c) TIP-7.

Electron diffraction (ED) patterns were recorded for several agglomerated areas ob-served in TEM images. At DBSA-to-aniline feed ratio of 5, ill defined ED patterns were observed indicating the presence of both crystalline (not shown in the figure) and amor-phous (Figure 7.36a; Page 120) regimes in the polymer. Well defined ED patterns having bright arcs of different lengths could be seen at DBSA-to-aniline feed ratio of 10 (Figure 7.36b; Page 120). Similar ED patterns were also observed for PANI-DBSA synthesized *via* an emulsion pathway and for an electrochemically synthesized PANI-CSA [138, 166]. Such a pattern is attributed to an orthorhombic crystal structure.

Figure 7.36. Electron diffraction patterns for selected agglomerated particles of (a) TIP-5 and (b) TIP-7.

Chapter 8
Summary

8.1 PANI-DBSA

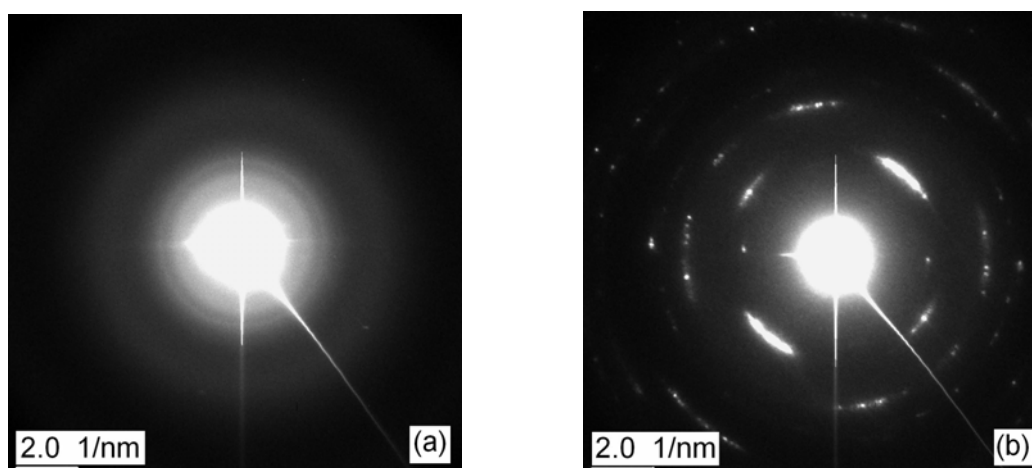A new inverse emulsion procedure is successfully employed to synthesize PANI-DBSA, which is completely soluble in common organic solvents such as chloroform and a 2:1 mixture of toluene+2-propanol. Remarkable improvement in the solubility of parent PANI is observed due to the surfactant dopant (DBSA) and the synthetic approach. PANI redissolved in these solvents can be spun-, drop- or dip-coated on metallic or glass substrates with very good adhesion. PANI suspension obtained during synthesis can also be used directly for practical applications. *In situ* conductivity measurements, which are, till date carried out only for the electrochemically deposited conducting polymers have been, for the first time, employed for the chemically synthesized PANI and the results are in agreement with the electrochemically synthesized ones. PANI-DBSA synthesized using present approach possesses fairly high electrical conductivity as noticed from the minimum resistance values (10 Ω) in the *in situ* conductivity measurements.

Solution state UV-Vis spectra of PANI-DBSA in chloroform do not show any shift in the position of the low energy polaron band (~800 nm) and the ratio of intensities of bands at 800 and 360 nm does not depend on the amount of PANI dissolved in it. These observations reveal that chloroform is the most suitable solvent to process the pristine PANI-DBSA. Electronic absorption spectroscopy also confirms the presence of strong interaction, probably due to hydrogen bonding, between 2:1 mixture of toluene+2-propanol and PANI-DBSA. UV-Vis responses of a drop-coated film of PANI-DBSA for the change in applied potential are similar to that of electrochemically deposited ones. *In situ* UV-Vis spectroscopy measurements reveal good electrochromic reversibility and electrochemical stability for the polymer.

In acidified aqueous electrolytes, PANI-DBSA does not show good electrochemical responses because of the surfactant nature of DBSA, whereas, cyclic voltammogram recorded in non-aqueous electrolyte shows two pairs of well defined redox waves which are very similar to the response of electrochemically synthesized PANI in aqueous electrolytes. At more positive potentials where emeraldine-to-pernigraniline transformation oc-

curs, CVs of PANI in aqueous acids show two oxidation waves due to the presence of two types of counter ions in the polymer film. Their peak position and shape are influenced by the slow anion exchange rate as also confirmed by the *in situ* UV-Vis spectroscopy.

In situ pre-resonance Raman spectroscopy is used to monitor metal-to-insulator transition in PANI. Raman spectra also give valuable structural information of PANI-DBSA. A regular change in the bulk morphology of PANI-DBSA from fiber-to-network-to-compact film could be achieved just by changing the concentration of DBSA in the feed. An increase in the feed ratio of DBSA to aniline increases the tendency of aggregation of spherical particles of PANI as indicated in transmission electron microscopy. TEM images also reveal that morphology of PANI at molecular level is different from that of the bulk morphology. However, the bulk morphology (SEM) could be correlated to the TEM images.

8.2 Poly(aniline-*co*-*o*-toluidine)s

The inverse emulsion polymerization method described for the synthesis of PANI-DBSA was also employed to synthesize poly(*o*-toluidine) and copolymers of aniline and *o*-toluidine. POT as well as copolymers were obtained in fairly good yields indicating that the bulky DBSA can efficiently dope POT chain even though it contains a methyl substituent which does not favor the presence of bulky counter ion in the vicinity of –N atoms of the polymer backbone. The effective doping of POT by DBSA is also confirmed from the elemental analysis data which indirectly provide the extent of doping in the polymer. The expected and calculated elemental compositions are in good agreement. However, DBSA, a well known dopant for PANI, which improves the solubility of PANI fails to improve the solubility of POT. Solubility of POT-DBSA is lower than that of PANI-DBSA which is due to the difference in their bulk morphologies. Flakes of PANI-DBSA possess porous network-type morphology and, therefore, the solvent can easily penetrate through the material making it soluble. Flakes of POT show highly compact morphology (no free volumes) with random three-dimensional growth of the polymer and hence the solubility is dramatically reduced. Copolymers of aniline and *o*-toluidine exhibit better solubility than POT, however, it is lower than that of PANI. UV-Vis, FTIR, Raman spectroscopies and cyclic voltammetry studies confirm the formation of real copolymer.

Electrical conductivity of the copolymers, as expected, is much lower than that of PANI-DBSA. Unlike PANI, in the applied potential range, conductivity of POT as well as

copolymers does not improve after the first potential cycle because of their degradation at much lower positive potentials. PANI-DBSA has wide, while POT has narrow potential window of electrical conductivity and the potential window of copolymers is strongly influenced by the fraction of comonomers in the feed. Higher fraction of aniline yields copolymers with wider potential window (similar to PANI) and *vice versa.*

Solution state UV-Vis spectra of POT in a 2:1 mixture of toluene+2-propanol reveal that the compact coil-type conformation of POT does not undergo any rearrangement. *In situ* UV-Vis responses of POT as well as copolymers resemble PANI except for the fact that emeraldine-to-pernigraniline transformation occurs at lower positive potential than that of PANI. In the applied potential range, POT as well as copolymers exhibit good electrochromic reversibility but lacks better electrochemical stabilities.

Electrochemical behavior of POT in aqueous acids does not exhibit a kinetic influence of anion-exchange during cycling. Electrochemical response of copolymers containing higher concentration of aniline is more similar to that of PANI, whereas, the copolymers containing higher fraction of *o*-toluidine behave like POT. As in the case of PANI, electrochemical responses in non-aqueous electrolyte are much better than those in aqueous electrolytes. FTIR spectroscopy reveals that amount of monomer present in the copolymer depends on the comonomer feed ratios. *In situ* Raman spectroscopy has been used to monitor the metal-to-insulator transition induced by the change in applied potential. Morphology of POT is completely different from that of PANI whereas morphology of copolymers shows greater similarity to POT.

The copolymer containing equimolar fractions of comonomers in the feed exhibits behavior quite different from the others. It was obtained in higher yield and the position of the band at ~800 nm show larger bathochromic shift in chloroform. Moreover, its morphology shows greater similarity to PANI with large numbers of free volumes present in it.

References

1. H. Shirakawa, E. J. Louis, A. G. MacDiarmid, C. K. Chiang and A. J. Heeger, *Chem. Commun.*, **1977**, 578.

2. A. A. Syed and M. K. Dinesan, *Talanta*, 38, **1991**, 815.

3. A. F. Diaz, J. F. Rubinson and Jr. H. B. Mark, *Adv. Polym. Sci.*, 84, **1988**, 113.

4. P. S. Rao, D. N. Sathyanarayana and T. Jeevananda, In *Advanced Functional Molecules and Polymers*, H. S. Nalwa (ed.), Gordon and Breach, Tokyo, Vol.3, **2001**, p. 79.

5. T. A. Skotheim, R. L. Elsenbaumer and J. R. Reynolds (eds.), *Handbook of Conducting Polymers*, 2nd ed., Marcel Dekker, New York, **1998**.

6. H. S. Nalwa (ed.), *Handbook of Conductive Organic Molecules and Polymers*, Wiley, Chichester, Vols. 1–4, **1997**.

7. H. S. Nalwa (ed.), *Advanced Functional Molecules and Polymers*, Gordon and Breach, Tokyo, Vols. 1–4, **2001**.

8. J. Y. Shimano and A. G. MacDiarmid, *Synth. Met.*, 123, **2001**, 251.

9. A. J. Heeger, *Angew. Chem. Int. Ed.*, 40, **2001**, 2591.

10. A. G. Green and A. E. Woodhead, *J. Chem. Soc.*, 97, **1910**, 2388.

11. A. F. Diaz and J. A. Logan, *J. Electroanal. Chem.*, 111, **1980**, 111.

12. R. Holze In *Advanced Functional Molecules and Polymers*, H. S. Nalwa (ed.), Gordon and Breach, Tokyo, Vol. 2, **2001**, p. 171.

13. A. G. Green and A. E. Woodhead, *J. Chem. Soc.*, 101, **1912**, 1117.

14. J. C Chiang, A. G. MacDiarmid, *Synth. Met.*, 13, **1986**, 193.

15. E. M. Genies, A. Boyle, M. Lapkowski and C. Tsintavis, *Synth. Met.*, 36, **1990**, 139.

16. Y. S. Negi and P. V. Adhyapak, *J. Macromol. Sci. - Polym. Rev.*, C42, **2002**, 35.

17. Y. B. Shim and S. M. Park, *Synth. Met.*, 29, **1989**, E169.

18. D. M. Mohilner, R. N. Adams and W. J. Argersinger, *J. Am. Chem. Soc.*, 84, **1962**, 3618.

19. H. Yang and A. J. Bard, *J. Electroanal. Chem.*, 339, **1992**, 423.

20. S. A. Brazovskii and N. N. Kirova, *Sov. Phys. JETP Lett.*, 33, **1981**, 4.

21. G. E. Wnek, *Synth. Met.*, 15, **1986**, 213.

22. B. Lundberg, W. R. Salaneck and I. Lundström, *Synth. Met.*, 21, **1987**, 143.

23. W. R. Salaneck, I. Lundström, T. Hjertberg, C. B. Duke, A. Paton, E. M. Conwell, W. S. Huang, N. L. D. Somasri, A. F. Richter and A. G. MacDiarmid, *Synth. Met.*, 18, **1987**, 311.

24. D. N. Sathyanarayana, In *Vibrational Spectroscopy: Theory and Applications*, 2nd ed., New Age International, New Delhi, **2004**.

25. D. J. Gardiner, In *Practical Raman Spectroscopy*, P. R. Graves (ed.), Springer-Verlag: Berlin Heidelberg, **1989**, p 9.

26. D. L. Andrews, In *Lasers in Chemistry*, Springer-Verlag, Berlin Heidelberg, **1986**, p 106.

27. R. Holze and J. Lippe, *Synth. Met.*, 38, **1990**, 99.

28. K. Aoki, J. Chen, Q. Ke, S. P. Armes and D. P. Randall, *Langmuir*, 19, **2003**, 5511.

29. E. Marie, R. Rothe, M. Antonietti and K. Landfester, *Macromolecules*, 36, **2003**, 3967.

30. M. T. Nguyen, P. Kasai, J. L. Miller and A. F. Diaz, *Macromolecules*, 27, **1994**, 3625.

31. B. Wessling, *Synth. Met.*, 102, **1999**, 1396.

32. R. V. Gregory, In *Handbook of Conducting Polymers*, 2nd ed., T. A. Skotheim, R. L. Elsenbaumer, J. R. Reynolds (eds.), Marcel Dekker, New York, **1998**, p.437.

33. M. Angelopoulos, A. Ray, A. G. MacDiarmid and A. J. Epstein, *Synth. Met.*, 21, **1987**, 21.

34. M. Inoue, R. E. Navarro and M. B. Inoue, *Synth. Met.*, 30, **1989**, 199.

35. R. Jiang and S. Dong, *Synth. Met.*, 24, **1988**, 255.

36. S. Li, Y. Cao and Z. Xue, *Synth. Met.*, 20, **1987**, 141.

37. S. K. Dhawan and D. C. Trivedi, *Synth. Met.*, 60, **1993**, 63.

38. L. G. Xu, S. C. Ng and H. S. O. Chan, *Synth. Met.*, 123, **2003**, 403.

39. H. S. O. Chan, P. K. H. Ho, S. C. Ng, B. T. G. Tan and K. L. Tan, *J. Am.Chem. Soc.*, 117, **1995**, 8517.

40. X. L. Wei, M. Fahlman and A. J. Epstein, *Macromolecules*, 33, **2000**, 8117.

41. J. Anand, S. Palaniappan and D. N. Sathyanarayana, In *Handbook of Organic Conductive Molecules and Polymers,* H. S. Nalwa (ed.), Wiley, Chichester, Vol. 2, **1997**, p. 573.

42. M. Probst and R. Holze, *Macromol. Chem. Phys.*, 198, **1997**, 1499.

43. A. L. Schemid, L. M. Lira and S. I. Cordoba de Torresi, *Electrochim. Acta*, 47, **2002**, 2005.

44. Y. Cao, P. Smith and A. J. Heeger, *Synth. Met.*, 48, **1992**, 91.

45. C. Huber, M. Sadogi, T. Huber and D. Chacko, *Adv. Mater.*, 7, **1995**, 316.

46. J. Anand, S. Palaniappan and D. N. Sathyanarayana, *Prog. Polym. Sci.*, 23, **1998**, 993.

47. S. Yang and E. Ruckenstein, *Synth. Met.*, 60, **1993**, 249.

48. V. Jousseaume, M. Morsli, A. Bonnet and S. Lefrant, *J. Appl. Polym. Sci.*, 67, **1998**, 1209.

49. P. Banerjee and B. M. Mandal, *Macromolecules*, 28, **1995**, 3940.

50. S. S. Im and S. W. Byun, *J. Appl. Polym. Sci.*, 51, **1994**, 1221.

51. P. S. Rao, S. Subrahmanya and D. N. Sathyanarayana, *J. Appl. Polym. Sci.*, 98, **2005**, 583.

52. Y. Wie, R. Hariharan and S. A. Patel, *Macromolecules*, 23, **1990**, 758.

53. C. C. Han, S. P. Hang, K. F. Yang, M. Y. Bai, C. H. Lu and C. S. Huang, *Macromolecules*, 34, **2001**, 587.

54. P. Savitha, P. S. Rao and D. N. Sathyanarayana, *Polym. Int.*, 54, **2005**, 1243.

55. J. Stejskal, M. Spirkova and P. Kratochvil, *Acta Polymer.*, 45, **1994**, 385.

56. K. E. J. Barret (Ed.), *Dispersion Polymerization in Organic Media*, Wiley, London, **1975**.

57. P. Banerjee, *Eur. Polym. J.*, 34, **1998**, 841.

58. P. R. Somani, *Mater. Chem. Phys.*, 77, **2003**, 81.

59. G. Gustafsson, Y. Cao, G. M. Treac, F. Klavetter, N. Colaneri and A. J. Heeger, *Nature*, 357, **1992**, 477.

60. D. Chattopadhyay and B. M. Mandal, *Langmuir*, 12, **1996**, 1585.

61. J. Stejskal and P. Kratochvil, *Langmuir*, 12, **1996**, 3389.

62. P. Banerjee, S. N. Bhattacharyya and B. M. Mandal, *Langmuir*, 11, **1995**, 2414.

63. E. C. Cooper and B. Vincent, *J. Phys. D: Appl. Phys.*, 22, **1989**, 1580.

64. S. P. Armes, M. Aldissi, S. Agnew and S. Gottesfeld, *Langmuir*, 6, **1990**, 1745.

65. S. H. Lee, D. H. Lee, K. Lee and C. W. Lee, *Adv. Funct. Mater.*, 15, **2005**, 1495.

66. J. Stejskal, *J. Polym. Mater.*, 18, **2001**, 225.

67. P. A. Hassan, S. N. Sawant, N. C. Bagkar and J. V. Yakhmi, *Langmuir*, 20, **2004**, 4874.

68. N. Kuramoto and E. M. Genies, *Synth. Met.*, 68, **1995**, 191.

69. N. Kuramoto and A. Tomita, *Polymer*, 38, **1997**, 3055.

70. L. Yu, J. I. Lee, K. W. Shin, C. E. Park and R. Holze, *J. Appl. Polym. Sci.*, 88, **2003**, 1550.

71. B. J. Kim, S. G. Oh, M. G. Han and S. S. Im, *Synth. Met.*, 122, **2001**, 297.

72. D. Han, Y. Chu, L. Yang, Y. Liu and Z. Lv, *Colloids and Surfaces A: Physicochem. Eng. Aspects*, 259, **2005**, 179.

73. S. Shreepathi and R. Holze, *Chem. Mater.*, 17, **2005**, 4078.

74. M. G. Han, S. K. Cho, S. G. Oh and S. S. Im, *Synth. Met.*, 126, **2002**, 53.

75. Y. Haba, E. Segal, M. Narkis, G. I. Titelman and A. Siegmann, *Synth. Met.*, 106, **1999**, 59.

76. Y. B. Kim, J. K. Choi, J. A. Yu and J. W. Hong, *Synth. Met.*, 131, **2002**, 79.

77. J. N. Barisci, P. C. Innis, L. A. P. Kane-Maguire, I. D. Norris and G. G. Wallace, *Synth. Met.*, 84, **1997**, 181.

78. A. Malinauskas and R. Holze, *Electrochim. Acta*, 43, **1998**, 2563.

79. A. Malinauskas and R. Holze, *J. Appl. Polym. Sci.*, 73, **1999**, 287.

80. A. Abd-Elwahed and R. Holze, *Curr. Top. Electrochem.*, 9, **2003**, 93.

81. R. Holze, *J. Solid State Electrochem.*, 8, **2004**, 982.

82. D. Chattopadhyay, S. Banerjee, D. Chakravorty and B. M. Mandal, *Langmuir*, 14, **1998**, 1544.

83. N. K. Svelko, S. Reynaud and J. Francois, *Synth. Met.*, 150, **2005**, 107.

84. P. S. Rao, S. Subrahmanya and D. N. Sathyanarayana, *Synth. Met.*, 128, **2002**, 311.

85. P. Ghosh, A. Chakrabarti and S. K. Siddhanta, *Eur. Polym. J.*, 35, **1999**, 803.

86. W. Yin and E. Ruckenstein, *Synth. Met.*, 108, **2000**, 39.

87. C. Li and S. Mu, *Synth. Met.*, 144, **2004**, 143.

88. M. Morita, *J. Appl. Polym. Sci.*, 52, **1994**, 711.

89. A. Abd-Elwahed and R. Holze, *Synth. Met.*, 131, **2002**, 61.

90. C. Liu, J. Zhang, G. Shi and F. Chen, *J. Appl. Polym. Sci.*, 92, **2004**, 171.

91. A. Hugot-LeGoff and M. C. Bernard, *Synth. Met.*, 60, **1993**, 115.

92. M. Bartonek, N. S. Sariciftci and H. Kuzmany, *Synth. Met.*, 36, **1990**, 83.

93. S. Quillard, M. I. Boyer, M. Cochet, J. P. Buisson, G. Louarn and S. Lefrant, *Synth. Met.*, 101, **1999**, 768.

94. C. Y. Xu, P. X. Zhang and L. Yan, *J. Raman Spectrosc.*, 32, **2001**, 862.

95. B. Vincent and J. Waterson, *J. Chem. Soc. Chem. Commun.*, **1990**, 683.

96. J. Stejskal, P. Kratochvíl and N. Radhakrishnan, *Synth. Met.*, 61, **1993**, 225.

97. K. Tzou and R. V. Gregory, *Synth. Met.*, 53, **1993**, 365.

98. P. Rannou, B. Dufour, J. P. Travers and A. Pron, *Synth. Met.*, 119, **2001**, 441.

99. X. Lu, J. Xu and L. Wong, *Synth. Met.*, 156, **2006**, 117.

100. P. Tsotra and K. Friedrich, *J. Mater. Sci.*, 40, **2005**, 4415.

101. P. Krzysztof and Y. Nan-Loh, *Abstracts, 36th middle Atlantic regional meeting of the Am. Chem. Soc. Princeton*, June **2003**, 366.

102. B. Dufour, P. Rannou, D. Djurado, H. Janeczek, M. Zagorska, A. deGeyer, J. P. Travers and A. Pron, *Chem. Mater.*, 15, **2003**, 1587.

103. L. W. Shacklette, G. G. Miller, R. L. Elesenbaumer, C. Han, B. M. Webling and B. Wessling, *U. S. Patent*, 5,281,363,**1994**.

104. M. Angelopoulos, N. Patel, J. M. Shaw, N. C. Labianca and S. A. Rishton, *J. Vac. Sci. Technol. B*, 11, **1993**, 2794.

105. Y. Cao, P. Smith and A. J. Heeger, *U. S. Patent*, 5,232,631, **1993**.

106. R. Madathil, R. Parkesh, S. Ponrathnam and M. C. J. Large, *Macromolecules*, 37, **2004**, 2002.

107. G. Li and Z. Zhang, *Macromolecules*, 37, **2004**, 2683.

108. K. S. Alva, J. Kumar, K. A. Marx and S. K. Tripathy, *Macromolecules*, 30, **1997**, 4024.

109. J. A. Akkara, K. J. Senecal and D. L. Kaplan, *J. Polym. Sci.*, 29, **1991**, 1561.

110. Y. Ma, J. Zhang, G. Zhang and H. He, *J. Am. Chem. Soc.*, 126, **2004**, 7097.

111. J. Kan, S. Zhang and G. Jing, *J. Appl. Polym. Sci.*, 99, **2006**, 1848.

112. X. Wang, N. Liu, X. Yan, W. Zhang and Y. Wei, *Chem. Lett.*, 34, **2005**, 42.

113. J. E. Osterholm, Y. Cao, F. Klavetter and P. Smith, *Synth. Met.*, 55, **1993**, 1034.

114. J. E. Osterholm, Y. Cao, F. Klavetter and P. Smith, *Polymer*, 35, **1994**, 2902.

115. P. J. Kinlen, J. Liu, Y. Ding, C. R. Graham and E. E. Remsen, *Macromolecules*, 31, **1998**, 1735.

116. J. Li, K. Fang, H. Qiu, S. Li and W. Mao, *Synth. Met.*, 142, **2004**, 107.

117. G. Odian, In *Principles of Polymerization*, 4th ed. John Wiley-interscience, New York, **2004**.

118. L. M. Gan, C. H. Chew, H. S. O. Chan and L. Ma, *Polym. Bull. (Berlin)*, 31, **1993**, 347.

119. E. Ruckenstein and Y. Sun, *Synth. Met.*, 74, **1995**, 107.

120. I. Kogan, L. Fokeeva, I. Shunina, Y. Estrin, L. Kasumova, M. Kaplunova, G. Davidova and E. Knerelman, *Synth. Met.*, 100, **1999**, 303.

121. Z. Sun, Y. Geng, L. Ji, X. Wang, X. Jing and F. Wang, *J. Appl. Polym. Sci.*, 72, **1999**, 1077.

122. A. Yasuda and T. Shimidzu, *Polym. J.*, 25, **1993**, 329.

123. A. Pron, F. Genoud, C. Menardo and M. Nechtschein, *Synth. Met.*, 24, **1988**, 193.

124. P. S. Rao, D. N. Sathyanarayana and S. Palaniappan, *Macromolecules*, 35, **2002**, 4988.

125. M. S. Ram and S. Palaniappan, *J. Mater. Sci.*, 39, **2004**, 3069.

126. Y. Wei, R. Hariharan and S. A. Patel, *Macromolecules*, 23, **1990**, 758.

127. P. S. Rao and D. N. Sathyanarayana, *Polymer*, 43, **2002**, 5051.

128. P. S. Rao and D. N. Sathyanarayana, *J. Polym. Sci. Part A: Polym. Chem.*, 40, **2002**, 4065.

129. B. C. Roy, M. D. Gupta, L. Bhowmik and J. K. Ray, *Bull. Mater. Sci.*, 24, **2001**, 389.

130. A. L. Sharma, V. Saxena, S. Annapoorni and B. D. Malhotra, *J. Appl. Polym. Sci.*, 81, **2001**, 1460.

131. F. R. Diaz, C. O. Sanchez, M. A. del Valle, J. L. Torres and L. H. Tagle, *Synth. Met.*, 118, **2001**, 25.

132. S. Vogel and R. Holze, *Electrochim. Acta*, 50, **2005**, 1587.

133. A. A. Shah and R. Holze, *J. Solid State Electrochem.*, 11, **2006**, 38.

134. A. A. Shah and R. Holze, *Synth. Met.*, 156, **2006**, 566.

135. S. Bilal and R. Holze, *J. Electroanal. Chem.*, 592, **2006**, 1.

136. M. R. Huang, X. G. Li, Y. L. Yang, X. S. Wang and D. Yan, *J. Appl. Polym. Sci.*, 81, **2001**, 1838.

137. D. D. Borole, U. R. Kapadi, P. P. Mahulikar and D. G. Hundiwale, *Mater. Lett.*, 58, **2004**, 3816.

138. C. H. Yang, T. C. Yang and Y. K. Chih, *J. Electrochem. Soc.*, 152, **2005**, E273.

139. P. Savitha and D. N. Sathyanarayana, *Polym. Int.*, 53, **2004**, 106.

140. S. J. Su, M. Takeishi and N. Kuramoto, *Macromolecules*, 35, **2002**, 5752.

141. L. Y. Xin, X. G. Zhang, G. Q. Zhang and C. M. Shen, *J. Appl. Polym. Sci.*, 96, **2005**, 1539.

142. S. Ito, K. Murata, S. Teshima, R. Aizawa, Y. Asako, K. Takahashi and B. M. Hoffman, *Synth. Met.*, 96, **1998**, 161.

143. S. A. Chen and G. W. Hwang, *J. Am. Chem. Soc.*, 117, **1995**, 10055.

144. J. Laska and J. Widlarz, *Synth. Met.*, 135-136, **2003**, 261.

145. S. Palaniappan and V. Nivasu, *New J. Chem.*, 26, **2002**, 1490.

146. A. A. Athawale, M. V. Kulkarni and V. V. Chabukswar, *Mater. Chem. Phys.*, 73, **2002**, 106.

147. J. Lippe and R. Holze, *Synth. Met.*, 41–43, **1991**, 2927.

148. D. Kumar, *Synth. Met.*, 114, **2000**, 369.

149. N. Ahmad, J. Naseer, N. Gadgil and F. Goodson, *J. Indian Chem. Soc.*, **2004**, *81*, 606.

150. H. V. Hoang and R. Holze, *Chem. Mater.*, 18, **2006**, 1976.

151. J. Stejskal and I. Sapurina, *Pure Appl. Chem.,* **77**, **2005**, 815.

152. A. J. Dominis, G. M. Spinks, L. A. P. Kane-Maguire and G. G. Wallace, *Synth. Met.*, 129, **2002**, 165.

153. T. Lindfors, C. Kvarnström and A. Ivaska, *J. Electroanal. Chem.*, 518, **2002**, 131.

154. J. E. de Albuquerque, L. H. C. Mattoso, R. M. Faria, J. G. Masters and A. G. MacDiarmid, *Synth. Met.*, 146, **2004**, 1.

155. R. Mazeikiene, G. Niaura and A. Malinauskas, *Synth. Met.,* 139, **2003**, 89.

156. M. C. Bernard, S. Joiret, A. Hugot-Le Goff and P. D. Long, *J. Electrochem. Soc.,* 148, **2001**, B299.

157. D. A. Buttry and M. D. Ward, *Chem. Rev.*, 92, **1992**, 1355.

158. M. Lapkowski, K. Berrada, S. Quillard, G. Louran, S. Lefrant and A. Pron, *Macromolecules*, 28, **1995**, 1233.

159. M. V. Kulkarni, A. K. Viswanath and U. P. Mulik, *Mater. Chem. Phys.*, 89, **2005**, 1.

160. A. Falcou, A. Duchene, P. Hourquebie, D. Marsacq and A. Balland-Longeau, *Synth. Met.*, 149, **2005**, 115.

161. X. Lu, H. Y. Ng, J. Xu and C. He, *Synth. Met.*, 128, **2002**, 167.

162. M. Baibarac, M. Cochet, M. Lapkowski, L. Mihut, S. Lefrant and I. Baltog, *Synth. Met.* 96, **1998**, 63.

163. N. S. Sariciftci and H. Kuzmany, *Synth. Met.*, 21, **1987**, 157.

164. P. S. Rao, S. Subrahmanya and D. N. Sathyanarayana, *Synth. Met.*, 139, **2003**, 397.

165. C. Y. Yang, P. Smith, A. J. Heeger, Y. Cao and J. E. Osterholm, *Polymer*, 35, **1994**, 1142.

166. P. C. Innis, I. D. Norris, L. A. P. Kane-Maguire and G. G. Wallace, *Macromolecules*, 31, **1998**, 6521.

167. P. A. McCarthy, J. Huang, S. C. Yang and H. L. Wang, *Langmuir*, 18, **2002**, 259.

Selbständigkeitserklärung

Hiermit erkläre ich an Eides statt, die vorliegende Arbeit selbständig und ohne unerlaubte Hilfsmittel durchgeführt zu haben.

Chemnitz, den 26.07.2006   (Subrahmanya S)

Curriculum Vitae

Personal Information

Name:	Subrahmanya Shreepathi
Date of Birth:	February 21, 1977
Place of Birth:	Ananthapur, India
Nationality:	Indian
Address:	Kumara Krupa
	Gurubhavana Road
	SORAB-577 429
	India

Education:

1994-1997:   L.B. College, Kuvempu University, India

B.Sc (Physics, Chemistry and Mathematics)

1997-1999:   Mysore University, India

M.Sc (Inorganic Chemistry)

2000-2002:   Project Assistant

Department of IPC, Indian Institute of Science, Bangalore, India

Project Title: Synthesis and characterization of conducting polyaniline blends with thermoplastic polymers

2003-Till date: **Ph.D.** Student, Institute of Physical Chemistry/Electrochemistry, TU Chemnitz, Germany

Publications:

1 "Benzoyl peroxide initiated inverse emulsion copolymerization of aniline and *o*-toluidine: effect of dodecylbenzenesulfonic acid on the physicochemical properties of the copolymers" **S. Shreepathi** and R. Holze, *Macromol. Chem. Phys.* (accepted).

2 "Corrosion protection performance and spectroscopic investigations of soluble conducting polyaniline-dodecylbenzenesulfonate synthesized *via* inverse emulsion procedure" **S. Shreepathi**, H. V. Hoang and R. Holze, *J. Electrochem. Soc.* in Press (2007).

3 "Spectroelectrochemistry and preresonance Raman spectroscopy of polyaniline-dodecylbenzenesulfonic acid colloidal dispersions" **S. Shreepathi** and R. Holze, *Langmuir,* 22 (2006) 5196.

4 "Spectroelectrochemical investigations of soluble polyaniline synthesized *via* new inverse emulsion pathway" **S. Shreepathi** and R. Holze, *Chem. Mater.* 17 (2005) 4078.

5 "Water-soluble conductive blends of polyaniline and poly(vinyl alcohol) synthesized by two emulsion pathways" P. S. Rao, **S. Subrahmanya** and D.N. Sathyanarayana, *J. Appl. Polym. Sci.* 98 (2005) 583.

6 "Polyaniline–polycarbonate blends synthesized by two emulsion pathways" P. S. Rao, **S. Subrahmanya** and D.N. Sathyanarayana, *Synth. Met.* 143 (2004) 323.

7 "Synthesis by inverse emulsion pathway and characterization of conductive polyaniline–poly(ethylene-*co*-vinyl acetate) blends" P. S. Rao, **S. Subrahmanya** and D.N. Sathyanarayana, *Synth. Met.* 139 (2003) 397.

8 "Inverse emulsion polymerization: a new route for the synthesis of conducting polyaniline" P. S. Rao, **S. Subrahmanya** and D.N. Sathyanarayana, *Synth. Met.* 128 (2002) 311.

International Conferences:

1. Poster presentation of article entitled "Spectroelectrochemistry of soluble polyaniline synthesized by a new inverse emulsion procedure" in *IUPAC World Polymer Congress MACRO 2004* at Paris, France from July 4-9, 2004.

2. Poster presentation of article entitled "Spectroelectrochemical investigations of soluble polyaniline synthesized *via* new inverse emulsion procedure" in *4th Baltic conference on Electrochemistry* at Greifswald, Germany from March 13-16, 2005